ProQuest LLC.
789 East Eisenhower Parkway
P.O. Box 1346
Ann Arbor, MI 48106 – 1346

THE MEASUREMENT OF TURBULENT SKIN FRICTION FOR SMOOTH AND ROUGH PLATES

by

John Anthony Harrison

A thesis submitted for the degree of

MASTER of PHILOSOPHY

of the

UNIVERSITY of SURREY

ABSTRACT

An analysis of the measurement of turbulent skin friction on smooth and rough plates using a hot wire anemometer, and surface Pitot tubes is here presented. Emphasis is placed on the use of a modified form of Stanton tube for use on rough surfaces.

In addition various parameters such as :- Roughness Reynolds number, centre line average roughness value, grit size etc., are correlated to the law of the wall, and boundary layer momentum thickness and shape factor. Further investigations are made into the relationship between turbulence intensity and roughness parameters.

The effect of a blunt-edged flat plate on the skin friction results is also considered, and a drag law taking into account free stream turbulence is presented.

The experimental results were obtained using plates mounted in a vertical plane in the test section of a low speed wind tunnel at velocities up to a maximum of 21 m/s with a plate Reynolds number of 750,000.

ACKNOWLEDGEMENTS

The author wishes to express his gratitude to Mr. D. Fargie for suggesting this research topic and for his very helpful supervision.

Sincere thanks are also due to Dr. Klemz and Dr. Marsden, and the technicians of the Mechanical Engineering department of the North East London Polytechnic, in particular the work of Mr. F.Marris has been most appreciated.

A special thank you to my wife for her kind assistance in typing and compiling this thesis.

CONTENTS

INDEX TO FIGURES

NOTATION

A, C – Calibration constants - Hot Wire Anemometer. (4.06..1).

B – Constant in the law of the wall.(2.02..2).

C_{fx} – Local Friction Factor.

CLA – Centre Line Average Value. (μ ins.)

d – Preston tube diameter. (ins.)

E – Bridge Voltage.

E_o – Bridge Voltage at Zero Flow Velocity.

E_{rms} – Root Means Square Voltage.

f – Pipe Friction factor $= 2\tau/\rho U^2$ (2.03..3)

F_r – Roughness Function - Nikuradse Equation.(2.03..1)

G – Constant in the law of the wall. (2.03..5)

h – Height of Stanton tube above surface (ins.).

H – Shape Factor $= \delta^*/\theta$.

I – Turbulence Intensity. (%).

K – Asperity Height (ins.).

K_s – Nikuradse Sand Particle Size (ins.).

L – Axial Length of Wall(ins.)

M – Manometer constant.

N – Speed of Fan (rev/min.).

p – Static Pressure at any height in Boundary Layer (ins.Water)

P – Static Pressure recorded by Pitot tube (ins.Water)

P_o – Total " " " " " "

P_a – Atmospheric Pressure (mm mercury).

Δp – Stanton Tube Total Pressure - Static Pressure (ins.Water)

Q – Volume Flow Rate (ft^3/s). (2.02..3).

r – Radius of Tube or Pipe (ins.)

R_r – Roughness Reynolds Number $K_s u_\tau/\nu$.

R_s - Stanton Tube Reynolds Number $u_p h/\nu$.(2.01..3)

R_x - Reynolds Number based on x Ux/ν.

R_y - Reynolds Number based on y Uy/ν.

R_θ - Reynolds Number based on θ $U\theta/\nu$.

t - Temperature ^oC.

T - Absolute Temperature ^oK.

u - Mean Velocity Component parallel to wall (ft/s).

u_p - Velocity equivalent of Pressure Difference Δ_p across a Stanton Tube (ft/s).

u_τ - Friction Velocity $\sqrt{\tau/\rho}$ (ft/s).

U - Mainstream Velocity.

U^+ - Dimensionless Velocity in the law of the wall u/u_τ

v - Mean Velocity Component Perpendicular to wall (ft/s

w - Width of Stanton Tube (ins.).

x - Distance along the plate (ins.).

x_k - Distance from the leading edge of a single roughness element.

y - Distance perpendicular to the plate (ins.).

y_p - Effective centre of Stanton tube, where the velocity equals u_p (2.01..1).

y_t - Abrasive paper thickness (ins.)

z - Distance sideways along the plate. (ins.).

y^+ - Dimensionless group in the law of the wall equation yu_τ/ν. (2.02..2).

x^* - Stanton tube calibration $= \text{Log}_{10}\left[\frac{1}{8}\left(\frac{u_p h}{\nu}\right)^2\right]$

y^* - Stanton tube calibration $= \text{Log}_{10}\left[\frac{1}{4}\left(\frac{u_\tau h}{\nu}\right)^2\right]$

β - Angle of Yaw of Stanton tube (2.01..7).

ρ - Density of Air. (lb/ft^3)

μ - Dynamic Viscosity of Air (lb/ft.s).

ν - Kinematic Viscosity of Air (ft^2/s)

δ - Local Height of Boundary Layer (ins.)

δ_L - Local Height of Laminar Sub Layer (ins.)

τ_w - Shear Stress at the wall.

δ^* - Displacement Thickness $\int_o^\delta \left(1-\frac{u}{U}\right)dy$

ϕ - Function.

θ - Momentum Thickness $\int_o^\delta \frac{u}{U}\left(1-\frac{u}{U}\right)dy$

K - Constant in the law of the wall (2.02..2).

λ - Prandtl Mixing length (2.02..5).

CHAPTER 1 INTRODUCTION

1.01 General

A substantial quantity of earlier work exists regarding skin friction measurements on a flat smooth plate at zero incidence. Generally however the surface to be considered in most engineering plant applications is far from smooth, consequently smooth surface methods cannot always be used.

The type of roughness referred to in the past has usually been geometrically regular in shape, or artificially produced by either a printing or machining process. The type of surface normally encountered in practice however usually consists of a uniformly distributed random roughness. There is a need therefore, for further information relating real engineering roughness to the law of the wall, friction factor, and the usual boundary layer parameters.

The aim of this thesis is to help to satisfy this requirement, and to provide a practical basis for assessing friction factor using either a hot wire anemometer, or a surface Pitot tube.

It is the intention to concentrate mainly on rough surfaces, but smooth surfaces will also be considered, primarily for the sake of completeness, but also as a control surface to which the rough surfaces can be compared.

Finally some work on turbulence has also been included; therefore the basic parts to this investigation may be said to fall into four main sections which are shown overleaf.

(a) Surface Pitot Tubes

Surface Pitot tubes play a vital role in this thesis, and it is as well at this stage to define those used. A Stanton tube is usually taken to be a flat surface Pitot tube where the width (w) is far greater than the height (h). A Preston tube which is also fixed to the surface facing into the air stream is cylindrical in form, and the outside diameter (d) is far greater than the height (h) of a Stanton tube.

(b) Smooth Plate Surfaces

An improved type of Stanton tube was used as a skin friction sensor; the basic calibration was obtained by means of a hot wire anemometer. A further check on friction factor was made using a Preston tube. Displacement, and momentum thicknesses were calculated from the velocity profiles obtained, and were used for the final calibration.

(c) Rough Plates

Skin friction readings were taken, as indicated above, but various other roughness parameters are now included in addition, and a relationship between these variables, and the law of the wall is developed.

(d) Turbulence Effects

Turbulence levels, parallel to, and at right angles to the plates, for smooth and rough surfaces were measured. The effect on turbulence of varying roughness for a particular flow, is also considered.

1.02 Aims and Objectives

The broad aim of the project has been mentioned in para.1.01 , the main objectives are as follows:-

(i) To develop, and calibrate an improved form of skin friction sensor of the Stanton tube type, and to use this, for smooth and rough surfaces under turbulent flow conditions. Also to compare the calibration with those of other workers.

(ii) To correlate the roughness parameters of a particular surface with the law of the wall for flat plates.

(iii) To ascertain how turbulence intensity is affected by varying the plate roughness.

(iv) To investigate how shape factor, and momentum thickness are affected by the roughness of the plate.

CHAPTER 2 REVIEW OF PREVIOUS WORK

As outlined in the introduction, the work falls broadly into four sections, hence it is logical to consider the review of previous work to conform to this format.

Paragraph 2.01 traces the history, and development of surface Pitot tubes, whereas paragraph 2.02, which deals with skin friction measurement concentrates mainly on the velocity distribution aspect and the law of the wall, and is solely concerned with smooth surfaces. The survey of work on rough surfaces is developed in paragraph 2.03, and that concerned with turbulence levels in paragraph 2.04.

2.01 Surface Pitot Tubes

The original form of the Stanton tube as conceived by Stanton, Marshall and Bryant [48] in 1920 consisted of a special form of Pitot tube in which the surface to which it is attached formed one wall of the Pitot tube; its width being much greater than its height so that the flow is effectively two dimensional.

Fage and Falkner [22] in 1930 next considered using a Stanton tube, but allowed for the height (h) to be varied, and developed the term effective centre (y_p). The effective centre y_p of a Stanton tube is defined as the distance from the wall where the velocity is equal to u_p and

$$y_p = \left[\left(1 - \sqrt{1 - \frac{2}{3}\frac{u_p}{U}}\right)\right]\frac{W}{2} \qquad \ldots(2.01..1)$$

Fage and Falkner [22] used their surface Pitot tubes for measurement of turbulent skin friction, but in fact calibrated them in laminar flow, and assumed the velocity profiles would agree.

In 1938 G.I.Taylor [50] extended the earlier work by relating effective centre y_p to a unique non-dimensional form called Stanton tube Reynolds number R_s. As in the manner of previous workers, Taylor calibrated his Stanton tube in laminar flow, hence

$$R_s = \frac{\rho \tau_w h^2}{\mu^2} = \frac{u_p h}{\nu}$$

$$y_p = \left(\frac{2\Delta p}{\rho}\right)^{1/2} \frac{\mu}{\tau_w} \qquad \ldots(2.01..2)$$

the final calibration takes the form

$$y_p/h = \phi(R_s) \qquad \ldots(2.01..3)$$

where ϕ = 'function of'.

In order to investigate the transition from laminar to turbulent flow Fage and Preston [23] carried out their classical experiment using a water tunnel and fluid motion microscope, they employed Stanton tubes to locate 'transition' in the boundary layer.

The measurement of skin friction before 1954 was a rather involved process except perhaps in pipes or channels owing to the rather cumbersome form of the Taylor relation. Preston [43] completely changed this with the introduction of his Pitot tube (Preston tube) and the correlation involving surface shear, and pressure difference in a non-dimensional form.

$$\frac{\tau_w d^2}{4\rho\nu^2} = F\left[\frac{\Delta p\, d^2}{4\rho\nu^2}\right] \qquad \ldots(2.01..4)$$

where F = 'function of'

This can be arranged in a Reynolds No. format.

$$\frac{1}{4}\left[\frac{u_\tau d}{\nu}\right]^2 = F\left[\frac{1}{8}\left(\frac{u_p d}{\nu}\right)^2\right] \qquad \ldots(2.01..5)$$

d = Preston tube outside diameter.

Which can be written in a more convenient log form as follows :-

$$x^* = \mathrm{Log}_{10}\left[\frac{1}{8}\left(\frac{u_p d}{\nu}\right)^2\right]$$

$$y^* = \mathrm{Log}_{10}\left[\frac{1}{4}\left(\frac{u_p d}{\nu}\right)^2\right] \qquad \ldots(2.01..6)$$

Preston's theory relies on the assumption that the velocity distribution in the wall region is common to boundary layers and pipe flow. Using the results of Laufer [38] for pipe flow and Klebanoff [37] for flat plates it is possible to show that Preston's assumptions about the 'inner law' are valid. Dutton [16] applied the boundary layer momentum equation to his investigation on surface Pitot tubes, and included terms to allow for turbulence; his experimental results substantially confirmed the accuracy of Preston's method. However experimental work by other writers appeared to contradict Preston's concept of a universal inner law for pipe and boundary layer flows.

Preston's work was finally proved, once and for all by the work of Head and Rechenberg [29], and at Liverpool by the work of Duffy [14] using a highly accurate Chattock gauge. In 1965 Patel [41] presented an extremely comprehensive calibration of the Preston tube which was in close agreement to Rechenberg's results.

In the meantime work on Stanton tubes had been progressing with Hool [32] in 1956 who first used sections of razor blades as surface friction sensors. Hool, like Fage and Falkner [22] and G.I.Taylor [50] calibrated his razor blades in laminar duct flow.

On the shape and theory for the Stanton tube, Gadd's [25] paper in 1958 presents a very useful step forward. He suggested that the precise geometry of the Stanton tube may not be important, in fact a solid step of the same height h as the tube would probably record the same pressure in the corner. Using the full Navier-Stokes equation an analysis was made assuming the flow past a solid step to be a Couette flow with a linear velocity profile; Gadd was thus able to predict the height of the undisturbed stream above a Stanton tube, and also the distance in front where the streamline divides.

Bradshaw and Gregory [6] in their paper of 1959 suggested that Stanton tubes which are calibrated in laminar duct flow, but subsequently used in turbulent flow may be liable to a 10% error. One further interesting feature should not be overlooked, and that is their definition of the various regions relating to the law of the wall.

(i) Linear Sub-Layer:- region where velocity profile is linear and

$$\frac{\delta u}{\delta y} = \frac{\tau_w}{\mu}$$

assuming no pressure gradient.

(ii) Viscous Sub-Layer:- is the region where turbulent shear stress is appreciable, but viscous shear stress predominates.

(iii) Universal Region:- in which the velocity profile is a unique function of skin friction for all turbulent flows.

(iv) Inner Law Region:- as with the universal region where the profile is a function of skin friction and independent of Reynolds No. for the flow considered.

The interpretation of these differing regions is bound to overlap at certain points, but their relevance to surface Pitot tubes is obviously important. One final result of Bradshaw and Gregory's paper is the significance of the geometrical limits ascribed to Stanton tubes so that they should function in the region of universality of turbulent velocity profile.

Smith, Gaudet and Winter [46] in 1962 extended the razor blade technique to supersonic flow in the transition range of Mach No., between 0.8 and 1.5. They also investigated the effect of yaw on the razor blades used; it appears that if u_p is the velocity

equivalent of the Stanton tube and the pressure difference Δp in the unyawed position, and Δp_β the pressure difference at an angle of yaw β, with velocity equivalent $u_{p\beta}$

then $$u_{p\beta} = u_p \cos\beta$$

hence $$\frac{\Delta p_\beta}{\Delta p} = \cos^2\beta \qquad \ldots(2.01..7)$$

The results they obtained clearly substantiate this, and indicate that a Stanton tube could possibly be used for three dimensional flow. Equation 2.01..7 suggests that if the maximum yaw is 15° (see sketch) then an error of 5% will occur in the skin friction result so obtained.

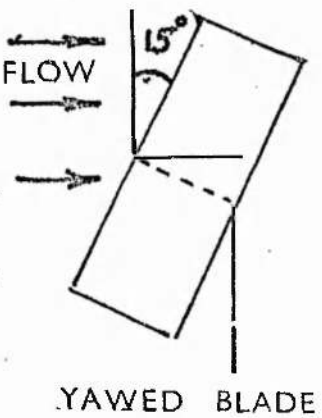

East [18] in 1966 carried out further tests in the R.A.E. (Bedford) low speed wind tunnel using razor blades; he first investigated the effect of altering Δx (the amount the pressure tap was covered - see sketch) and various other geometric parameters. It is important to remember that East took the razor blade height as half the razor blade thickness, asymmetric blades however were investigated as will be the case in the present work.

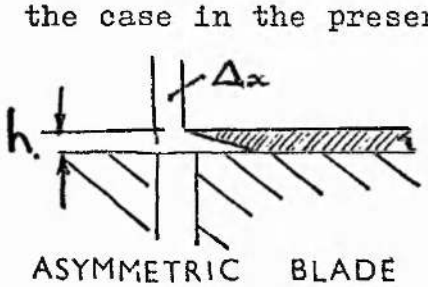

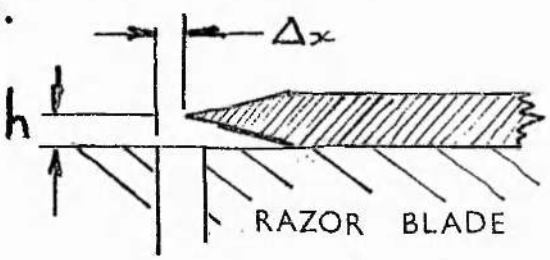

Holmes and Luxton [31] in 1967 used Preston tubes in the presence of heat transfer, and found that provided the fluid properties are evaluated at a suitable reference temperature, the constant property calibration curve of Preston may be used. Satisfactory results being obtained by using wall temperature as the reference temperature for fluid properties.

More recently Duffy and Norbury[15] in 1968 proposed dispensing altogether with the surface Pitot tube, and simply having two wall static holes of differing diameter to act as a skin friction sensor. Their results indicate that such a method is quite feasible, and agree to within 2% of those obtained with a conventional Preston tube, however the measurement of small pressure differences with a high degree of accuracy is still a difficulty.

Finally on the subject of surface Pitot tubes, and skin friction measurement Head and Ram[30] have recently presented a much simplified type of Preston tube calibration in which u_p/u is plotted against $Log_{10}(ud/\nu)$ for varying values of C_{fx}. This simplification greatly reduces the calculation time when using Preston tubes.

2.02 Turbulent Velocity Profiles - Smooth Plates

The paper of Preston, already discussed in para. 2.01 depends heavily on the law of the wall, and the universal form of the velocity distribution. The velocity distribution must therefore play a major role in the calculation of friction factor.

Clauser [9] in 1954 suggested a method of plotting all turbulent equilibrium velocity distributions on the same curve; by plotting $(u - U)/u_\tau$ against $(y/\delta^*)\sqrt{C_f/2}$ a universal curve is obtained which can also include rough surface results (see Fig. 21), however it is probably more convenient to use the more conventional form of von Karman and plot U^+ against y^+, that is u/u_τ against $\text{Log}_e(yu_\tau/\nu)$.

Clauser also extended the use of the law of the wall by plotting a family of curves on coordinates of u/U against yU/ν or R_y, each one being for a given value of U/u_τ or $\sqrt{2/C_f}$. This type of chart may be used for the experimental determination of skin friction, being usually called a Clauser chart, and is described further in Chapter 4.

Before proceeding further, it is advisable at this stage to clearly define the significance of the main sections of boundary layer laws. In the laminar sub-layer close to the wall, viscous forces predominate and

$$\frac{u}{u_\tau} = \frac{y\,u_\tau}{\nu} = y^+ \qquad \ldots(2.02..1)$$

Further out beyond the point where $y\,u_\tau/\nu = 30$ the graph takes the familiar straight line 'LOG-LAW' form, and this is often called the inner law or more frequently the law of the wall since it is the region that is still partly influenced by the wall and

$$U^+ = \frac{u}{u_\tau} = \frac{1}{K}\text{Log}_e\, y^+ + B \qquad \ldots(2.02..2)$$

At the edge of the boundary layer viscous forces are insignificant and the turbulent Reynolds stresses predominate, the law characterising this section is often called the defect or outer law and is dealt with later in more detail. Having clearly defined the meaning of these sections of the boundary layer it is now possible to continue, and discuss further some of the earlier developments in this section.

Laufer[38] whilst investigating turbulence levels, and spectral distributions with a hot wire anemometer confirmed the existence of the region of similarity, made use of by Preston, where turbulent and viscous stresses are both significant.

Klebanoff[37] employing similar methods to Laufer, but using a smooth flat plate tended to concentrate more on the outer, or defect law. His observations in the region where the outer law overlaps the inner law confirmed several of Laufer's results.

Dutton[17] also showed that where the law of the wall, and defect law overlap the boundary layer shape factor H can be expressed as a universal function of R_θ.

Brunello[8] whilst investigating forced convective heat transfer from rough surfaces obtained velocity profiles very similar to those of Clauser, for rough and smooth surfaces.

Bradshaw [3] in 1959 put forward a far simpler method of calculating skin friction, using an intersection method, rather than plotting a Clauser chart.

Rotta[45] showed that such a method as Clauser's, or Bradshaw's was far more suitable in practice than the von Karman momentum integral equation which was rather susceptible to errors particularly in a rising pressure gradient, or if the flow, was not two dimensional.

Head[28] whilst considering the concept of entrainment in turbulent boundary layers suggested that the velocity distribution in the outer layer or 'wake' can be assessed by means of form parameters such as H, as Dutton had previously suggested. The amount of fluid entrained by the boundary layer per unit time is given by

$$\frac{dQ}{dx} = \frac{d}{dx}\left[U \quad (\delta - \delta^{**}) \right] \qquad \ldots(2.02..3)$$

Jayatillaka[35] used a universal relation of the type

$$U^{+} = \frac{1}{K} \; \mathrm{Log}_e \; (E', y^{+}) \qquad \ldots(2.02..4$$

for rudimentary Couette flow, where E' is a parameter into which the sub-layer effects are put.

The recent work of Huffman and Bradshaw[33] on the constant used in the von Karman law of the wall equation (2.02..2) suggests that K may vary by as much as 3% at low Reynolds number. The viscous sub-layer apparently is more sensitive to external influence than the fully turbulent section. For small distances from the wall the Prandtl hypothesis is valid $\lambda = K.y$ ...(2.02..5)

where λ = Prandtl mixing length.

K is usually considered to be 0.4.

2.03 Turbulent Flow - Rough Plates

When considering the flow past rough surfaces, obviously the first name to be considered is that of Nikuradse [40] whose classical paper in 1933 formed the foundation for this subject. Nikuradse used tightly-packed sand grains of fixed size glued to the inside of pipes, and took K_s/r as the main roughness parameter, which is called the relative roughness. The sand particle size, as defined by Nikuradse was obtained by using sieves of varying aperture size so as to produce graded grains of differing size K_s. In the case of boundary layer flows the relative roughness is defined in terms of the distance from the wall i.e. y/K_s . It naturally follows that the 'log law' for velocity distribution must include relative roughness and take the form

$$U^+ = 2.5 \text{ Log}_e (y/K_s) + F_r \qquad \ldots(2.03..1)$$

where F_r = Nikuradse roughness function which depends on the nature of the roughness.

Prandtl and Schlichting [44] in 1934 extended Nikuradse's work on rough pipes to include both smooth and rough surfaces on plates. The results were calculated using the above logarithmic velocity distribution.

In 1935 Streeter [47] carried out experiments using artificially roughened pipes. Various regular roughness shapes and spacings were employed, and close agreement with Nikuradse's work was obtained. Two interesting points emerge, the first being that roughness elements can be placed too close together so that the effective frictional resistance is reduced. Secondly, the shape of the roughness element appeared to have almost as much effect on pressure drop as its size.

Goldstein [26] suggested that for roughness to have a significant effect, the height of roughness elements K must protrude through the sub-layer. All roughness falling below the sub-layer would be considered as hydraulically smooth. The value δ_L of the thickness of the sub-layer was calculated by Goldstein from the criterion that a von Karman vortex street is about to form on an individual protrusion; he obtained $\delta_L = 5\nu/u_\tau$ ...(2.03..2) which is the limit of the range in which the laminar velocity distribution law is valid for the sub-layer.

The transition region in between completely smooth, and rough pipe laws was investigated by Colebrook [10] in 1939 who developed the following transition law for the section of the Nikuradse curve falling between the hydraulically smooth, and the fully rough.

$$\frac{1}{\sqrt{f}} = -2 \text{ Log } \frac{K}{3.7d} + \frac{2.51}{R\sqrt{f}} \qquad \ldots(2.03..3)$$

One of the earliest workers to consider using artificially roughened pipes for heat transfer was Cope[11] who used a knurling device to roughen the inside of the pipes; his work was mainly concerned with heat transfer, but one fact emerges relevant to this discussion, that is that the ratio of K_s to K was found to be about 2 whereas earlier workers had obtained much higher figures. Cope also suggested that form drag might also affect results, particularly where roughness elements are quite large. Cope utilised the Colebrook roughness function.

Following the war, Dryden [13] in 1953 wrote a paper giving a survey of literature on the effect of using a single roughness element as a turbulence promoter.

Dryden was concerned with causing transition to occur prematurely on a flat plate by the use of a cylindrical wire placed perpendicularly to the stream at a distance x_k from the leading edge. Distributed roughness can also stimulate transition much earlier, reference is made to the use of emery and glass paper, and it is noted by Dryden that the paper thickness y_t must be included in the asperity height K .

At the same time as Dryden's paper was published Arni and Myers [2] presented a paper to the American Society of Refrigeration Engineers regarding pressure drop and heat transfer effects on internally integral finned tubes. It was concluded that a greater number of fins per inch reduced the value of C_f to almost the smooth pipe values, whereas 7 fins/inch increased C_f to a value 10% greater than that for a plain tube. This paper again stresses the importance of roughness spacing on friction. No mention was made of the relationship between K_s and K however.

Brunello [8] whilst studying heat transfer cn rough surfaces carried out extensive work on the hydrodynamic effect of rough surfaces on boundary layer growth. He used three different rough plates, and obtained excellent agreement with Nikuradse and others. The displacement of velocity profiles, and the shift of the momentum thickness θ when plotted against Reynolds number were reported.

Brun and Plum [7] carried out further tests on the basis of Brunello's work, using a uniformly distributed rough plate, formed by a printing technique. They obtained close agreement to Clauser on the basis of the defect-velocity profile; in fact both the smooth and rough plate results fell on the same curve.

Rotta [45] (in his work on page 75) refers to the fact that some skin friction at a rough surface is due to form drag, whereas the rest consists of viscous effects. In the case of a flat plate covered with uniform roughness elements there exists a layer of constant shear stress adjacent to the wall where viscous forces and the scale of roughness are of paramount importance. If in fact dynamical similarity is considered

$$u = u_\tau \phi\left[\frac{y\, u_\tau}{\nu} \quad , \quad \frac{K_s\, u_\tau}{\nu}\right]$$

The effect of roughness is only effective near the wall hence $u = u_\tau\left[\frac{1}{K} \mathrm{Log}_e\left(\frac{y\, u_\tau}{\nu}\right) + C\left(\frac{K_s\, u_\tau}{\nu}\right)\right]$...(2.03..4)

Rotta also refers to the shift of the universal velocity distribution, and the value of the constant F_r in equation 2.03..1.

Dipprey and Sabersky [12] in their valuable paper on heat and momentum transfer showed that the function F_r bears a direct relationship to the roughness Reynolds number R_r.

Tewfik's [51] (49) results indicate that roughness has a more pronounced effect nearer the front of a flat plate, and that this decreases as x increases. Tewfik used rough cylinders roughened on the outside mounted in a low speed wind tunnel. The results obtained are comparable with flat plate results, and excellent correlation with the Prandtl-Schlichting relation was obtained.

Jayatillaka's paper has already been referred to, but it is now important to consider his work on rough surfaces. Jayatillaka classified roughness under two headings (i) irregular i.e. sand grain - natural roughness etc., and (ii) regular - knurling threads etc., Defining the law of the wall as

$$U^+ = \frac{1}{K} \text{Log}_e \ (G.\ y^+) \qquad \ldots(2.03..5)$$

where G is a constant, then Jayatillaka analysed the relationship between G and the roughness Reynolds number R_r for a variety of roughness types, and the following facts emerged:-

(i) In the case of distributed roughness two further geometrical parameters are needed to account for lateral and longitudinal spacing.

(ii) A statistical method based on sand grain size produces a useful curve to fit the transition portion of Nikuradse curve.

(iii) In general, roughness of the same basic type will have the same 'fully rough' characteristic.

The effect of surface roughness on steam turbine blades was investigated by Forster[24] who carried out extensive work using emery paper of various grades. Forster was able to correlate CLA roughness values with K_s, and also the makers size of grit, and showed that $K_s = 1.5\ K$ was a satisfactory guide to the roughness scale.

Finally in 1972 Antonia and Luxton [1], whilst investigating the effect of a step change from a rough surface to a smooth surface showed that the value of the constant B in the law of the wall equation (2.02..2) increased considerably at a point downstream over the comparable smooth law value. The value of the constant K in this equation also appeared to vary slightly.

2.04 The Effect of Turbulence

Fage [21] used a hot wire anemometer to determine how free stream turbulence affected transition from laminar to turbulent flow; the signal from the hot wire being displayed on an oscilloscope. It was found that an increase in turbulence caused a later transition, that is one further from the leading edge. The free stream turbulence was of the order

$$\frac{\sqrt{(\overline{u'^2})}}{U} = 0.0018.$$

Fage undoubtedly pioneered this work on transition, and later collaborated with Preston on a statistical approach to turbulence.

Laufer [38] presents, in his paper on the structure of turbulence a valuable comprehensive work on turbulence in pipe flows. He showed that the turbulent energy rates reach a sharp maximum near the edge of the laminar sub-layer. The spectrum measurements taken are relative to pipe flows so have not a great bearing on the present investigation.

Klebanoff's paper is more concerned with the outer section of the boundary layer but agreement is reached with Laufer on the overlapping sections.

Bradshaw [5] presents an up-to-date view on turbulence; experiments with three boundary layers show several unifying features regarding turbulence intensity and spectrum analysis.

CHAPTER 3 APPARATUS

The apparatus consisted of essentially an open-circuit wind tunnel, for use with the various rough surfaces, together with hot wire anemometer measuring equipment. General views of the apparatus are shown in figures 1 to 7.

3.01 Wind Tunnel

The wind tunnel used in this investigation was a low-speed open-circuit type (see Figs. 1. 2A, &2B). The air entered the wind tunnel through a bell-mouthed inlet 64" (2.5m) square fitted with a fine nylon mesh wind tunnel screen; the air being drawn through the wind tunnel by a fan at the discharge end. The nylon screen was fitted to improve the stability, but mainly to prevent the ingress of dust particles and grit which could damage the hot wire anemometer probes.

The wind tunnel had a ratio of convergence of 4, and after the bell-mouthed inlet there followed a straight section 16" (41cms) square by 39" (1 metre) long during which the air could stabilise itself prior to entering the test-section.

The test-section was 16" (41cms) square and 47" (1.2m) in length. Access to the test-section was available on all sides. The Sindanyo frame with the brass plates (para. 3.02) was mounted in a vertical plane affixed to the centre of the floor plate of the test-section. Perspex side-panels were used to facilitate easy viewing, one of them being supplied with a static-pressure tapping for calibrating the wind tunnel (para.4.01). If desired the traversing equipment (para.3.05) could be used in place of the standard perspex window.

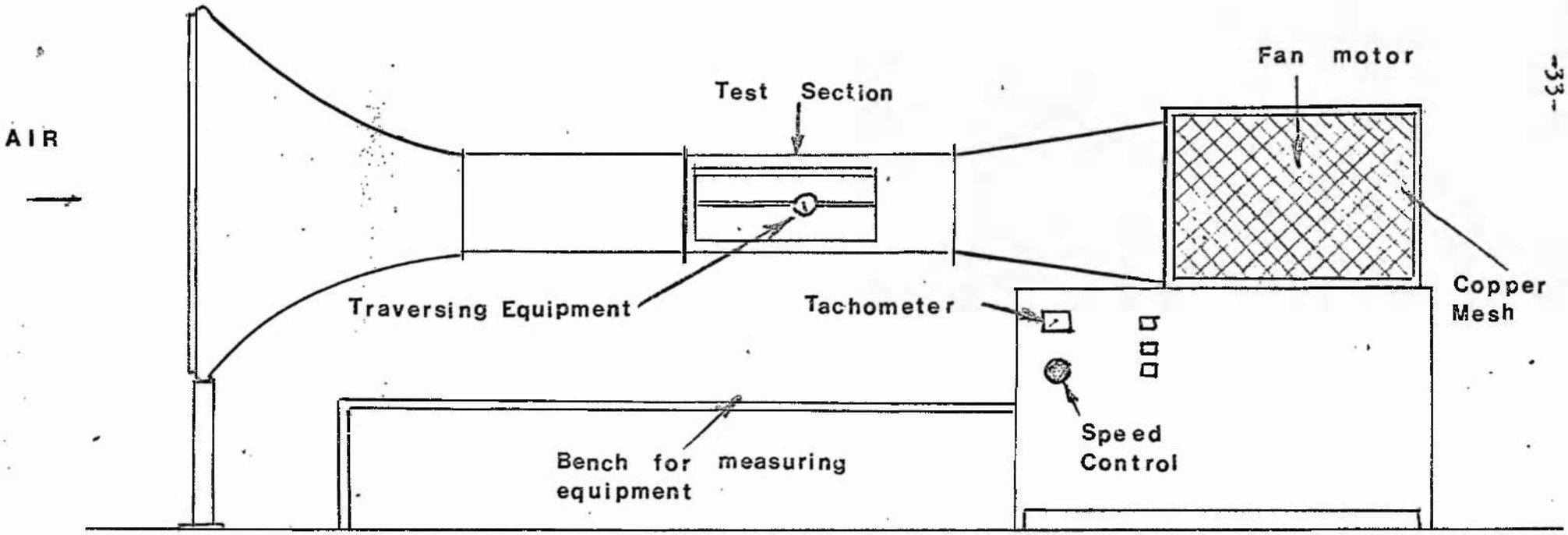

FIG 1A GENERAL VIEW OF WIND TUNNEL

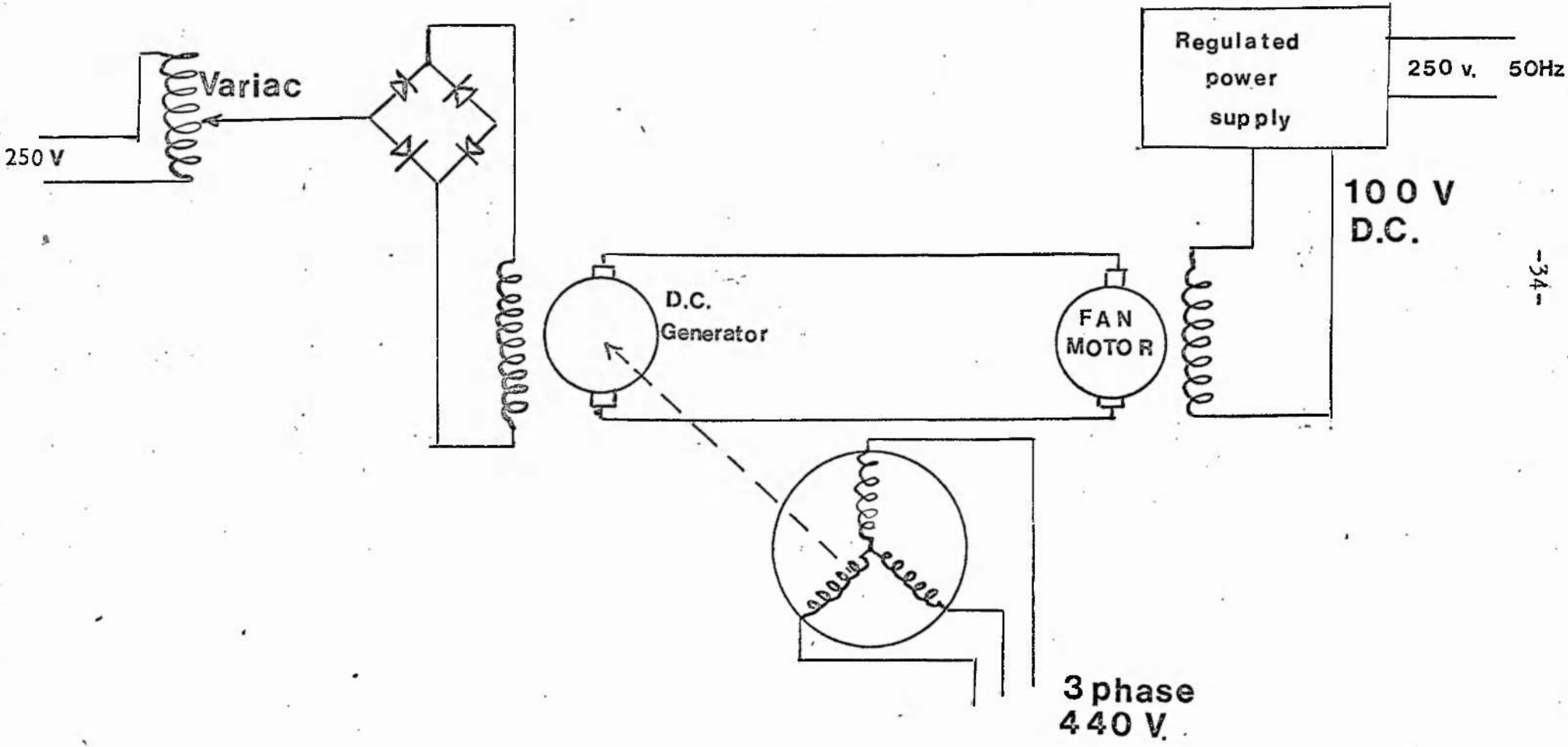

FIG 1B. CIRCUIT DIAGRAM OF WIND TUNNEL

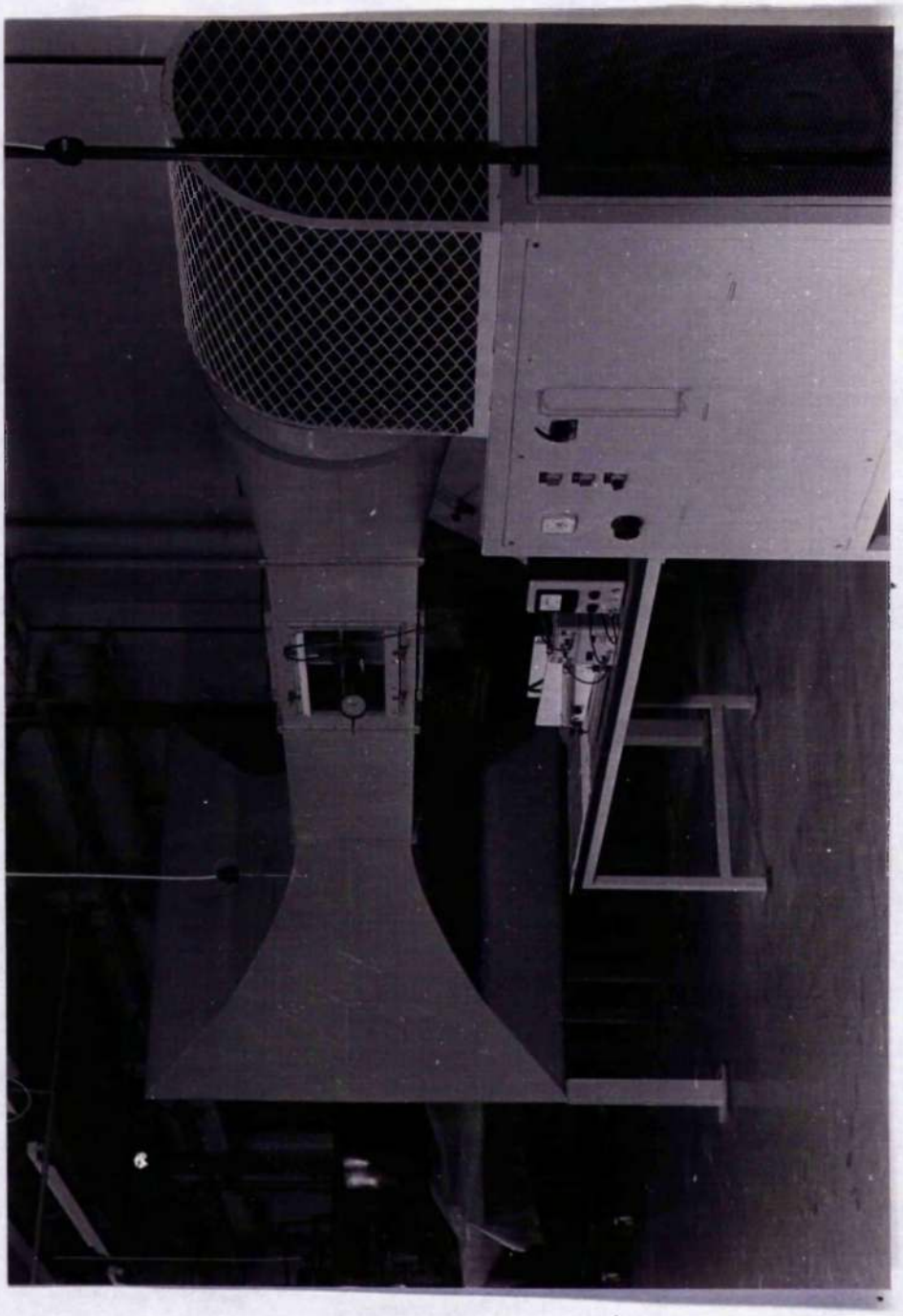

FIG 2A. VIEW FROM FAN MOTOR END.

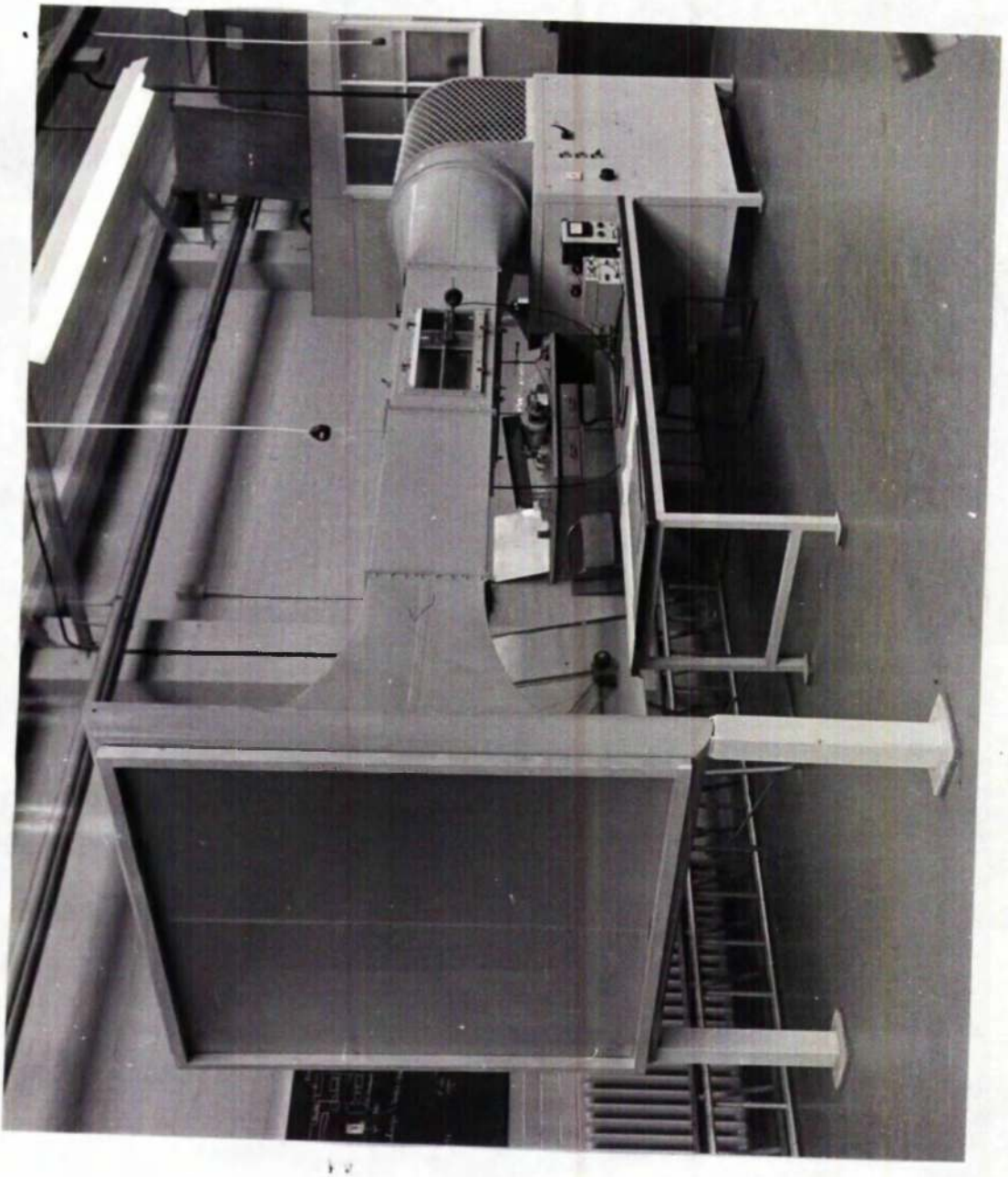

FIG 2B. VIEW FROM SCREEN END

The top of the test section was constructed with a perspex window to allow better viewing conditions, and also contained several holes placed at necessary points for the insertion of Pitot-static tubes. Following the test-section the air passed through a honeycomb, and then through a divergent portion in order to reduce the velocity.

A four-bladed fan driven by a 110v DC motor was located at the tunnel exit. The circuit diagram used for the variable-speed drive is shown in Figure 1A. A three-phase motor was used to drive a 110v generator. The excitation for which came from a rectified 240v supply fitted with a Variac. The Variac thus supplied a variable A.C. voltage which was subsequently passed to a full wave rectifier, prior to exciting the field. The armature of the DC generator was coupled directly to the armature of the DC fan motor. The excitation for the fan motor coming from a separate, stabilised DC supply.

The fan speed was infinitely variable between 0-1900 rev/min by adjusting the Variac control situated on the front panel (see Fig.2A). The speed being indicated by a tachometer also mounted on the front panel. The advantage of this system is the excellent stability of the fan motor once it has been set. The air was finally discharged through a copper mesh which completely shrouded the fan motor.

3.02 Sindanyo Frame

The frame for mounting the brass plates to be tested, was fixed in a vertical plane in the centre of the test section. The frame, which exactly divided the test section in half, was mounted on the lower removable side panel by aluminium angles; the top being located with pegs to the top panel.

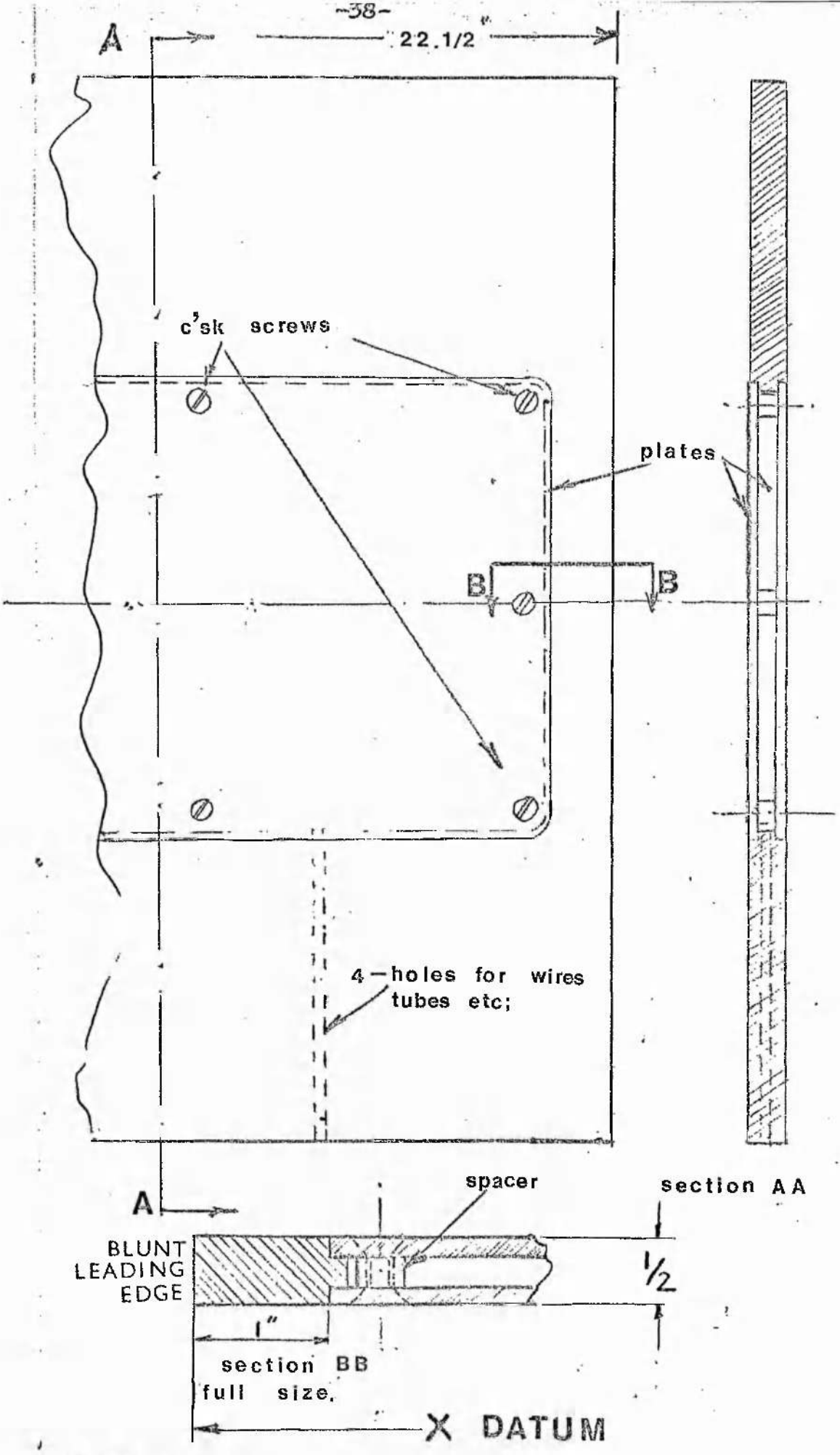

FIG 3A SINDANYO FRAME ASSEMBLY

(1/2 FULL SIZE)

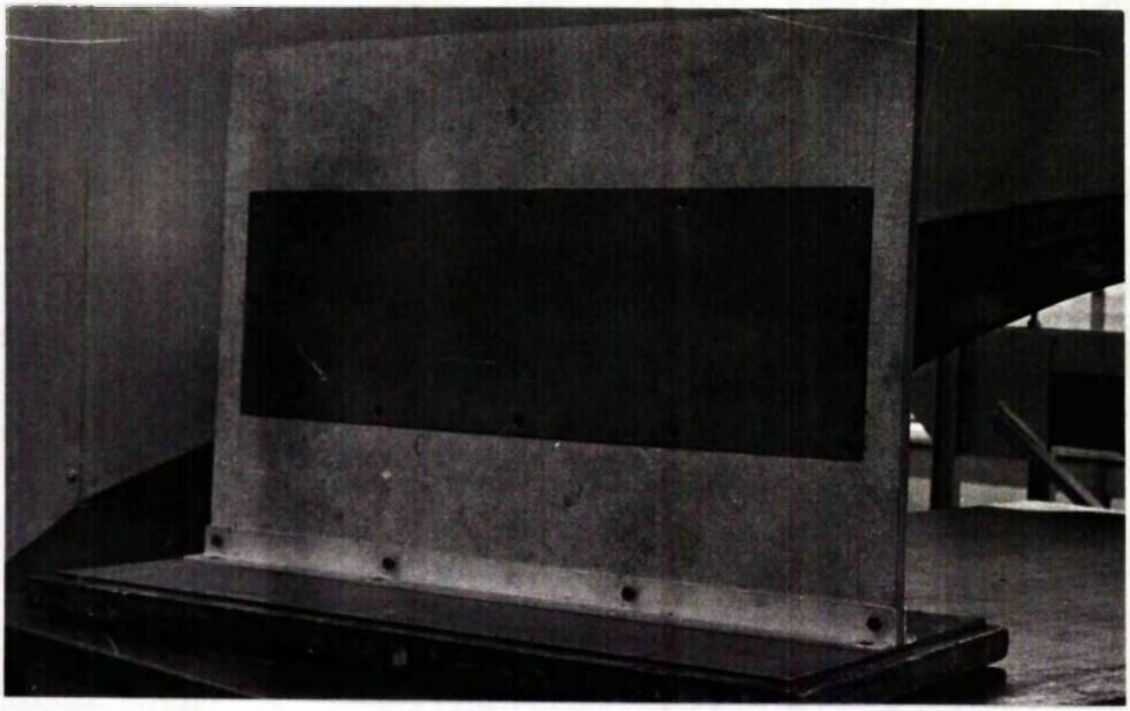

FIG 3B LEADING EDGE OF SINDANYO FRAME

The original intention was to carry out heat transfer tests with the brass plates, and it was for this reason that Sindanyo was selected for mounting the plates. Provision was made for a heating element to be installed between the two plates, which are separated by a 1/4 inch (6½mm) gap (see Figs. 3A & 3B). Small spacers, 2 BA threaded holes, were used to hold the plates in position; countersunk 2 BA screws being employed to fix the spacer to the plate. Care being taken to ensure that the screw heads did not project above the working surface of the plate. The plate itself was recessed into the Sindanyo frame so as to present a level surface to the air flow(see Fig. 3).

The necessary pressure connections from the surface of the brass plates down to the inclined manometer, situated on the bench below were made through holes drilled up through the thickness of the Sindanyo into the heating element cavity.

3.03 Brass Plates

The brass plates used for this investigation were fixed to each other with twelve spacers, as mentioned in Para. 3.02, the thickness of each plate being 0.125 inch (3.2mm).

The plates were finished to a nominal surface finish of between 5-10 μ ins. The length of each plate was 20.5 ins. (0.52m) and the height 7 ins. (178mm). All measurements taken with the hot wire equipment, and the surface tubes were taken on one side of the Sindanyo frame, and on a horizontal line equidistant from the sides of the plate. This was done so as to reduce to a minimum any possible side effects where the plate and the Sindanyo surfaces meet.

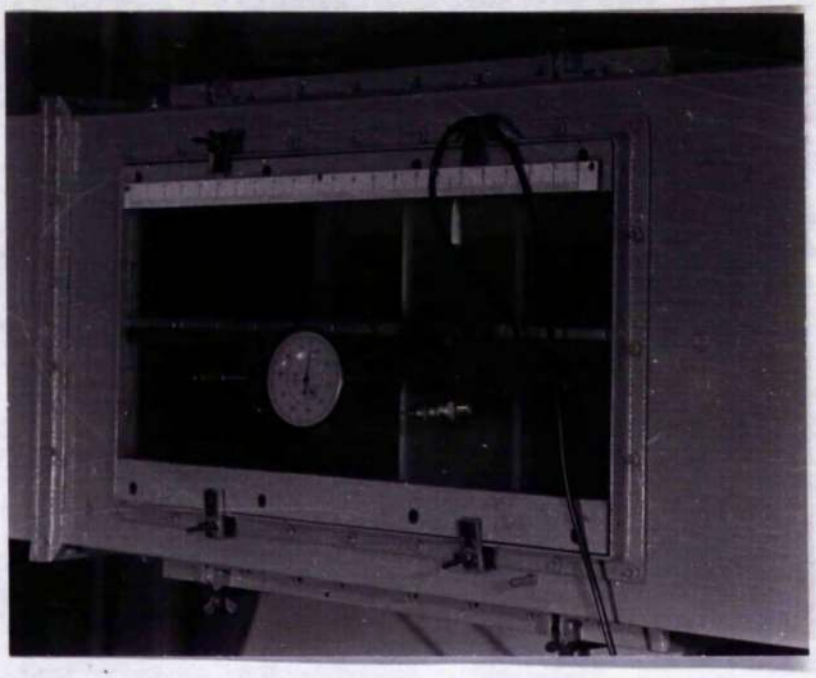

FIG 4A TRAVERSING EQUIPMENT

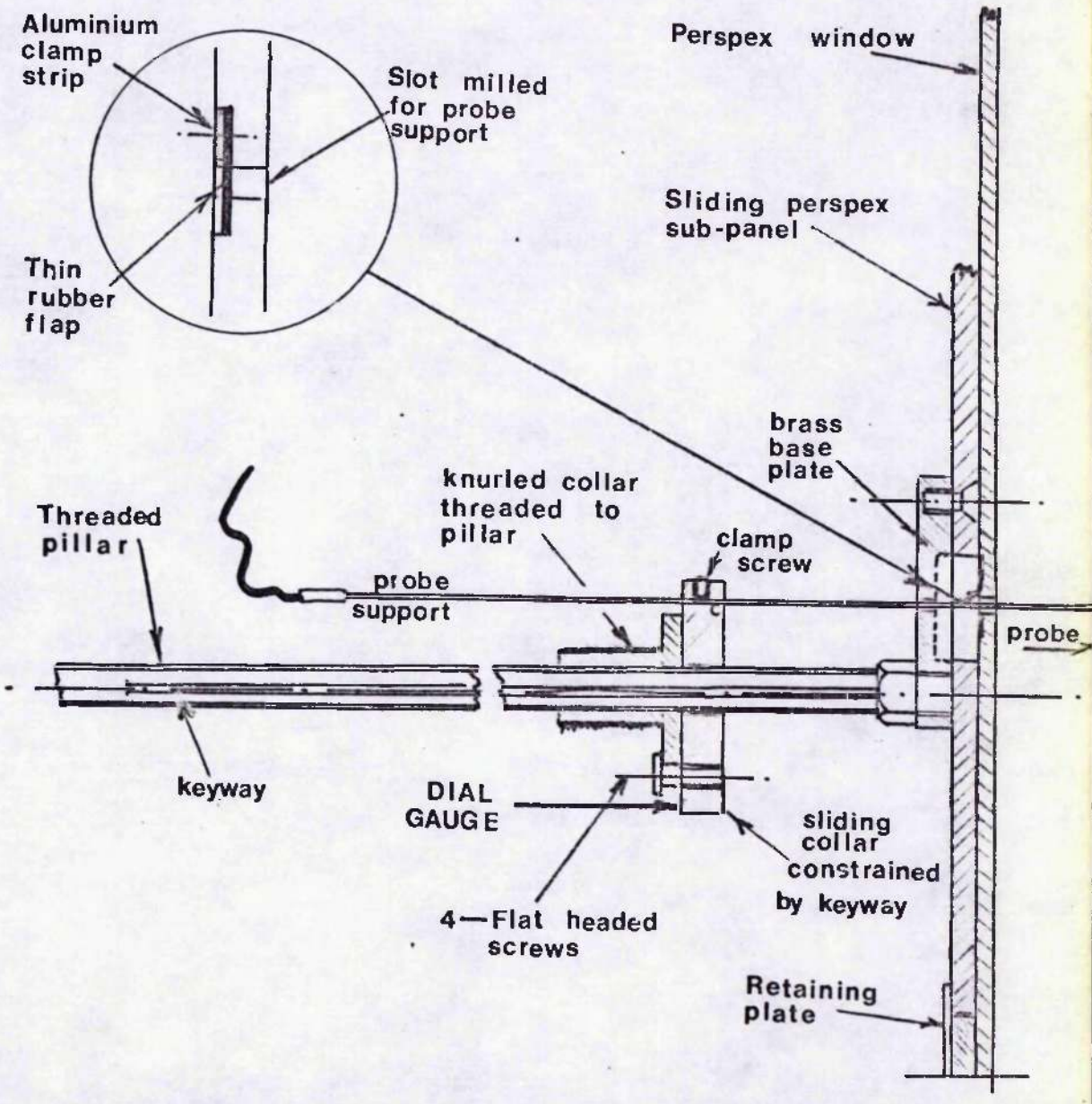

FIG 4B – SECTION OF TRAVERSING EQUIPMENT

'B' SURFACE X (5) CLA 210 μ ins

'C' SURFACE X (5) CLA 250 μ ins

FIG 5A SAND BLASTED BRASS PLATES

For the low, and intermediate roughnesses, sand-blasting of the brass plates to different degrees was used. The full particulars being given in para. 4.09 and para. 6.04. For the fully-rough surfaces it was not possible to sand-blast to a higher degree as bowing took place so consequently emery and glass paper strips were glued to each plate.

3.04 Hot Wire Equipment

The measurement of friction factor, for calibrating the plates for the surface Pitot tubes together with all the measurements on turbulence etc., were made using a hot wire anemometer.

The probes used throughout this investigation were of the right-angle-support variety manufactured by D.I.S.A. With this type of probe it was possible to traverse quite close towards the brass plate. The long probe-support was used which enabled velocity profiles to be obtained over a range of y = 0.020 in. to y = 1.8 ins. (o.5mm to 45mm).

Five metres of probe cable were used to connect the probe to a 55 D05 Battery operated Constant Temperature Anemometer made by D.I.S.A. The anemometer operated on a Wheatstone-bridge principle. and so as to compensate for different probe resistance, and cable length the bridge resistance could be varied between 2.4 to 13 ohms. An additional external resistance of up to 50 ohms could be used if required.

The main switch had three positions 'Off' 'Adj' and 'Operate'. With the probe connected to the probe socket the switch was turned first to 'adjust', and the bias was adjusted so as to bring the meter to the balance position. Subsequently the switch was then turned to 'operate' and the probe was then ready for use.

GRADE 100 X (5) K = 0·006 ins

ALUMINIUM OXIDE CLA 600μ ins

GLASS PAPER X (5) GRADE 36 K = 0·017 ins

FIG 5B ABRASIVE PAPER SURFACES

The anemometer's frequency response, when operating at the 10:1 bridge ratio is very dependent on accurate coil adjustment. This was achieved by using a square wave generator and tuning according to the maker's instructions.

The output from the anemometer was normally connected to D.I.S.A. type 55D30 Digital DC voltmeter, and also to a RMS voltmeter. Occasionally a storage oscilloscope was used for studying turbulence patterns.

The probe wire was always in the vertical position facing the air stream. So that accurate measurements could be made of y on the traversing equipment (Para.3.05) the length of the probe, from the wire to the shoulder of the probe (see Fig.7) was measured using a travelling microscope.

3.05 Traversing Equipment

The traversing equipment used for these tests was specially designed so that velocity profiles could be obtained at numerous positions along the plate axis. It was possible to obtain either an orthodox traverse in the y direction out from the plate, or to traverse in the x direction along the length of the plate at a constant value of y. Fig. 4A, and 4B shows a general view of this equipment.

(a) y - Traverse

The y-direction traversing equipment consisted of a circular brass base 3 ins. (75mm) diameter by 5/8 in. (16mm) thick mounted on the sliding perspex panel. Rigidly fixed to this base, and offset from the centre was a 6 ins.(150mm) long by a 5/8 in. (16mm) diameter pillar, threaded down its length with a 0.050 in. (2mm) pitch thread. A keyway 0.125 in. (3.1mm) wide was also milled along the length of the pillar.

A collar was fitted onto the pillar so that it could slide freely, but was constrained from rotating by a pin engaged in the keyway. This collar also formed the mounting for the probe support, which was clamped to it, and penetrated through a hole in the brass plate ultimately into the working section of the wind tunnel.

A knurled threaded nut, screwed to the pillar, and connected to the collar provided the necessary movement to the collar. The connection between the collar, and the nut was formed by four flat-headed screws fitting over a lip on the knurled nut.

A 0-2 ins. (50mm) dial gauge clamped to the pillar, and pressing on the collar recorded the movement of the probe support. Any unwanted back-lash between the collar and nut was overcome by a compression spring fitted internally between them. The maximum amount of free movement never exceeded 0.002 in.

(b) x - Traverse

The main perspex panel had a slot formed down the centre through which the probe support could slide. This slot was covered by a thin rubber flap, and held in place by the air pressure except where the probe penetrated. A smaller sub-panel, used for mounting the y traverse apparatus, was able to move on the main perspex side panel by means of slides at the top and bottom. A scale on the top slide indicated the distance x from the leading edge of the Sindanyo frame.

3.06 Stanton Tubes

One of the main reasons for developing a surface Pitot-tube of the Stanton type was its ease in fitting to a given surface. Bradshaw and Gregory[6] state that the Stanton tube, and hot wire methods involve the least restrictive assumptions and are probably the easiest to apply for obtaining friction factor.

Initially it was decided to use actual razor blades, but grinding them down to produce an asymmetric knife edge resulted in the internal stresses being relieved with consequent bowing.

Laminated shim steel therefore was chosen, as layers 0.002 in. (0.05mm) thick could be peeled off to reduce the effective thickness. Originally the ground edge was placed uppermost in the air stream, but subsequently it was decided to have the ground edge facing downwards in order to reduce the separation points (see Fig. 6), and to comply with the theory presented by earlier workers. Para. 4.08 gives further details of Stanton tube geometry.

The fixing of the Stanton tube to the brass plates was carried out using either double-sided cellulose tape, or rubber latex adhesive. The important fact was to have a method that was quick to apply, and gave consistent thickness results.

The final configuration (Fig. 6) shows the manometer hole just underneath the knife edge, and the static pressure hole in the same vertical line, but about 1.5 ins.(38mm) below . For spanwise velocity variation refer to Para.4.04.

A height gauge fitted with a dial gauge was used to measure the Stanton tube height 'h' above the brass plate.

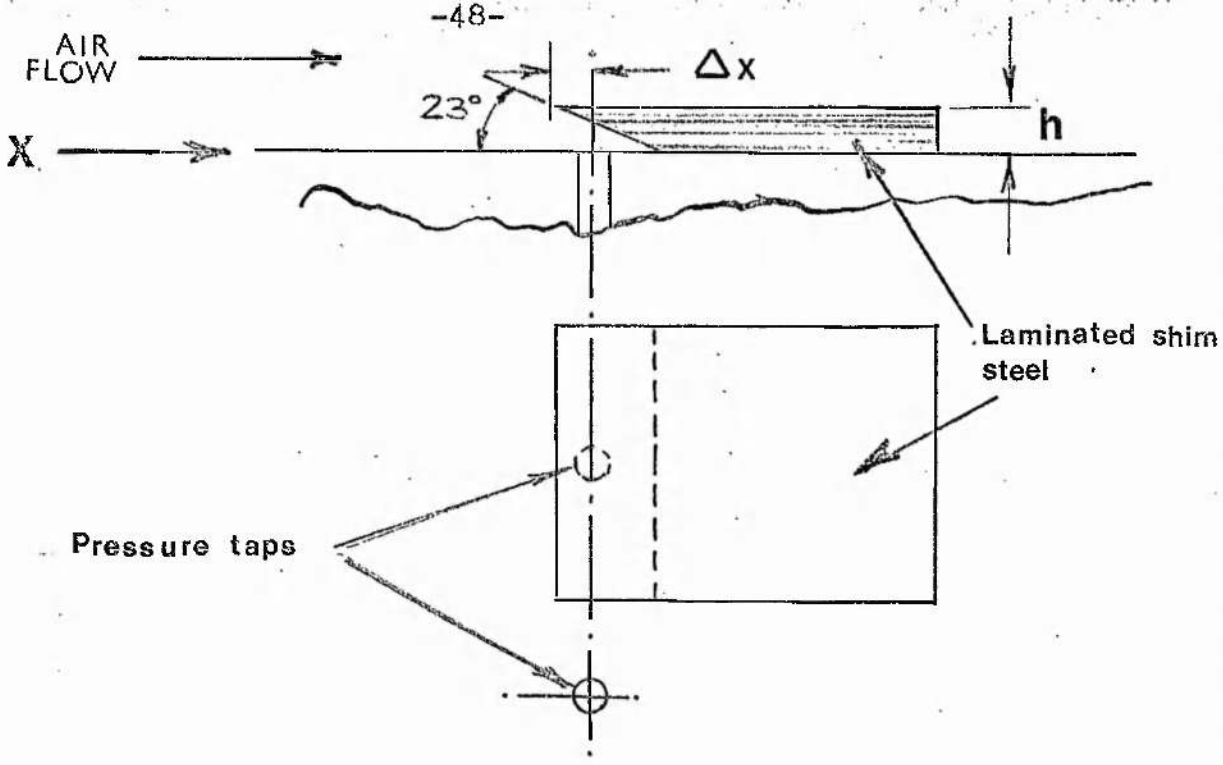

FIG 6 – DIAGRAM OF SURFACE PITOT TUBE (STANTON TUBE)

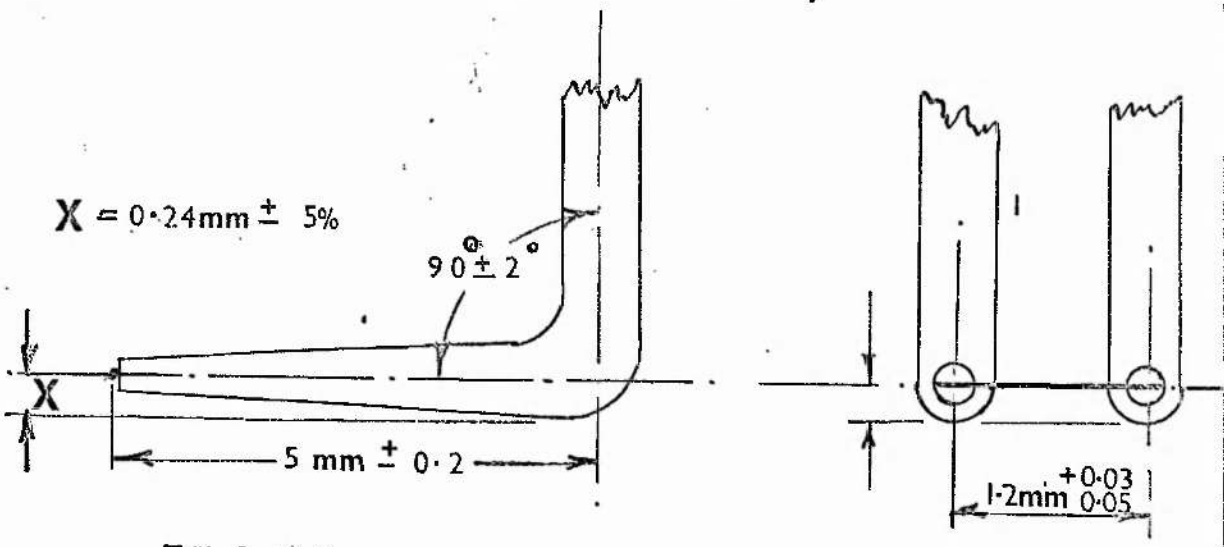

55 A 86 probe tip dimensions by courtesy of D.I.S.A.

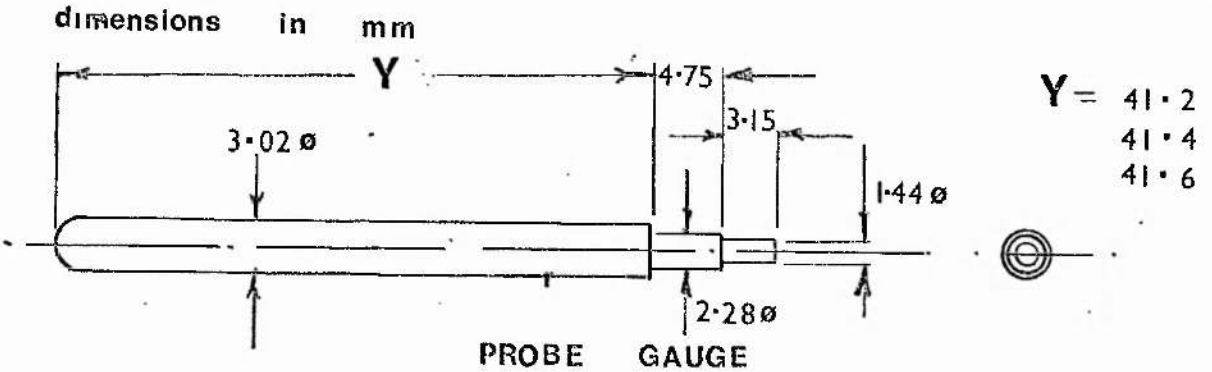

FIG 7 DIAGRAM OF PROBE TIP and PROBE GAUGE

CHAPTER 4 PRELIMINARY EXPERIMENTS & GENERAL ANALYTICAL PROCEDURES

Before any viable hot wire, or Stanton tube readings could be taken various preliminary tests were necessary to ensure the accuracy and reliability of the results obtained. These preliminary tests and calibrations are discussed in paragraphs 4.01 to 4.06, and their importance emphasised.

The principal measurements taken, the techniques adopted, and the procedure for processing these readings using different computer programs are dealt with in paragraphs 4.07 to 4.10, and can also be seen in Fig.10. In addition a mathematical analysis is presented linking the law of the wall with roughness.

Paragraphs 4.11 and 4.12 deal mainly with methods for validating the results obtained, and checking the findings with those of other workers.

4.01 Calibration of the Wind Tunnel

In order to eliminate the need for continually having a Pitot-static tube penetrating into the test-section, the wind tunnel was frequently calibrated as follows.

A Pitot-static tube was mounted in the tunnel at the mid-height position facing the air flow through a suitable hole in the top panel, such that the nose of the Pitot-static tube was 14.7 ins. (390mm) from the leading edge; care being taken to ensure that the nose of the Pitot-static tube was well outside the boundary layer of the plate, and at least 2 ins. (50mm) from it in the free stream. (i.e. $x = 14.7$ ins., and $y > 2$ ins.)

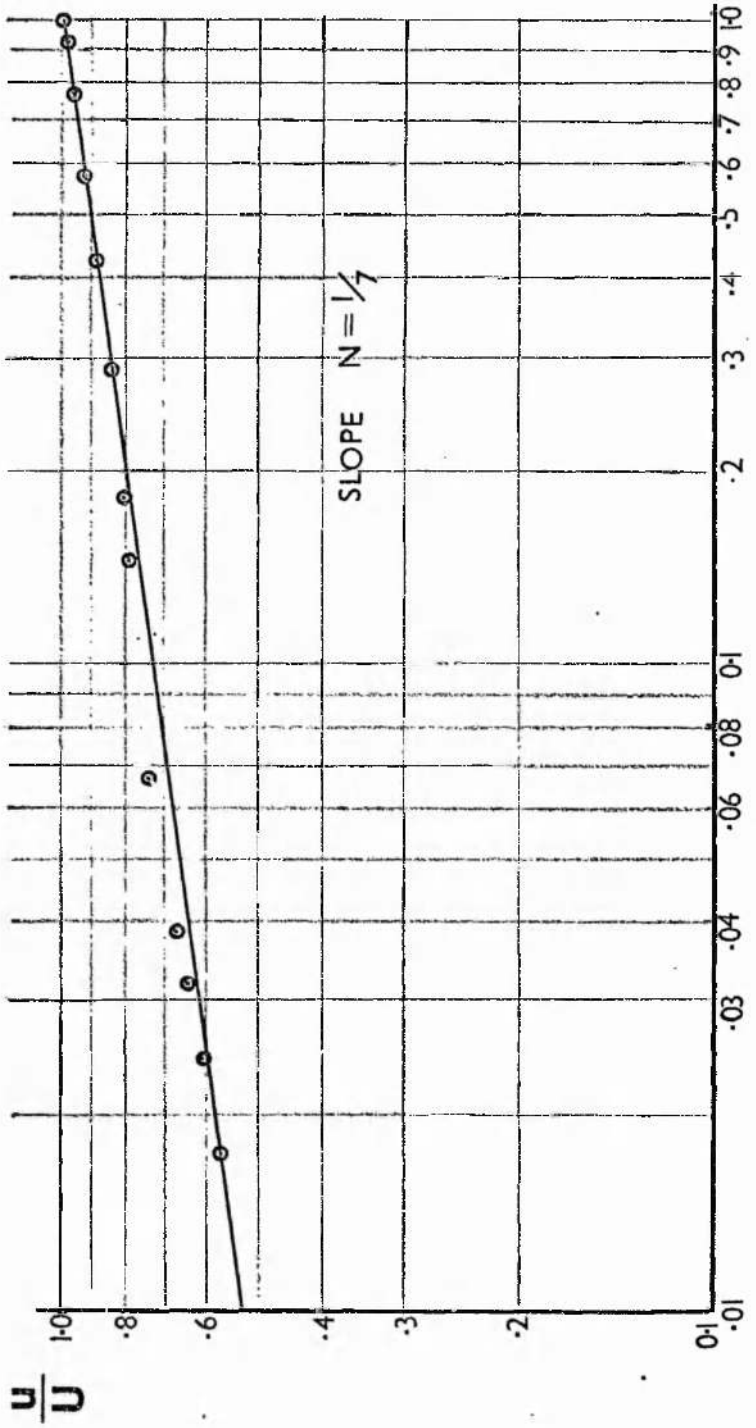

FIG 8 LOG PLOT OF VELOCITY PROFILE

A static pressure tapping was provided on the side perspex panel, and this was connected to an inclined manometer. Both the kinetic, and static heads were measured on inclined manometers manufactured by 'Airflow Developments'.

Before a major series of tests, the wind tunnel was always calibrated, as dust on the wind tunnel screen appeared to slightly modify the calibration. A typical calibration graph is shown in Appendix 1.(Fig. A1., page 142)

4.02 Test for Zero Pressure Gradient

The purpose of this check is to investigate whether the mainstream velocity U is constant along the plate axis. A lot of boundary layer theory deals with flows where zero pressure gradients predominate. In fact the law of the wall equation

$$u^+ = \frac{1}{K} \text{Log}_e\, y^+ + B \qquad \ldots(2.02..2)$$

is based on the assumption of constant mainstream velocity.

From von Karman's momentum integral equation for flat plates at zero incidence in incompressible flow.

$$\frac{d\theta}{dx} = \frac{\tau_w}{\rho U^2} - \frac{\theta}{U}\left[H+2\right]\frac{dU}{dx} \qquad \ldots(4.02..1)$$

obviously if there is zero pressure gradient then dU/dx = 0,and the mainstream velocity is constant, the above simplifies to $\frac{d\theta}{dx} = \frac{\tau}{\rho U^2} = \frac{C_{fx}}{2}$

from which expression relationships can be derived for obtaining C_{fx}. Realising the importance of these relationships, and the need for zero pressure gradient on

skin friction calculations, two investigations were made to verify this condition.

A Pitot-static tube was inserted through the top panel at several positions along the length of the plate and always at 2 ins. (50mm) from it to check if there was any axial velocity variation. The maximum kinetic head variation was found to be less than 0.5%. As a further test the hot wire probe was traversed in the x direction well away from the wall at y =1.60 ins. (40mm) the variation in bridge voltage only being 1.515 to 1.512. It was therefore concluded that zero pressure gradient existed along the plate, and U was constant.

4.03 Velocity Profile - 1/7th Power Law

To satisfy the condition that the flow was turbulent, the velocity profile marked with an asterisk in Table 1 (1100 Rev/min.U = 40ft/s) was plotted in the form $\text{Log}_e(u/U)$ vs $\text{Log}_e(y/\delta)$. Fig.8 indicates that the points conform to the 1/7th Power Law.

4.04 Spanwise Variations on Nominal Two-Dimensional Flow

To verify that the boundary layer existing along the plate was two-dimensional, and to satisfy that no side effects were apparent from the Sindanyo frame a spanwise investigation was performed. Bradshaw [4] refers in his paper to the effect of wind tunnel screens on spatial stability and claims that variations of as much as 10% in friction factor may occur when the open area ratio is less than 0.57.

Whilst all the readings in this investigation were made on the centre line, it was felt none the less important to check for spanwise variations. East [19] more recently, has subsequently confirmed Bradshaw's work and extended it.

This investigation was carried out as follows, two static-pressure holes were drilled in the smooth brass plate. One hole was placed on the centre line at a distance of 14.8 ins. (376 mm) from the leading edge; the other hole 2 ins. (50mm) below it. It was essential to ensure that the pressure-taps did not protrude above the surface of the brass plate as this could cause reduction in static-pressure (Ref. 52). Connections were made between the static holes and a standard inclined manometer fitted on the 0 to 0.5 in. water gauge range.

The wind tunnel was operated at six different flow rates, and the pressure difference in each case noted. In the majority of cases the difference in pressure was constant at 0.001 in. water gauge ($0.25\ N/m^2$) ; the maximum difference encountered at the maximum flow rate was 0.005 in. water gauge ($1.25\ N/m^2$). In view of these small pressure differences it was concluded that the boundary layer was nominally two-dimensional.

4.05 Kinematic Viscosity

To avoid continually referring to tables for accurate values of kinematic viscosity ν, as atmospheric conditions varied, it was decided to use Sutherland's formula for dynamic viscosity μ.

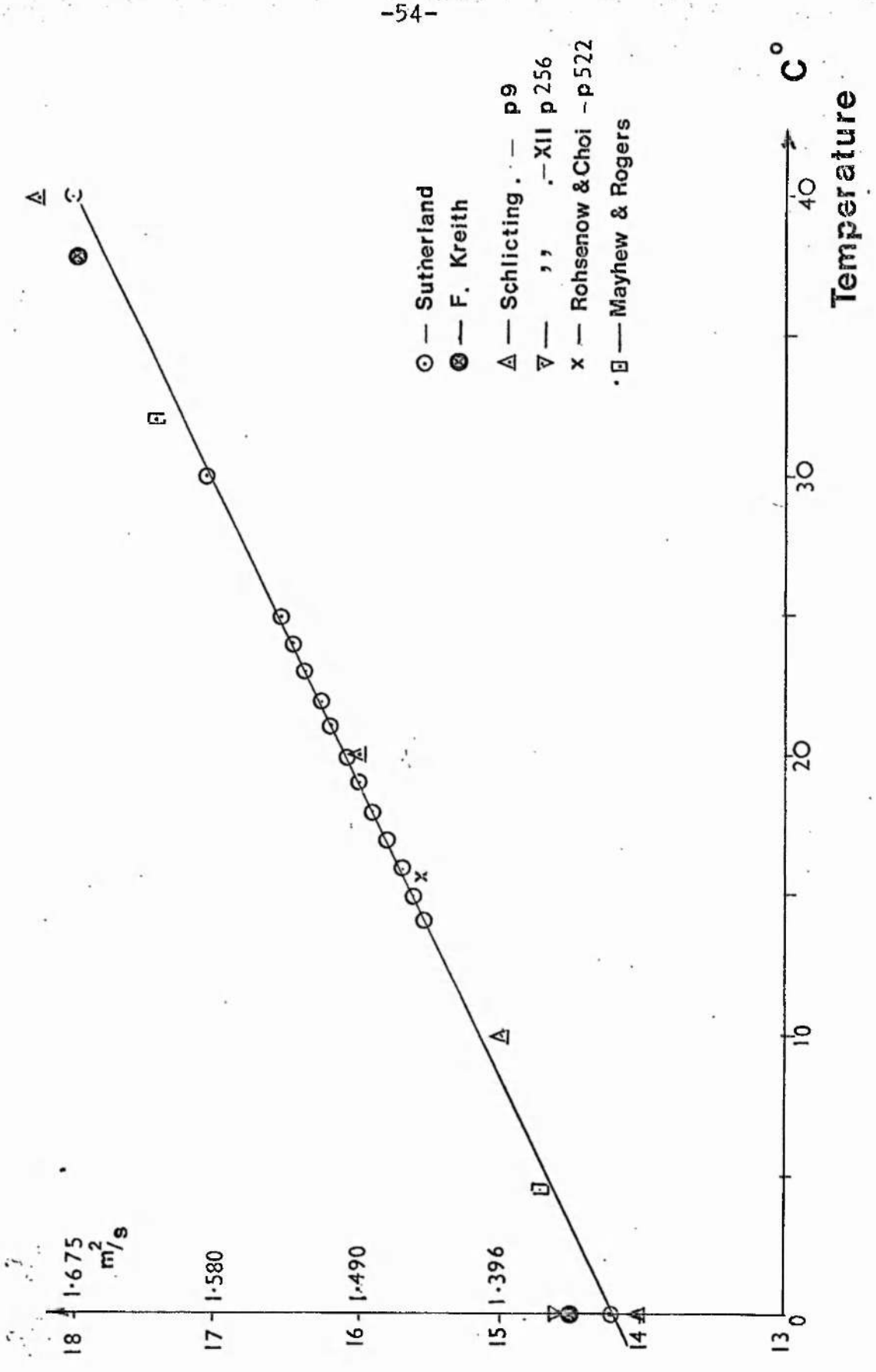

FIG 9 VARIATION OF KINEMATIC VISCOSITY WITH TEMPERATURE FOR AIR

Another reason for using a formula of this type was the extensive use made in this investigation of computing techniques.

Schlichting (sixth edition)[46] refers on page 312 to the Sutherland formula.

$$\frac{\mu}{\mu_o} = \left(\frac{T}{T_o}\right)^{3/2} \left(\frac{T_o + S_1}{T + S_1}\right) \qquad \ldots(4.05..1)$$

where μ_o denotes the viscosity at a reference temperature T_o

and T = the temperature in ^oK

S_1 = 124 for the range 0-100^oC for air.

For higher temperatures S_1 decreases.

For air $$\mu = \frac{150.\ 10^{-7}.\ T^{3/2}}{T + 124} \quad \text{(poise)} \qquad \ldots(4.05..2)$$

Density $$\rho = \frac{MW.\ 273.\ P_a}{22.41\ T.\ 760} \quad \text{(gm/cc)} \qquad \ldots(4.05..3)$$

which at 760 mm pressure for air gives:-

$$\rho = \frac{0.001293}{1+0.00367t} \quad \text{(gm/cc)} \qquad \ldots(4.05..4)$$

The value of ν thus obtained from 4.05..2 and 4.05..4 will be in centistokes units, which can be converted to ft^2/s units. All the values used on the graph of ν against temperature are given in Appendix 1B. Some extra values from other sources are also included.

It is apparent that the Sutherland formula provides an accurate and reliable means of computing kinematic viscosity. The straight line obtained was for standard atmospheric pressure of 760 mm mercury; for other values, the kinematic viscosity should be multiplied by $760/P_a$ so as to obtain the correct value of ν.

The final formula used in the computer program was derived from the graph (see Fig. 9).

$$\nu = (0.00014205 + t.\ 9.37.\ 10^{-7}).\ 760/P_a.$$

in ft^2/s units. ...(4.05..5)

4.06 Calibration of Probe

Prior to any velocity traverses being made it was necessary to calibrate the probe in two modes:-

(a) Position of Probe relative to brass plate

Primarily the probe had to be accurately positioned relative to the brass plate so that there was no zero error on the dial gauge. As mentioned in para.3.04 the length of the probe from the heel of the supports to the shoulder where it connected to the probe support, was measured using a travelling microscope. The probes were found to vary quite considerably, and it was necessary to measure each individually. The nominal size of a 55A36 probe was 41 mm according to DISA.

The probe gauges were constructed as shown in Fig. 7 so as to fix into the probe support in the traversing equipment.

Three gauges were constructed one being 1.620 ins. (41mm), one 1.630 ins. (41.4mm), and the last 1.640 ins. (41.6mm) between the shoulder and the tip.

The procedure for setting up the probe, was to choose a probe gauge as near to the actual probe as possible, and insert it in the probe support. A torch bulb holder was wired to the brass plate, and a battery; the probe support, and the gauge completed the circuit. With the flashlight bulb and battery in position the gauge was slowly advanced inwards until the bulb just lit up. The zero on the dial gauge was set, and the probe support withdrawn. It was now possible to insert the actual hot wire probe in the wind tunnel, with the sure knowledge that the distance from the wire to the plate was accurately known.

(b) Calibration of Bridge Voltage and Velocity

Considerable information exists on the DISA equipment in the handbooks provided. (Instruction and Service Manual for Type 55D00 Universal Anemometer.) and (Instruction and Service Manual for Type 55D05 Battery operated CTA.)

The normal calibration was performed using a Pitot-static tube* to obtain velocity, and thence plotting the square of bridge voltage against the square root of flow velocity (see Appendix 1C) also Fig.A2. This resulted in a straight line which passed through E_o^2 (the zero flow position). By extrapolating back, lower velocities may be obtained from the original calibration.

* Pitot-static tube by 'Airflow Developments' 8 mm diameter - 19 inches long to BS-1042.

The turbulence intensity measurements rely considerably on being able to obtain an accurate value of dE/dU. Incorrect data points can cause considerable errors if they are not taken at reasonable spacing. R.Kinns [36] suggests a logarithmic spacing, however if sufficient points are taken to provide an accurate straight line, and the intercept is obtained the results can be processed through a computer with a high degree of accuracy.

The intercept on the E^2 scale is measured and called C in the computer program. The reciprocal of the slope of this line is called A, and is shown on Fig. A2, page 145.

In the computer program

$$\sqrt{u} = (E^2 - C) \cdot A \qquad \ldots(4.06..1)$$

4.07 Velocity Profile - Measurements & Procedures

Once the probe has been calibrated, and the traversing equipment correctly positioned (see para. 4.06) then the principal velocity profile readings can be made.

It was found necessary initially to position the probe well away from the wall, so as to ensure that the probe was in the free stream, well outside the boundary layer. This could be ascertained by moving the probe 0.1 in. (2.5 mm), from a mean position and noting if there was any alteration in bridge voltage.

The velocity profile was obtained by moving the probe towards the wall in steps of 0.1 in., and recording the bridge voltage E for every value of distance y. If turbulence measurements were to be taken then the root mean square voltage E_{rms} was also recorded. When the probe was 0.1 in. away from the wall, then the incremental steps were reduced to 0.01 in. (0.25 mm) and the readings noted until a minimum distance of 0.05 in. (.13 mm) was reached.

The probe was then withdrawn, and one or two outward bridge voltages checked against those obtained previously; a check was also made to see if the mainstream velocity had altered. The probe calibration constants A and C, together with 'the no flow voltage' E_o were noted. The laboratory temperature, t^oC and the barometric pressure P_a mm were recorded for the purpose of obtaining kinematic viscosity ν ft^2/s.

For the smooth plate surface twenty-one profiles were obtained in the above manner, for varying positions of x ranging from x = 4 ins. (101 mm) to x = 20 ins. (0.507 m); the mainstream velocity U varying between 10.5 ft/s (3.2 m/s) and 64.6 ft/s (19.6 m/s). The complete results are shown in Table 1. on page 81.

In the case of rough surfaces all the profiles were obtained at the x = 1.380 ft (0.420 m) position. Twenty profiles were taken for the sand blasted surfaces, with U varying between 7.18 ft/s (2.2 m/s), and 68.77 ft/s (21 m/s). For the abrasive paper surfaces, three profiles were used for the Glass Paper grade 36 surface, and seven for the Aluminium Oxide grade 100 surface; the range of mainstream velocity varying between 8.5 ft/s (2.59 m/s) and 67.6 ft/s (20.6 m/s).

Having obtained the experimental data for a particular point on the plate at a known value of mainstream velocity three or four possibilities present themselves in the procedure for calculating friction factor, depending on the nature of the surface. These are introduced in general terms at this point, and considered in more detail in Chapter 5 and Chapter 6. The various computer programs and procedures are shown graphically in the flow diagram Fig. 10.

(1) Bradshaw Intersection Method

If the surface is smooth then the technique suggested by Bradshaw [3] has a lot to recommend it, although it does depend on a prior knowledge of the law of the wall. The method is as follows :- a graph of u/U is plotted against distance from the wall y. Now suppose an arbitrary value such as $y\,u_\tau/\nu = 200$, corresponding to $u/u_\tau = 18.75$ is selected on the law of the wall.

A second graph of the law of the wall using this value is also plotted on the same axes where

$$u/U = (u/u_\tau) \Big/ (U/u_\tau)$$

and

$$y = \left(\frac{y u_\tau}{\nu}\right) \cdot \frac{\nu}{U} \cdot \frac{U}{u_\tau} \qquad \ldots(4.07..1)$$

hence taking $yu_\tau/\nu = 200$ and $u/u_\tau = 18.75$, and substituting ν and U for the given flow, and for varying values of U/u_τ, pairs of u/U and y values are calculated and plotted, this curve intersects the measured velocity profile at a value of u/U which can be related to U/u_τ thus C_{fx} can be found using $U/u_\tau = \sqrt{2/C_{fx}}$.

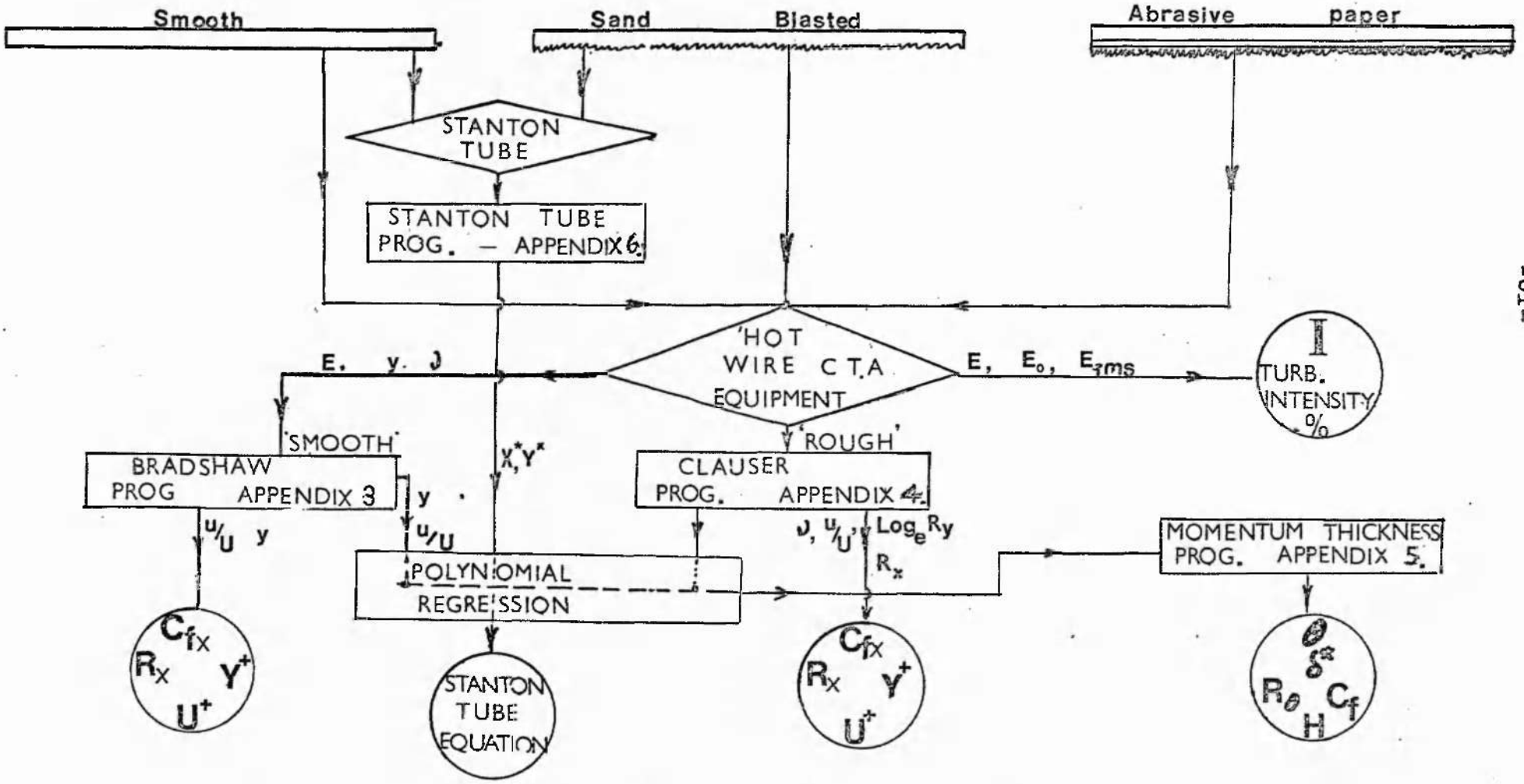

FIG – 10 Flow Diagram of Computational Procedures

In view of the large number of results required, it was thought advisable to have a computer program to process the hot wire readings. Use was made of plotting sub-routines, so that provided A, C, and ν are included a graph was plotted by the computer of u/U against y, together with the necessary Bradshaw intersection simply by supplying data of E and y. Details of the program, and a typical velocity curve and intersection are shown in Appendix 3. program 1.

(2) Velocity - Defect Method

Another method which may be used for obtaining skin friction results from the hot wire readings is the velocity defect, or outer law already referred to in Chapter 2 which is applicable to smooth or rough surfaces.

With $\frac{1}{K} = 2.5$, u can be written using the law of the wall equation (2.02..2)

$$u = u_\tau 5.75 \text{ Log}_{10} (yu_\tau/\nu) + B \quad ...(4.07..2)$$

Now when $y = \delta$ then $u = U$

$$U = u_\tau 5.75 \text{ Log}_{10} (\delta u_\tau/\nu) + B \quad ...(4.07..3)$$

Subtracting (4.07..3) from (4.07..2)

$$u - U = 5.75\, u_\tau \text{Log}_{10} (y/\delta)$$

Dividing both sides by U

$$\frac{u - U}{U} = 5.75 \frac{u_\tau}{U} \text{Log}_{10} (y/\delta) \text{ but } \frac{u_\tau}{U} = \sqrt{\frac{C_{fx}}{2}}$$

Hence $$\frac{U - u}{U} = 5.75 \sqrt{\frac{C_{fx}}{2}} \text{ Log}_{10} (\delta/y) \quad ...(4.07..4)$$

which is usually called the velocity-defect law, and is independent of Log law intercept B.

If $(1-u/U)$ is plotted against $\text{Log}_{10}(\delta/y)$ the slope will give the value of C_{fx}. This method has its limitations, as will be discussed later partly due to the fact that it requires prior knowledge of the local boundary layer thickness δ, and for this reason has only been used in a few instances for confirming results by different methods (see Table 1).

(3) Clauser Method

Clauser [9] in his paper suggests another possibility for the determination of turbulent skin friction if the law of the wall is known. The velocity profile, is plotted as u/U against $\text{Log}_e(yU/\nu)$. The law of the wall is plotted as a family of curves for various values $U/u_\tau = \sqrt{(2/C_{fx})}$. The particular curve which the velocity profile blends into gives the required value of U/u_τ and hence the value of C_{fx} may be obtained.

The required computer program for this method calculates u/U and $\text{Log}_e(yU/\nu)$ from the input velocity profile data of E and y together with the calibration constants of A, C, t, and P_a. It is also used to plot experimental results on axes of u/U against $\text{Log}_e(yU/\nu)$; a typical computer plot with the relevant 'print out' is shown in Appendix 4 Program 2.

A slight modification to this method which the author has found particularly useful for rough surfaces is to construct a Clauser grid. Using the familiar law of the wall equation for smooth surfaces

$$U^+ = 2.5 \text{ Log}_e y^+ + 5.5$$

A family of straight lines is drawn on tracing paper each being for a particular value of U/u_τ (see Fig.11). By placing this Clauser grid over the computer plot it is immediately apparent from the slope of the line which is the correct value of U/u_τ.

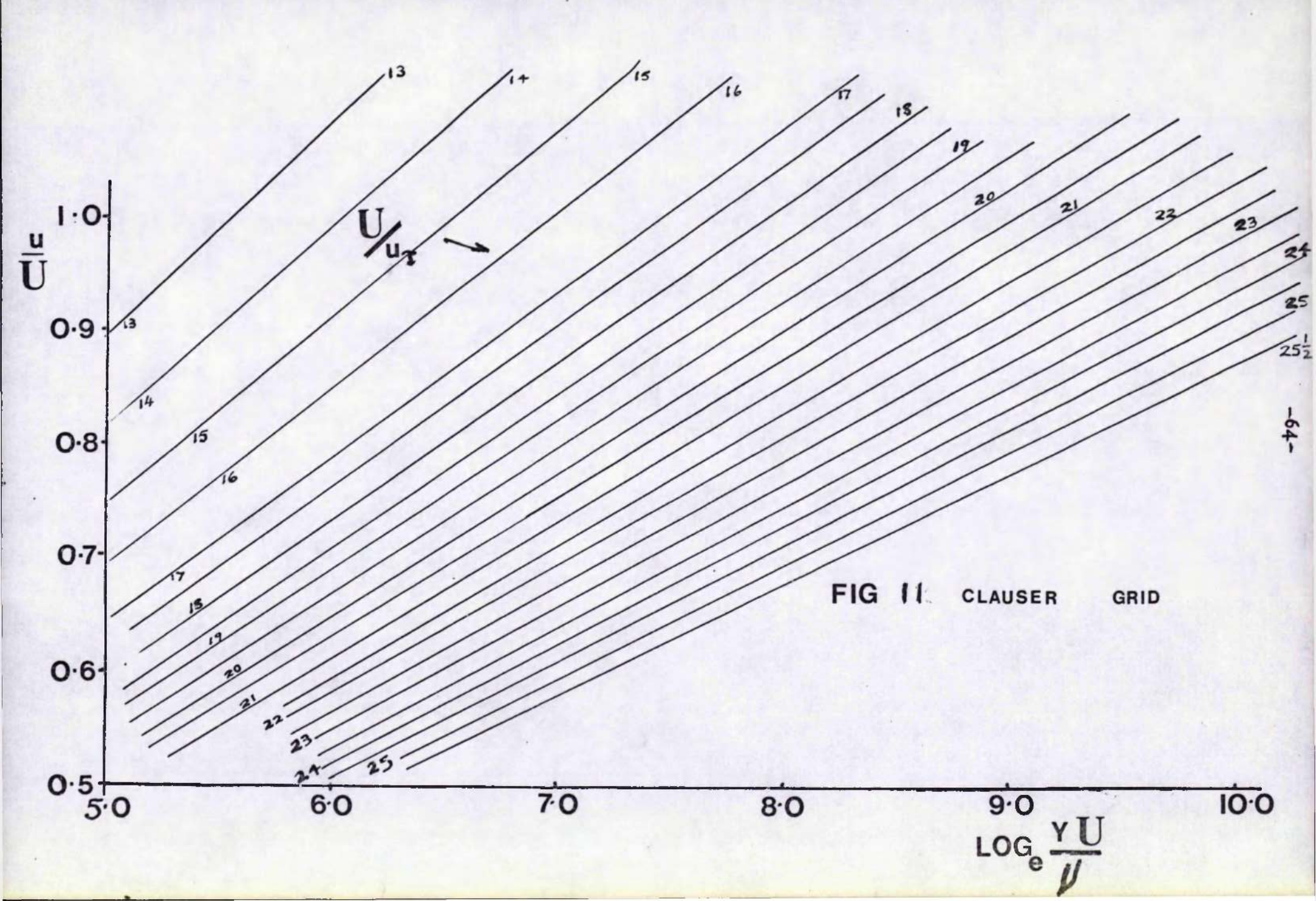

FIG 11 CLAUSER GRID

This technique assumes that the slope $1/K$ of the law of the wall is independent of roughness, this fact is verified later in para. 4.09.

This Clauser tracing paper overlay method must not be confused with the Clauser defect velocity profile method referred to in para. 2.02, which is outlined further in para. 5.06 as a means of validating the skin friction results, and is shown in Fig. 21.

(4) Momentum Integral Method

Having found θ and as explained in para.4.11, it is possible to use a formula due to Schlichting (46) (page 600 Eq.21.12) for smooth surfaces. This is based on the 1/7 power law, and enables friction factor to be checked without resorting to the law of the wall, it is also independent of distance x.

$$C_{f\theta} = 0.0256/R_{\theta}^{1/4} \qquad \ldots(4.07..5)$$

Friction factor obtained by this means using computer Program 3. Appendix 5 is only used as a means of confirming some of the smooth plate results; it cannot be used on rough surfaces.

4.08 Stanton Tube - Geometry and Measurements

One of the main objectives discussed earlier was to develop a new form of Stanton tube to be used on either smooth or rough surfaces.

Laminated shim steel was used for the construction of the Stanton tube, (para.3.06 and Fig.6). A knife edge of 23° was ground along the leading edge with a special fixture on an oil stone.

This was checked by means of shadowgraph equipment, and kept constant throughout all the tests.

At the commencement of the Stanton-tube tests the earlier readings obtained with the ground edge facing upwards, and the height 'h' under the tube taken as the height parameter have been omitted for the following two reasons :-

(1) The actual height h, the surface Pitot tube projects into the air stream is the main criteria; as stated by Gadd[25] an equivalent solid step would produce the same flow patterns as a Stanton tube of the same height.

(2) The effect of having the knife edge downwards i.e. the ground edge upwards would be to radically deviate from the solid step notion, by inducing new separation points farther downstream.

With the above points in mind it was decided to standardise the surface Pitot tube with the ground section underneath, consequently readings of Δp were obtained for various mainstream velocities U at a particular height 'h'. The height h could be reduced in a stepwise manner by removing layers of shim steel. Values of barometric pressure P_a, and temperature $t^{\circ}C$ were also recorded so that kinematic viscosity ν could be derived.

It was thought advisable to comply as far as possible with limits mentioned by Bradshaw and Gregory [6], in which paper reference is made to the need to calibrate surface Pitot tubes only in turbulent flow, if the calibration is carried out in laminar flow incorrect results may occur.

For this reason a lower limit $u_\tau h/\nu = 2$ was adopted.

Corresponding to $y^* = \text{Log}_{10}\left[\frac{1}{4}\left(\frac{u_\tau h}{\nu}\right)^2\right] = 0$ see equation 2.01..6.
Also so as to remain within the region of universality of the law of the wall where viscous stresses are still appreciable the height of the Stanton-tube must not exceed a value given by $\frac{u_\tau h}{\nu} = 30$ corresponding to $y^* = 2.352$.

The Stanton tube calibration is presented in a similar manner to that of a Preston-tube, i.e. x^* and y^* are obtained in the same manner except 'h' the Stanton-tube height replaces 'd' the Preston-tube diameter. For this reason another computer program (Appendix 6 Program 4) was devised to compute x^* and y^* from the experimental readings. The value of u_τ was obtained using the value of C_{fx} derived by the following method. A graph of $\text{Log}_{10} R_x$ was plotted against $\text{Log}_{10} C_{fx}$ using the hot wire results for C_{fx} and R_x (see Appendix 1D) and also Fig.A3. This resulted in a relationship of the form

$$C_{fx} = \frac{\text{Const}}{(R_x)^{0.21}}$$

where the constant depends on the nature of the surface, this was subsequently used in the computer program for deriving y^*.

The effect of using a standard razor blade was also studied. A further test was carried out to ascertain the effect of altering the longitudinal position of the Stanton-tube relative to the hole underneath. By just uncovering or exposing the hole in front of the tube three values of x were used (see Fig. 6).

Altogether sixty-one sets of results were obtained all with x = 1.220ft (376 mm) for values of height 'h' ranging between 0.004 in. (0.1 mm) to 0.023 in. (0.59 mm); the range of x^* being 1.04 to 4.17.

4.09 Rough Plate Measurement

This section is concerned with surface roughness, and the means adopted to measure it. The main section deals with how the surface roughness was produced and assessed, covering such items as CLA roughness value, and particle size. The second part deals with how skin friction results were obtained using the Clauser grid; the reliance of such a method on the law of the wall is also investigated.

(1) Assessment of Surface Roughness

The rough surfaces used, were either sand-blasted brass plates, or abrasive paper fitted to the smooth plate surfaces with adhesive.

(a) Sand-Blasted Surfaces

Three different sand-blasted surfaces were produced as follows all with compressed air at 60 lbf/in^2 (400 kN/m^2) gauge pressure.

Standard sand-blasting equipment was used, the abrasive material being either 'No.1 Uniblast' (a fine sand-blasting abrasive) or a coarser material G34 Angular grit. The surfaces produced are as follows :-

Surface A :- Using No.1 Uniblast with the standard gun.

Surface B :- Using No.1 Uniblast but with the major gun.

Surface C :- Using G34 Angular grit chilled iron.

These three techniques produced surfaces of increasing roughness. Unfortunately it was impossible to obtain a rougher surface than C by sand or shot-blasting as it would have caused severe bowing of the plate. Brass plate C tended to show slight bowing, and had to be sand-blasted on the inner side in order to minimise this.

Readings of centre line average (CLA) roughness were taken at several positions on the plate in the axial and spanwise direction using standard Talysurf equipment. The reason this was done was to check that the roughness was truly isotropic, which in fact it was. The readings were also checked using a B & K roughness meter.

In order to correlate the CLA roughness values to the Nikuradse sand particle size K_s referred to in para. 2.03 it was necessary to introduce a corresponding abrasive grit size K, so that both types of rough surface may have the one roughness height in common. This was achieved using the Talysurf results and some due to Forster [24], and can be seen in Fig. 24.

(b) Abrasive Paper Surface

As the sand-blasted surfaces did not provide a sufficient range of surface roughness, it was necessary to use various types of abrasive paper stuck to the brass plates with adhesive.

Unfortunately equipment of the Talysurf type was found to be completely unsuitable for measuring the high roughnesses required for this type of work; consequently other methods of surface assessment had to be employed. Measurements were taken of overall thickness and grit size. The grit size was obtained from either BSS 871 or the F.E.P.A. (Federation of European Producers of Abrasives) Handbook. Typical values of grit size for various abrasive papers are shown in Table 4.‡ The relationship between grit size K and the Nikuradse sand particle size K_s is discussed in para. 6.05.

(2) Law of the Wall for a Rough Surface

The method used for obtaining friction factors utilising the Clauser plot from the computer, and a tracing paper grid has been fully described in para. 4.07. This technique however relies considerably on the constant $1/\chi$ in the law of the wall equation (2.02..2) remaining constant irrespective of the degree of roughness. The following analysis validates that assumption.

It is generally accepted (12) that the influence of roughness is felt only near the wall, and that farther away from the wall, outside the sub-layer the velocity gradient du/dy is independent of roughness and viscosity (Rotta (45) page 75).

‡ see page 110.

For a rough surface using dimensional similarity

$$U^+ = \frac{u}{u_\tau} = \phi \left[y^+ , R_r \right]$$

where $y^+ = \frac{y u_\tau}{\nu}$ and $R_r = \frac{K_s u_\tau}{\nu}$

u_τ, the friction velocity $= \sqrt{\frac{\tau}{\rho}}$

$$\therefore u = u_\tau \phi \left[y^+ , R_r \right]$$

$$\therefore \frac{du}{dy} = u_\tau \left[\frac{d\phi}{dy^+} \cdot \frac{dy^+}{dy} + \frac{d\phi}{dR_r} \cdot \frac{dR_r}{dy} \right]$$

$\frac{dR_r}{dy}$ is obviously 0.

$$\therefore \frac{du}{dy} = u_\tau \frac{d\phi}{dy^+} \cdot \frac{u_\tau}{\nu} = \frac{u_\tau^2}{\nu} \cdot \frac{d\phi}{dy^+}$$

but as stated above du/dy is independent of ν and R_r

$$\frac{du}{dy} = \frac{u_\tau^2}{\nu} \frac{d\phi}{dy^+} \neq \psi(\nu . R_r)$$

Hence $\frac{d\phi}{dy^+}$ must be a function of y^+

such that ν cancels in $\frac{u_\tau^2}{\nu} \frac{d\phi}{dy^+}$

i.e. $$\frac{d\phi}{dy^+} = \frac{C \nu}{u_\tau y} = \frac{C'}{y^+}$$

where C' is a constant.

Hence $$\frac{du}{dy} = \frac{C' u_\tau^2}{\nu} \cdot \frac{\nu}{u_\tau y} = \frac{C' u_\tau}{y}$$

Introducing U^+ and y^+

$$\frac{du}{dy} = \frac{u_\tau dU^+}{\frac{\nu}{u_\tau} dy^+} = \frac{u_\tau^2}{\nu} \frac{dU^+}{dy^+} = C' \frac{u_\tau}{y}$$

$$\frac{dU^+}{dy^+} = \frac{C' \nu}{y u_\tau} = \frac{C'}{y^+}$$

Integrating $U^+ = C' \text{Log}_e y^+ + f(R_r)$

Hence the familiar form of U^+ versus y^+ plot.

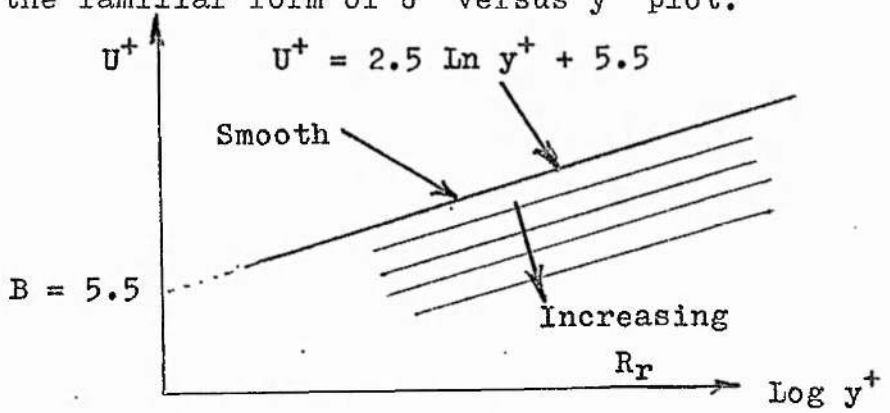

Which demonstrates that the slope C' is independent of roughness Reynolds No., whereas the intercept B is a function of R_r such that B decreases with increasing R_r.

4.10 Turbulence Measurements

The required turbulence measurements were obtained in the following manner, the fluctuating voltage from the hot wire probe was indicated on a B & K true RMS voltmeter, and the DC component on a mechanical display digital voltmeter.

Turbulence Intensity measurements are usually obtained from the slope dE/du of the probe calibration graph.

From Kings law

$$Nu = C_1 + A_1 \sqrt{R_d} \qquad \ldots(4.10..1)$$

but $Nu = \dfrac{E^2}{R\pi k(T-T_a)L}$ and $R_d = \dfrac{ud}{\nu}$

where $(T-T_a)$ = the temperature difference between the hot wire and the ambient temperature, and d = the wire diameter, L = length of wire.

$$\therefore \quad \frac{E^2}{R\pi k(T-T_a)L} = C_1 + A_1 \sqrt{\frac{ud}{\nu}}$$

This can be written in the simpler form for constant temperature wire, and uniform property isothermal flow using alternative constants.

$$\frac{E^2}{R} = \frac{E_o^2}{R} + A_2 \sqrt{u} \qquad \ldots(4.10..2)$$

where E_o = Bridge voltage at zero flow

Differentiating equation (4.10..2)

$$\frac{2E}{R} \cdot \frac{dE}{du} = \frac{A_2}{2\sqrt{u}}$$

$$\therefore \quad \frac{dE}{du} = \frac{A_2 R}{2\sqrt{u}.2E} = \frac{A_2 R}{4\sqrt{u}.E}$$

$$\therefore \quad \frac{u\,dE}{du} = \frac{A_2 R\sqrt{u}}{4E}$$

but from (4.10..2) $\sqrt{u} = \left(\dfrac{E^2}{R} - \dfrac{E_o^2}{R}\right)\dfrac{1}{A_2}$

$$\therefore \quad \frac{u\,dE}{du} = \frac{A_2 R}{4E} \cdot \frac{(E^2 - E_o^2)}{R A_2}$$

$$= \frac{(E^2 - E_o^2)}{4E} \qquad \ldots(4.10..3)$$

$$\text{Now \% Turbulence} = \frac{\text{RMS of velocity fluctuations}}{\text{mean velocity}}$$

$$= \frac{\text{Bridge RMS volts}}{\left(\begin{matrix}\text{Bridge volts per}\\ \text{unit RMS velocity}\end{matrix}\right).\left(\begin{matrix}\text{Mean}\\ \text{velocity}\end{matrix}\right)}$$

$$\text{hence \% Turbulence} = \frac{E_{rms}\ 100}{u\ dE/du}$$

which from (4.10..3) using the linear section of the graph gives :-

$$\text{Turbulence Intensity} = \frac{4.\ E_{rms}.E.100}{(E^2 - E_o^2)}\ \% \qquad \ldots(4.10..4)$$

Since the flow rate was comparatively low, and the ambient temperature was constant it was possible to assume a linear section of the graph of E^2 plotted against $\sqrt{u}$. Consequently equation (4.10..4) was used throughout.

A typical traverse from outside the boundary layer in the y direction is shown in Fig. 12. The main objective however in measuring turbulence intensity is to study the effect roughness has on turbulence levels.

Two investigations were carried out, in the first case the turbulence intensity along the length of the plate was obtained for a constant value of y, and a constant roughness. Next turbulence measurements were taken at fixed values of x, and at constant mainstream velocities for varying degrees of surface roughness with y = o.2 in. (5 mm) throughout. The results obtained and the graphs plotted are discussed in Chapter 8.

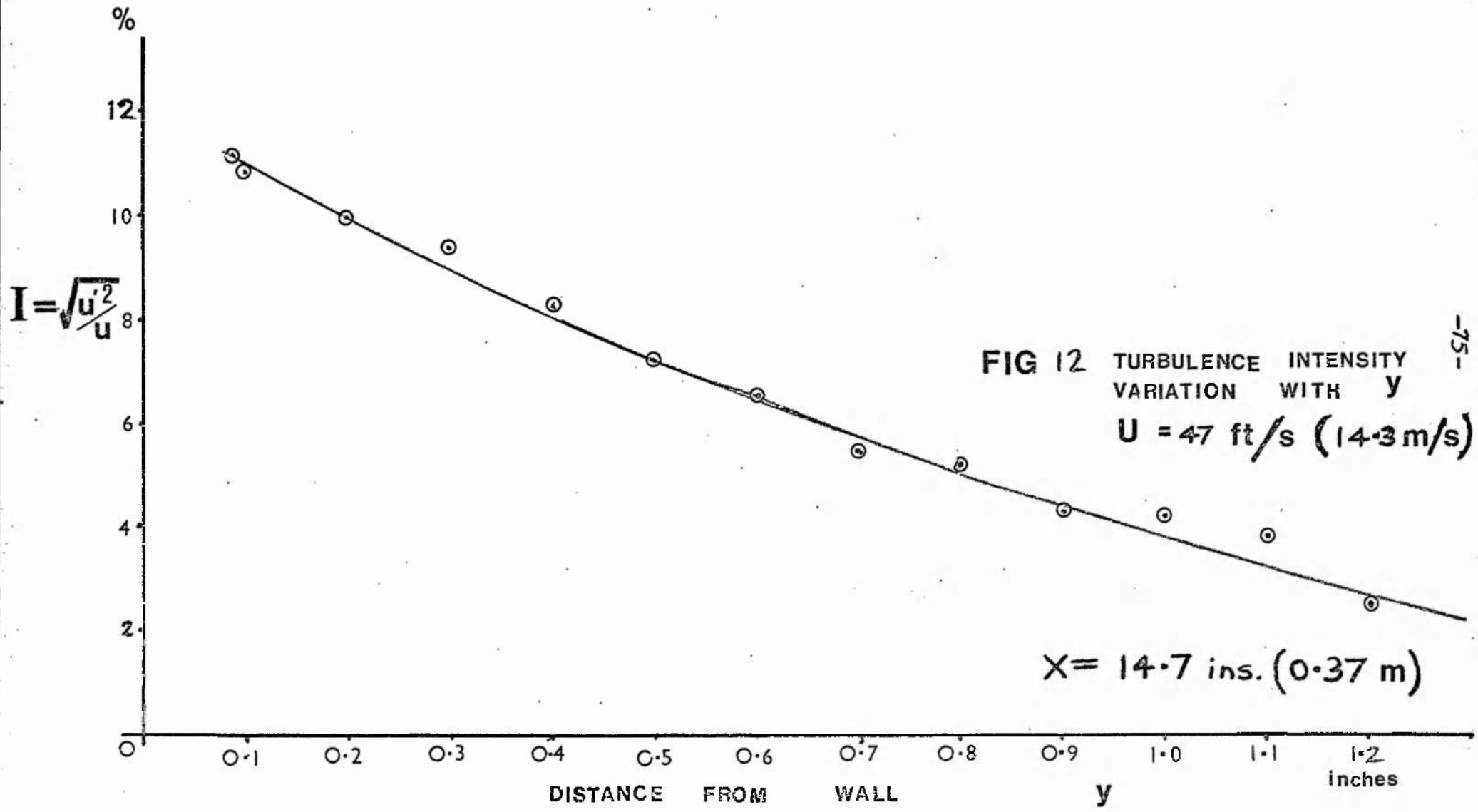

FIG 12 TURBULENCE INTENSITY VARIATION WITH y

U = 47 ft/s (14·3 m/s)

4.11 Calculation of Boundary Layer Parameters

δ^*, θ and H.

These quantities were determined primarily as a means of confirming some of the skin friction results, as mentioned in the introduction to this chapter.

The displacement thickness δ^* was used in obtaining the graph (Fig. 21) for smooth and rough surfaces using the Clauser defect velocity profile (9). Details of these results are given in para. 5.06. The friction factor based on momentum thickness $C_{f\theta}$ was obtained for comparison with the other values.

Momentum thickness, displacement thickness and shape factor were determined from a given velocity profile using the following procedure.

The experimental velocity profile of u/U versus y was represented by a polynomial of the fifth order. Putting Y = u/U, and X = y a standard Fortran computer program called POLRG was used to obtain the regression coefficients A_o, A_1, A_2 etc., in the equation

$$Y = A_o + A_1X + A_2X^2 + A_3X^3 + A_4X^4 + A_5X^5 \quad \ldots(4.11..1)$$

A further computer program was developed in order to be able to integrate and obtain δ^*, θ, H and R_θ etc., Details of the program are given in Program 3 Appendix 5, and are shown graphically in the flow diagram (Fig. 10).

Now displacement thickness δ^{**} for incompressible flow.

$$= \int_0^{\delta} (1-u/U)\, dy$$

$$= \int_0^{\delta} dy - \int_0^{\delta} u/U.dy$$

therefore $\delta^{**} = \delta - \int_0^{\delta} YdX$ ...(4.11..2)

Also momentum thickness θ for incompressible flow

$$= \int_0^{\delta} u/U(1-u/U)dy$$

$$= \int_0^{\delta} YdX - \int_0^{\delta} Y^2dX$$ ...(4.11..3)

The value of δ has been taken as that value which makes $u/U = 0.99$. The shape factor $H = \delta^{**}/\theta$.

4.12 Calibration of Preston-Tubes

As mentioned in the introduction to this chapter this section deals with the further verification of the smooth plate skin friction results, using two different diameters of Preston-tube. A small hole was drilled through the brass plate, at the principal measuring station, and a small section of hypodermic needle tube was inserted into the cavity behind. The front of the tube was carefully examined for burrs etc., and was fixed with adhesive, facing into the air flow (see sketch).

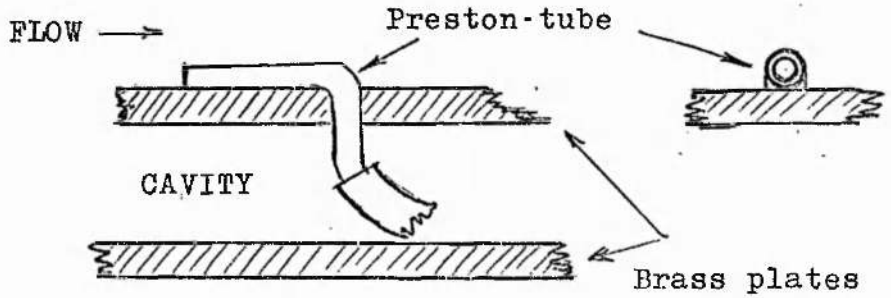

Two diameters of needle tubing were used one of 0.028 in. (0.71 mm), and the other 0.0635 in.(1.61 mm) external diameter. It was particularly important to ensure that the front of the tube was placed firmly against the brass plate.

The pressure difference between the Preston tube and a static pressure hole, sited adjacent to it was recorded on a standard 0-½ in. inclined manometer; values of Δp thus obtained were very accurate as the manometer had a high sensitivity combined with a comparatively low time lag. The connections to the Preston tube passed through the brass plate cavity, and had of necessity to be of small bore tubing, Seven to eight minutes was allowed for the system to reach equilibrium conditions for each set of readings taken.

Having obtained a value of Δp, (as indicated in the previous paragraph) for a given flow, it was then possible to derive u_p , once atmospheric temperature and pressure were known. The value of x^* was next determined, in the standard manner using Preston's approach [43], (refer to equation 2.01..6) for a given tube diameter d, and kinematic viscosity ν.

The calibration due to V.C.Patel[41], shown graphically on Fig. 13, was then used to obtain y^*, (see also equation 2.01..6) from which u_τ could be obtained. Finally C_{fx} was derived, utilising the relationship $U/u_\tau = \sqrt{2/C_{fx}}$.

The relationship between x^* and y^* obtained by V.C.Patel[41] was used to derive the friction factor for the smooth plates, as outlined above; but Patel's calibration was carried out in pipe flow. It would however appear applicable to flat smooth plates since East [18] has used it throughout. The Preston tube results are given in Table 1A page 83, and can be seen plotted in Fig. 16 together with the hot wire results.

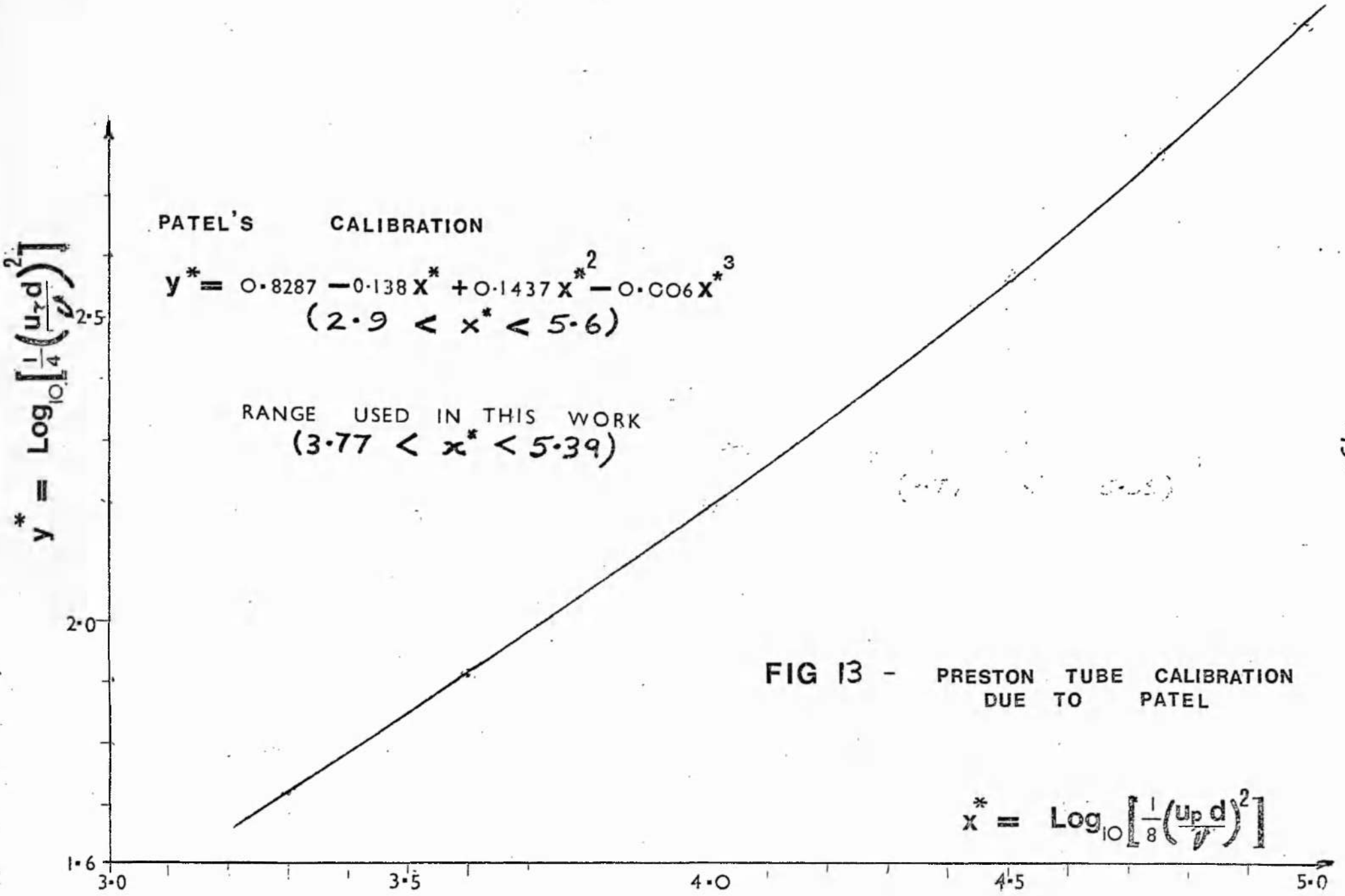

FIG 13 - PRESTON TUBE CALIBRATION DUE TO PATEL

CHAPTER 5 SMOOTH PLATES - EXPERIMENTAL RESULTS & COMPUTATIONS

The experimental results, derived by the procedures and techniques outlined in Chapter 4 are now considered in more detail. The hot wire results for the smooth plate are presented in tabular form in Table 1, and are shown graphically, along with the Preston-tube results in Fig. 16. Local friction factors C_{fx} were calculated for five measuring stations varying between x = 20 ins. (0.5 m) and x = 4 ins. (0.1 m) for mainstream velocities U in the range 65 ft/s (21 m/s) to 10 ft/s (3.2 m/s).

The following six paragraphs analyse the results calculated by the various techniques in more detail.

5.01 Bradshaw's Procedure

The method of determining skin friction as advocated by Bradshaw [3], and involving the intersection of the law of the wall with the measured velocity profile has been referred to in para.4.07. The results obtained by this method compare very favourably with the Preston tube results (Table 1A), and with other methods. (see Fig.16).

This method is very easy to apply, and as a computer program is used with the plotter, the results were obtained very quickly, however the method does require prior knowledge of the law of the wall, and it is for this reason that other methods employing momentum thickness have been adopted to verify these results.

TABLE I

SMOOTH PLATE - HOT WIRE RESULTS

x ins	N rev/min	U ft/s	ν ft^2/s	Friction Factor Cf_x				R_x
				I	II	III	Mean	
14.7	330	10.52	0.0001600	0.00500	0.00490	0.00550	0.00510	80600
"	450	14.80	0.0001575	0.00467	0.00463	0.00480	0.00465	115100
"	550	18.90	0.0001575	0.00450	0.00440	0.00460	0.00450	147000
"	745	25.61	0.0001575	0.00407	0.00405	0.00430	0.00410	199100
"	860	31.50	0.0001600	0.00385	0.00375	0.00380	0.00380	242000
"	1000	35.10	0.0001575		0.00376		0.00376	273000
"	1000	39.40	0.0001600	0.00379	0.00380		0.00380	302000
* "	1100	40.00	0.0001615	0.00375	0.00375	0.00378	0.00376	303400
"	1430	54.50	0.0001588	0.00358	0.00357	0.00364	0.00360	421000
8.0	340	10.70	0.0001610	0.00540	0.00545		0.00543	44400
"	450	13.52	0.0001610		0.00470		0.00470	56000
"	700	24.77	0.0001610		0.00400		0.00400	103000
"	850	32.90	0.0001630		0.00378		0.00378	134500
"	1080	39.70	0.0001630		0.00375		0.00375	162200
"	1720	64.60	0.0001610	0.00330	0.00310		0.00320	268000
4.0	1640	59.60	0.0001605		0.00309		0.00310	123700
"	1030	38.60	0.0001630		0.00388		0.00388	77600
"	750	26.52	0.0001605		0.00390		0.00390	54500
12.0	1180	45.40	0.0001655		0.00370		0.00370	274300
20.0	740	26.50	0.0001605		0.00440		0.00440	275290
"	1270	47.00	0.0001605		0.00418		0.00418	488000

I Clauser Method.
II Bradshaw Method.
III Defect Method.

* Used for 1/7 Power Law.

The one serious objection to this method is that it cannot be used for rough surfaces since the value of the intercept B does vary according to the surface considered (as established in para.4.09). The smooth plate results obtained by this method (Table 1) compare exceedingly well with the momentum thickness results,(see Table 2A) page 91 and for this reason most smooth plate results have been obtained by this procedure.

5.02 Defect Law

As can be seen from Table 1, some results have been checked using the velocity-defect method. A graph was plotted, but is not shown in this thesis, of $1-(u/U)$ against $\text{Log}_e(y/\delta)$,‡ the slope of which is $2.5 \cdot u_\tau/U$, hence C_{fx} could be found. This has not been applied to many results because it depends on accurate knowledge of the local boundary layer height δ. To be able to obtain δ sufficiently accurately is rather difficult, however the results in Table 1 for this method agree well with those derived by the other methods.

The outer law or defect law is really only valid for values of $y/\delta > 0.15$.

The defect law can be written in the form

$$\frac{U-u}{u_\tau} = -8.6 \text{ Log}_{10}(y/\delta) \qquad \ldots(5.02..1)$$

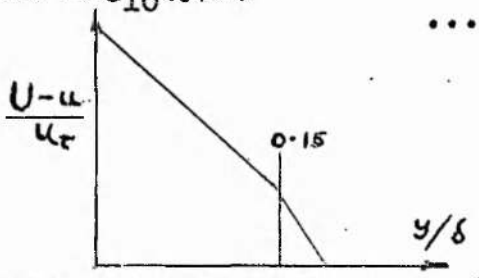

The law of the wall which is valid for $y/\delta < 0.15$ can be written $\frac{U-u}{u_\tau} = -5.6 \text{ Log}_{10}(y/\delta) + 2.5$ ...(5.02..2)

as can be seen on the sketch above the defect law is really only suitable for examination of the outer part of the boundary layer. Further reference to the outer, or defect law is made in Chapter 8.

‡ (Refer to Eq. 4.07..4 on page 62).

TABLE I A

PRESTON TUBE CALIBRATION OF SMOOTH FLAT PLATE (1)

x = 14.7 ins.

N Rev/ min	d in.	Kinetic Head in. H_2O	ν ft^2/s	R_x	U ft/s	C_{fx}
1680	0.0635	0.925	16.30×10^{-5}	4.90×10^5	65.0	0.00365
1510	"	0.730	"	4.31	57.6	0.00372
1400	"	0.616	"	4.00	53.0	0.00378
1200	"	0.455	"	3.42	45.5	0.00384
1000	"	0.312	"	2.84	37.7	0.00389
800	"	0.199	"	2.26	30.1	0.00397
620	"	0.108	"	1.67	22.2	0.00455
440	"	0.049	"	1.12	14.9	0.00495
790	0.0635	0.184	16.23×10^{-5}	2.17×10^5	28.8	0.00406
730	"	0.156	"	2.00	26.5	0.00405
580	"	0.090	"	1.52	20.2	0.00450
420	"	0.046	"	1.08	14.4	0.00520
1100	0.280	0.392	15.30×10^{-5}	3.30×10^5	41.1	0.00387
1300	"	0.575	16.15 "	3.84 "	50.6	0.00410
1610	"	0.870	16.01 "	4.43 "	58.1	0.00392

(1) This uses Patel's Calibration see Fig. 13.

Range of x^* 3.77 to 5.39.

Refer to para. 4.12

5.03 Stanton Tube Results

Using the shim steel it was possible to peel off a layer 0.002 in. (0.05 mm) thick and thus stepwise reduce the height h as mentioned in para. 4.08.

Altogether sixty-one sets of readings were taken at x = 1.220 ft. for varying heights of laminated shim, and also using a standard razor blade; the results are shown on x^*, y^* axes in Fig. 14. The values of h used, together with the range of $u_\tau h/\nu$, and y^* are shown in Appendix 2C.

The effects of varying h, on the calibration, are very minor as can be seen from Fig.14. The results agree well with those of East, ~~and Bradshaw and Gregory.~~

A computer program was used for the Stanton tube calculations, and is shown in Appendix 6; together with a typical 'print out'. Experimental data of temperature, barometric pressure, and manometer readings etc., were transposed into the familiar x^* and y^* form, as shown on the flow diagram Fig.10. The value of $y^* = \text{Log}_{10}\left[\frac{1}{4}\left(\frac{u_\tau h}{\nu}\right)^2\right]$ was derived using values of u_τ obtained from $u_\tau = U\sqrt{(C_{fx}/2)}$. From the hot wire results in Table 1 a graph of $\text{Log}_{10}C_{fx}$ vs $\text{Log}_{10}R_x$ (Fig. A3) was plotted resulting in a relationship of the form $C_{fx} = \frac{\text{Const}}{R_x^{0.21}}$ see Appendix 1D.

...(5.03..1)

For a given value of R_x it was then possible to compute C_{fx} using (5.03..1) and subsequently derive u_τ and y^*.

With the constant = 0.055, equation (5.03..1) compares favourably with the normal published flat plate relationship [46] of $C_{fx} = 0.0576/R_x^{0.2}$; the discrepancy in part being due to the blunt leading edge. Further reference is made to this in para. 5.04 and para.8.02.

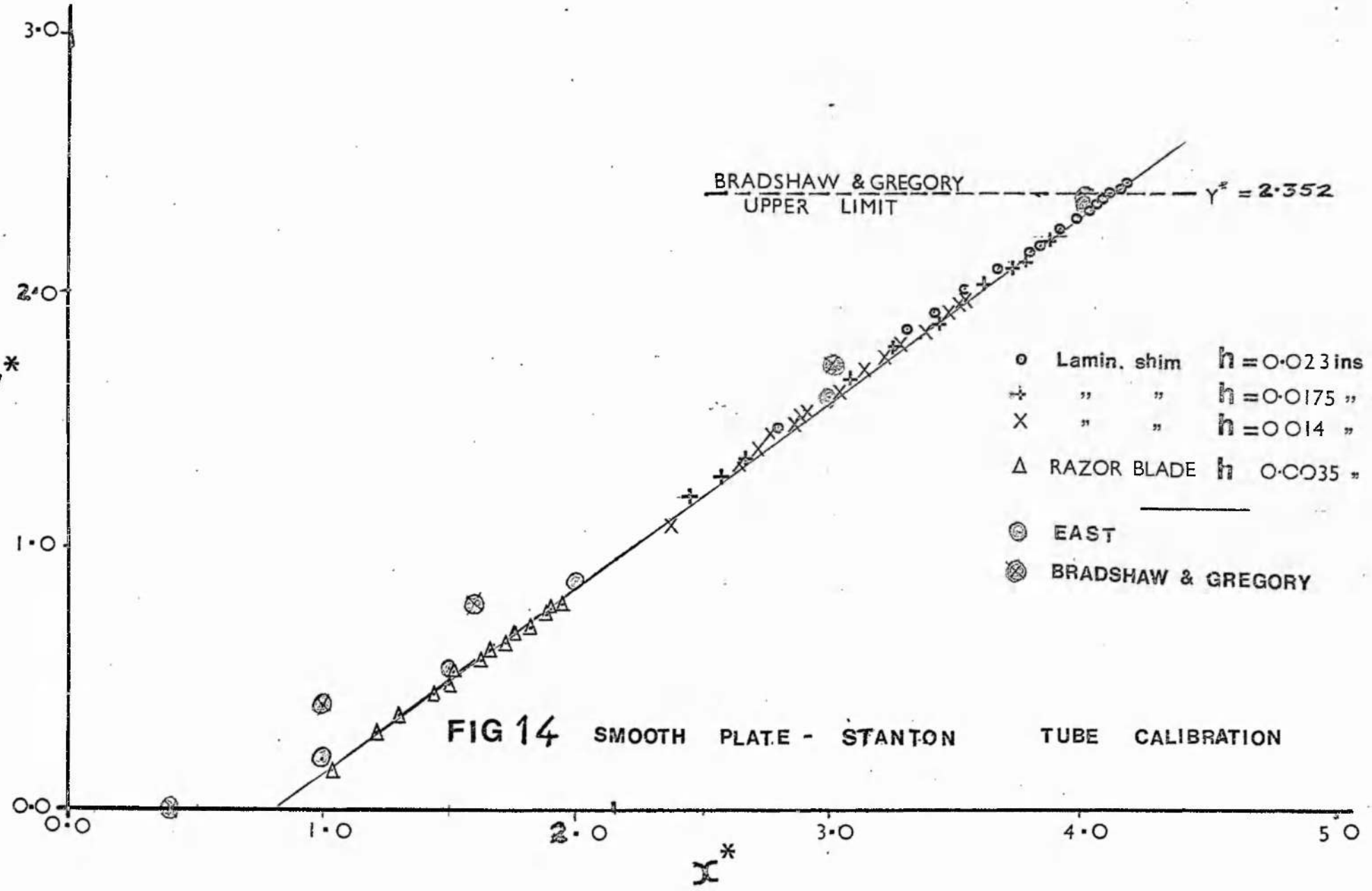

FIG 14 SMOOTH PLATE - STANTON TUBE CALIBRATION

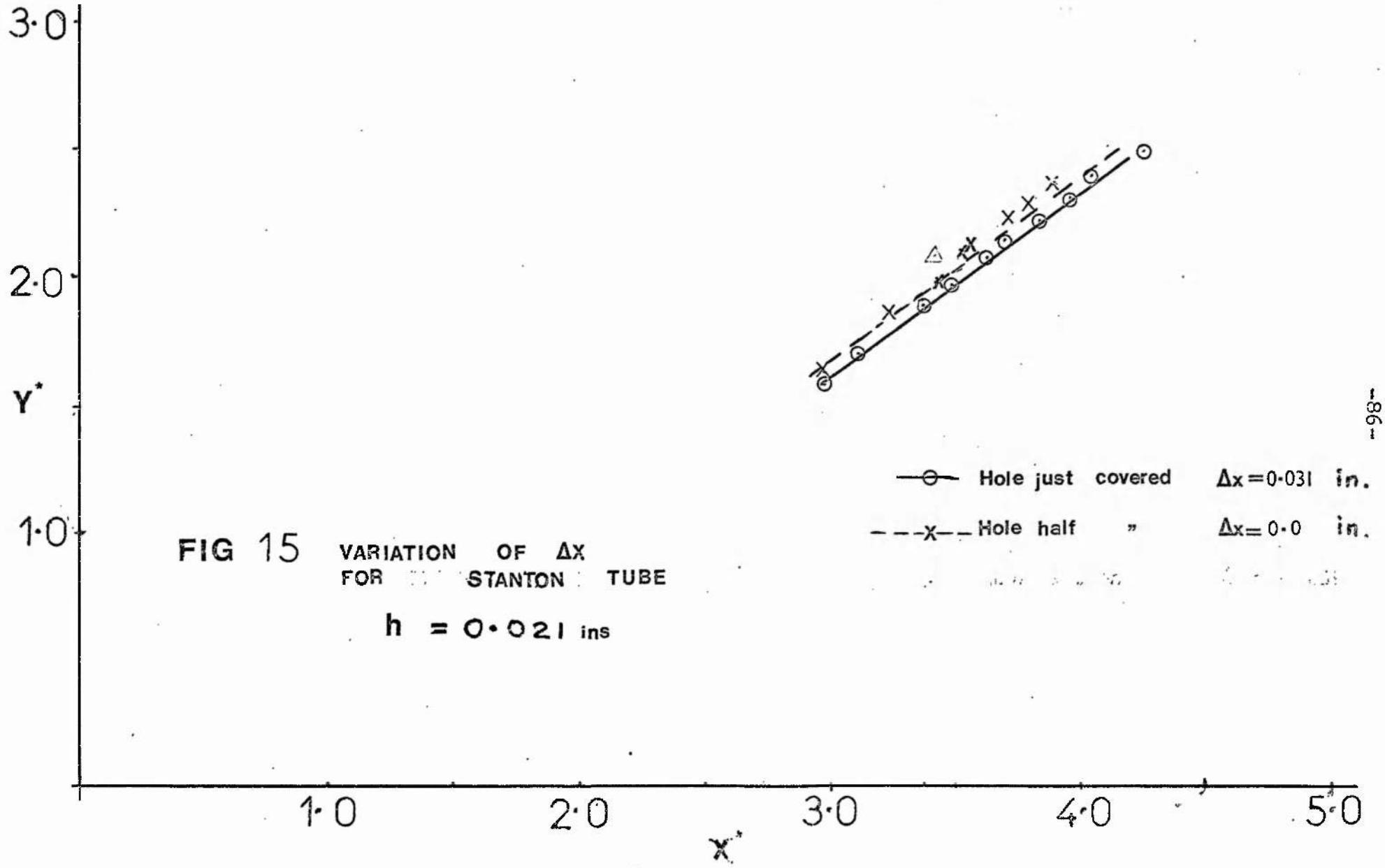

FIG 15 VARIATION OF Δx FOR STANTON TUBE

h = 0·021 ins

A polynomial regression program (POLRG) was used to formulate the polynomial equation of x^{*} and y^{*} for each value of h. The regression program was also applied to the complete set of sixty-one readings, and good agreement with East was observed. The regression results together with the range of y^{*}, and yu_{τ}/ν are shown in Appendix 2C.

Most of the results fell within the range suggested by Bradshaw and Gregory, all the points being above the lower limit of $yu_{\tau}/\nu = 2$ or $y^{*} = 0$, and only a few of the higher h values falling above the upper limit of $yu_{\tau}/\nu = 30$ or $y^{*} = 2.352$ (see Fig. 14).

The graph showing the effect of changing Δx, (the degree to which the Stanton tube knife edge covers the pressure hole) is shown in Fig. 15. This stresses the importance of the knife edge covering the hole, otherwise errors of between 5-8% may result in the values of y^{*}.

5.04 Leading Edge Effects

As can be seen in Fig. 3A, the front of the Sindanyo frame was left deliberately square in order to promote turbulence. Normally of course x would be measured from the leading edge of the plate, where the boundary layer starts to form; having a blunt leading edge however does give rise to considerable uncertainty regarding the datum for x.

The graphs of C_{fx} against R_x for different positions of x should of course fall on a single curve if the flat plate had a sharp leading edge. Measuring the distance from the blunt leading edge results in a different curve for each value of x see Fig. 16. In view of this it was decided to adopt Dutton's[18] procedure and plot C_{fx} versus R_{θ}.

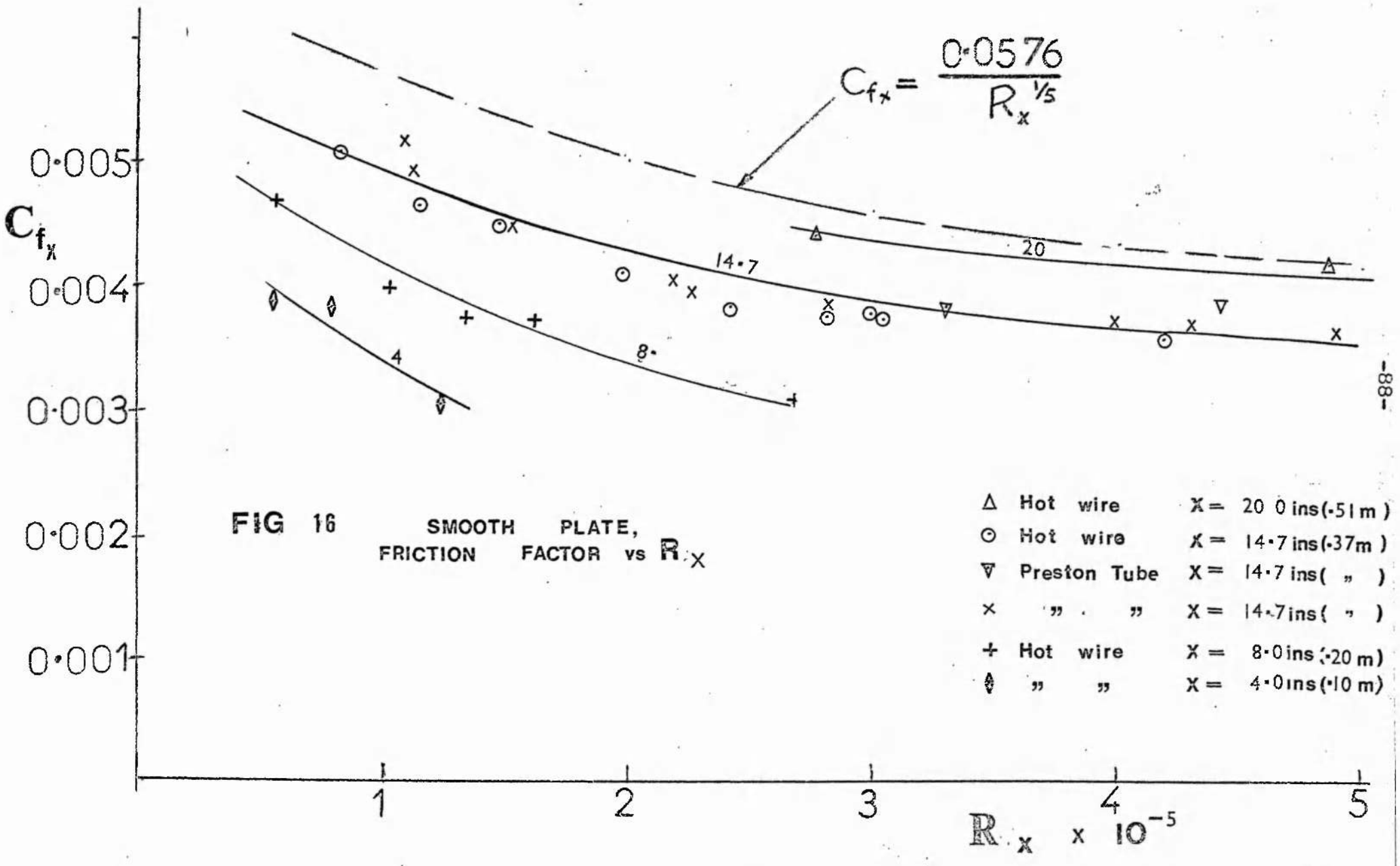

FIG 16 SMOOTH PLATE, FRICTION FACTOR vs R_x

This results in a single curve irrespective of the value of x, and this method of plotting is used from henceforth for smooth and rough surfaces.

Further reference is made to this effect of the blunt leading edge, and its effect on turbulence patterns in Chapter 8. An average drag law for a blunt-edged flat smooth plate, suitable for designers, utilising the smooth plate results from Table 1 and Fig. 16 is also presented in para. 8.02.

5.05 Momentum Thickness and Shape Factor

It is obvious from the previous paragraph that momentum thickness must be calculated for most of the hot wire results shown in Table 1 in order to obtain R_θ. Also the confirmation of the skin friction results referred to in paragraph 4.07 using equation (4.07..5) requires θ to be known, consequently the procedure referred to in para. 4.11. has been used to obtain θ and δ^* using the computer program shown in Appendix 5.

The graph of C_{fx} against R_θ in Fig. 18 shows a single curve for all values of x, unlike the relationship between C_{fx} and R_x in Fig. 16.

A typical graph showing the relationship between R_x and R_θ for two values of x is shown in Fig. 17, this clearly indicates an almost linear relationship between the two quantities. All these results, together with the two values of C_{fx} obtained by the different methods are included in Table 2A. The values of C_{fx} obtained from θ are in very close agreement with the value obtained relying on the law of the wall. (i.e. Bradshaw or Clauser technique).

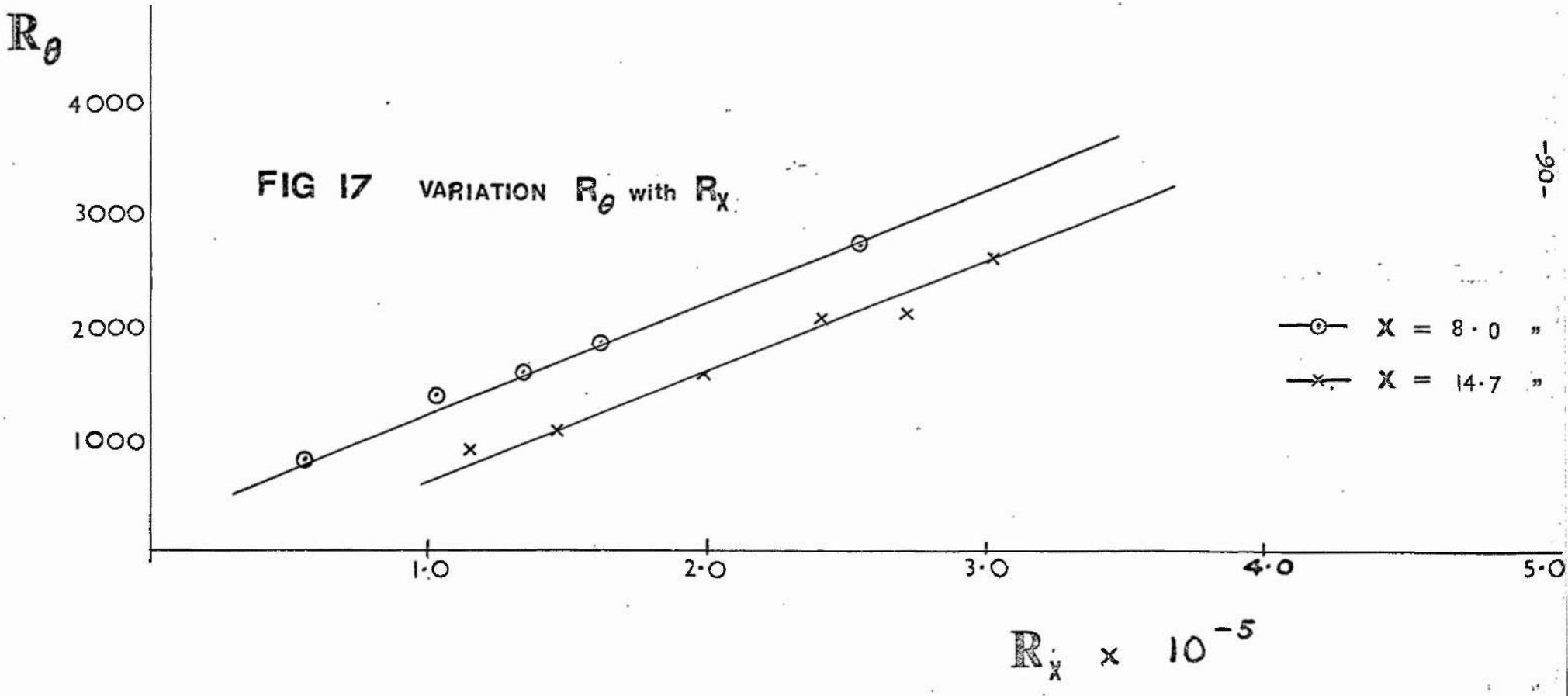

FIG 17 VARIATION R_θ with R_X

TABLE 2 A

SKIN FRICTION AND

MOMENTUM THICKNESS RESULTS

(para. 5.05 and Fig. 18)

(A) Smooth Plate

x in	U ft/s	ν ft^2/s	δ^* in	θ in	Cf_x	Cf_θ*	R_x	R_θ	H
14.7	10.52	0.0001600	0.224	0.138	0.00510	0.00490	80600	755	1.62
"	14.58	0.0001575	0.215	0.117	0.00465	0.00465	115100	915	1.76
"	18.90	0.0001575	0.203	0.110	0.00450	0.00446	147000	1098	1.75
"	25.60	0.0001575	0.210	0.115	0.00410	0.00406	199100	1567	1.82
"	31.50	0.0001600	0.160	0.123	0.00380	0.00381	242000	2026	1.29
"	35.10	0.0001575	0.197	0.109	0.00377	0.00380	273000	2028	1.80
"	40.00	0.0001615	0.160	0.122	0.00376	0.00360	303400	2568	1.29
8.0	13.52	0.0001610	0.204	0.117	0.00470	0.00478	56000	823	1.73
"	24.77	0.0001610	0.175	0.108	0.00400	0.00410	103000	1386	1.62
"	32.90	0.0001630	0.136	0.093	0.00378	0.00400	134500	1576	1.45
"	39.70	0.0001630	0.129	0.091	0.00375	0.00390	162200	1843	1.42
"	64.60	0.0001610	0.190	0.128	0.00320	0.00318	268000	4300	1.48
4.0	59.60	0.0001605	0.190	0.098	0.00310	0.00330	123700	3056	1.93
"	38.60	0.0001630	0.174	0.103	0.00388	0.00381	77600	2047	1.68
"	26.52	0.0001605	0.142	0.080	0.00390	0.00400	54500	1153	1.70
12.0	45.40	0.0001655	0.147	0.110	0.00370	0.00360	274300	2552	1.31
20.0	47.00	0.0001605	0.116	0.077	0.00440	0.00447	275290	1069	1.50

* Derived from Equation (4.07..5) using θ.

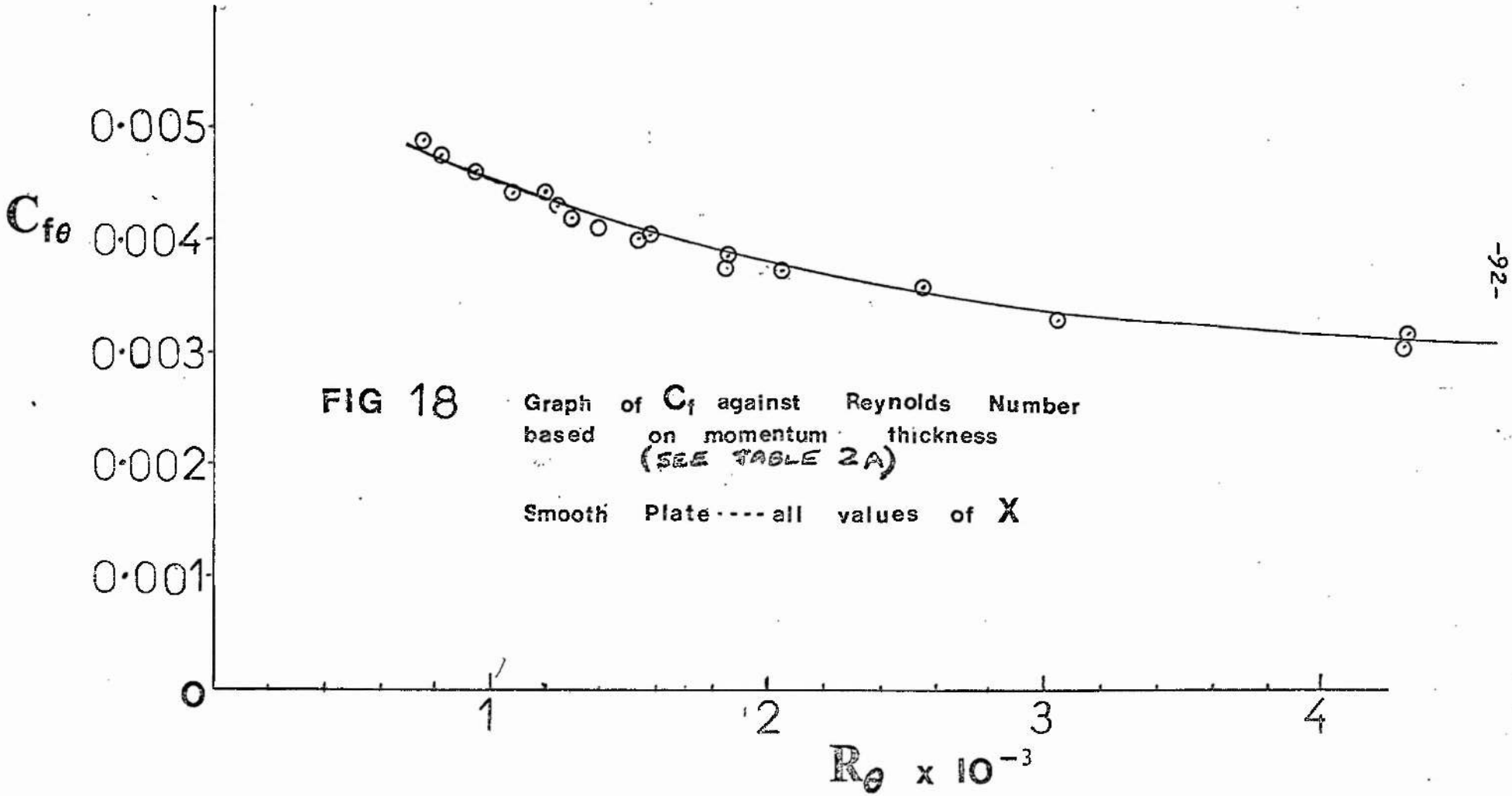

FIG 18 Graph of C_f against Reynolds Number based on momentum thickness (SEE TABLE 2A)

Smooth Plate ---- all values of X

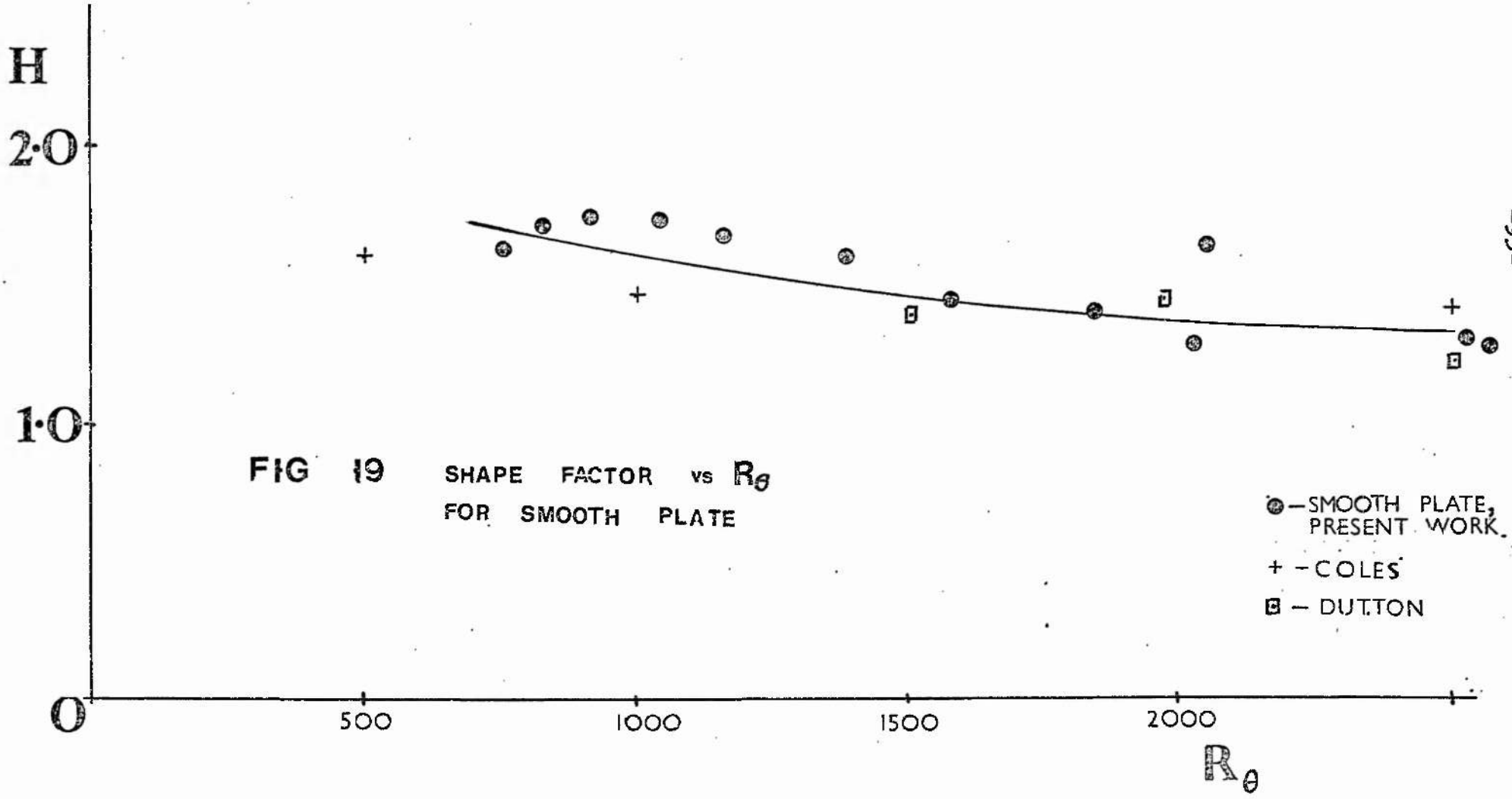

FIG 19 SHAPE FACTOR vs R_θ FOR SMOOTH PLATE

Dutton [17] and Head [28] suggested that where the velocity defect law, and the law of the wall overlap, a suitable common parameter to both laws is the shape factor H. In Fig. 19 shape factors H found from the present results are plotted against R_θ. Although the results are subject to a fair amount of scatter they are seen to agree favourably with those of Dutton and other workers especially in the range $1000 < R_\theta < 2500$.

5.06 Velocity Profile Laws

All the hot wire results for the smooth plate shown in Table 3A have been plotted on axes of U^+ versus $\text{Log}_e y^+$ in Fig. 20, where $U^+ = u/u_\tau = (u/U).(U/u_\tau) = u/U.\sqrt{2/C_{fx}}$ and $y^+ = (yu_\tau/\nu) = (yU/\nu) \cdot (u_\tau/U) = (yU/\nu).\sqrt{C_{fx}/2}$. the values in Table 3A have been selected from the hot wire velocity profiles so as to encompass as wide a range of U and x as possible. The large majority of the points fall on a straight line irrespective of the value of x. By the method of least squares the slope of this line was found to be 2.5 suggesting a value of 0.4 for the constant K, and an intercept B of 5.5. The results shown in Fig. 20, clearly indicate the accuracy of the method adopted; only two points falling slightly below the upper limit for the transition region of $yu_\tau/\nu = 30$.

An alternative form of velocity profile plot, but rather more cumbersome is the defect-velocity profile method due to Clauser [9] referred to in para. 4.02. this curve is obtained by plotting $\frac{u-U}{u_\tau}$ against $\frac{y}{\delta^*}\sqrt{\frac{C_f}{2}}$ and can be seen plotted in Fig. 21.

This was introduced as a means of checking the skin friction results and comparing with Brun and Plum [7]. A specimen calculation is shown in Appendix 2 section E.

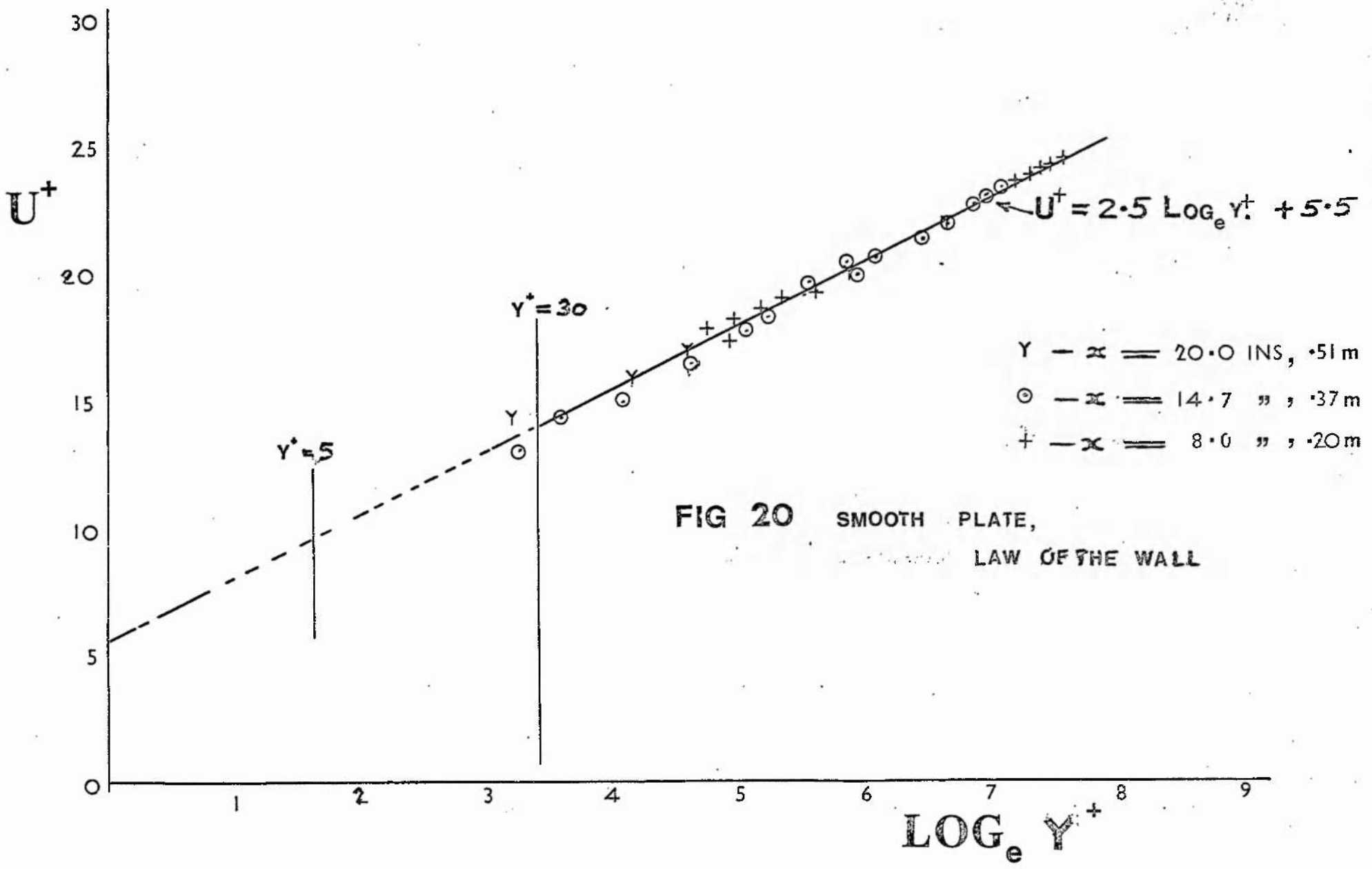

FIG 20 SMOOTH PLATE,
LAW OF THE WALL

TABLE 3A

LAW OF THE WALL PLOT
(para. 5.06) - results plotted on Fig. 20

Smooth Plate

x ins.	U/u_τ	U^+	y ins.	$\text{Log}_e yU/\nu$	$\text{Log}_e y^+$
14.7	20.40	20.40	1.30	8.88	5.86
14.7	20.40	19.60	0.95	8.55	5.53
14.7	20.40	19.10	0.80	8.36	5.34
14.7	20.40	18.20	0.70	8.26	5.23
14.7	20.40	17.60	0.60	8.10	5.08
14.7	20.40	16.30	0.40	7.61	4.61
14.7	20.40	14.90	0.20	7.10	4.08
14.7	20.40	14.50	0.15	6.70	3.72
14.7	20.40	12.95	0.10	6.30	3.28
14.7	23.00	23.00	1.40	10.10	6.95
14.7	22.90	22.90	1.30	9.96	6.83
14.7	22.90	22.00	1.10	9.76	6.63
14.7	22.40	22.00	1.00	9.50	6.40
14.7	22.40	20.60	0.90	9.20	6.10
14.7	22.40	18.80	0.40	8.45	5.35
8.0	24.50	24.50	1.40	10.80	7.59
8.0	24.50	24.19	1.30	10.70	7.48
8.0	24.50	24.00	1.20	10.60	7.40
8.0	24.50	23.80	1.10	10.50	7.31
8.0	24.50	23.60	1.00	10.40	7.20
8.0	24.50	23.30	0.90	10.30	7.10
8.0	24.50	22.90	0.80	10.20	7.00
8.0	24.50	21.32	0.50	9.70	6.51
8.0	24.50	17.17	0.10	8.10	4.91
8.0	22.95	17.40	0.19	8.06	4.93
8.0	22.95	15.40	0.07	7.05	3.92
20.0	21.30	20.80	0.80	9.27	6.21
20.0	21.30	20.20	0.60	8.95	5.89
20.0	21.30	17.00	0.20	7.65	4.59
20.0	21.30	14.50	0.05	6.24	3.18
1	2	3	4	5	6

Columns 1, 2, 4 are experimental data.
" 3, 5, 6 calculated by computer.

Brun and Plum [7] claim that results for smooth and rough surfaces fall on the same curve. The law of the wall for rough surfaces is very dependent on the intercept B as was shown in para. 4.09. Each type of roughness having a unique value of B (see para. 6.02). The defect profile method of Clauser, although it requires knowledge of δ^* has the advantage that all values whether for rough or smooth when plotted fall on a single curve, since none of the variables depend on the intercept B.

The results obtained, although subject to a fair amount of scatter do tend to confirm Brun and Plum's findings, which are also shown in Fig. 21.

This defect profile method of Clauser must not be confused with the Clauser tracing-paper overlay method which requires prior knowledge of the law of the wall.

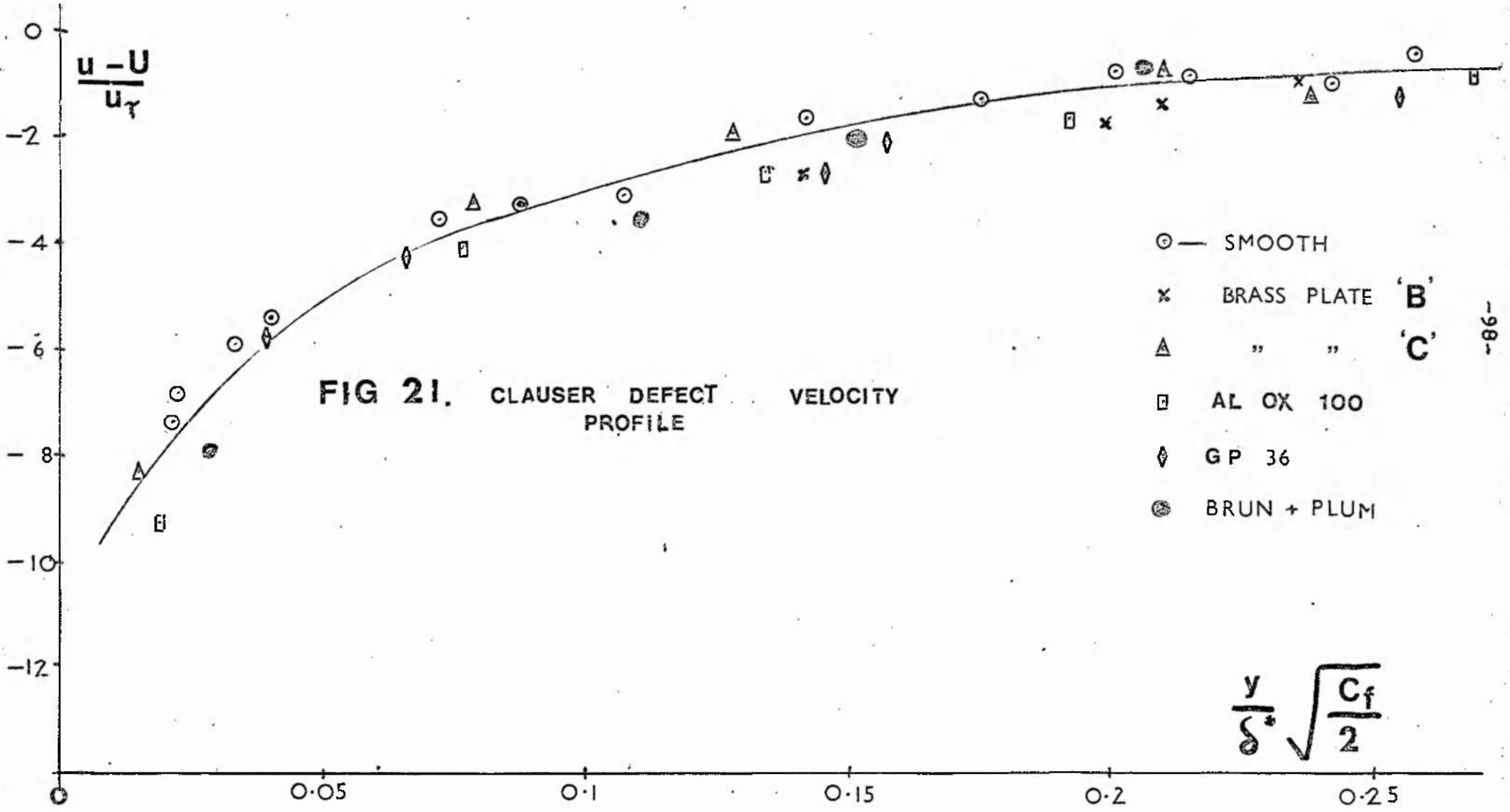

FIG 21. CLAUSER DEFECT VELOCITY PROFILE

CHAPTER 6 ROUGH PLATES - EXPERIMENTAL RESULTS & COMPUTATIONS

The methods used for obtaining skin friction for smooth surfaces outlined previously cannot all be employed on rough surfaces. The main technique used throughout the present work for rough surfaces has been the Clauser method, making use of the fact that the slope in the law of the wall equation is independent of roughness. (see para. 4.09).

Additional work has been performed using the Stanton tube on rough surfaces, and further work on the boundary layer shape factor H, and its relation to R_θ is presented. All the results of skin friction, and momentum thickness θ, measurements, are presented in Tables 2B and 2C. All the rough plate results were taken at the station x = 1.380 ft. (0.36 m).

6.01 Clauser Grid Method

The technique employed by Bradshaw for the determination of C_{fx} is obviously not applicable to rough surfaces since the constant B varies with roughness.

The hot wire data and experimental results were processed by computer (Appendix 4 Program 2). Using the computer plotter a plot of u/U against $\text{Log}_e(y\ U/\nu)$ was obtained in the customary Clauser manner. A maximum family of six curves could be plotted although it was found advisable to avoid too many sets of points, and usually only three were plotted on the one axis at a time in order to avoid confusion.

The Clauser grid plotted as shown in Fig. 11 but on tracing paper using $u/u_\tau = 2.5\ \mathrm{Log}_e(yu_\tau/\nu)+5.5$ may be used to determine the slope of the data points (and hence U/u_τ) by adjusting the position of the tracing paper overlay until the experimental points coincide with the grid. This procedure has been referred to in para. 4.07 and relies only on the slope of the law of the wall equation.

6.02 Intercept B

The skin friction results using the Clauser method for rough surfaces are given in tabular form in Table 2B and Table 2C, and are shown graphically in Fig. 22 in the usual law of the wall format. The law of the wall results used to plot Fig. 22 are given in Table 3B, and have been derived in the following manner from the velocity profile data to give as wide a range of U^+ and $\mathrm{Log}_e\ y^+$ as possible. Now $U^+ = (u/U).(U/u_\tau)$ was readily derived once u/U was known, and U/u_τ obtained from the tracing paper overlay,

hence $$\mathrm{Log}_e\ y^+ = \mathrm{Log}_e\left(\frac{y\ U}{\nu}\right) - \mathrm{Log}_e\left(\frac{U}{u_\tau}\right)$$

$\mathrm{Log}_e\ (yU/\nu)$ was obtained directly from the computer program.

The rapid decrease in the value of the intercept B as the roughness increases is clearly demonstrated. Nikuradse [40] defining a roughness Reynolds number R_r based on sand particle size K_s, as $(K_s\ u_\tau/\nu)$, states that the transition from the smooth to the fully rough condition extends over the range $5 < R_r < 70$. The degree to which the roughness elements protrude through the laminar sub-layer governs the value of R_r; when all the roughness projections have penetrated into the turbulent region the surface can be described as fully rough, and the friction factor C_{fx} is independent of the value of the local Reynolds number R_x. When the roughness elements all fall below the laminar sub-layer the surface is termed hydraulically smooth and B = 5.5.

TABLE 2 B

SKIN FRICTION AND

MOMENTUM THICKNESS RESULTS

(B) Sand Blasted Surfaces

x = 1.380 ft.

Type	N	U ft/s	ν ft^2/s	δ^* in	θ in	Cf_x	R_x	R_θ	H
'C'	300	7.18	0.0001614	0.183	0.114	0.00570	61400	421	1.61
"	600	22.97	0.0001616	0.160	0.107	0.00420	196140	1275	1.50
"	900	36.40	0.0001605	0.139	0.097	0.00394	312975	1843	1.43
"	1250	49.38	0.0001636	0.116	0.077	0.00380	416400	1944	1.49
"	1650	60.25	0.0001622	0.120	0.087	0.00347	512600	2500	1.48
"	1760	68.77	0.0001636	0.178	0.125	0.00314	580052	4401	1.42
'B'	740	23.64	0.0001622	0.194	0.145	0.00414	201129	1763	1.33
"	860	34.87	0.0001582	0.169	0.116	0.00396	304175	2136	1.45
"	1180	45.31	0.0001612	0.132	0.090	0.00396	387889	2111	1.47
"	1450	55.61	0.0001622	0.127	0.089	0.00378	473130	2568	1.42
"	1740	65.42	0.0001631	0.168	0.120	0.00347	553520	4026	1.39
"									

TABLE 2 C

(C) Abrasive Paper Surfaces

x = 1.380 ft.

Type	N	U	ν ft^2/s	δ^*	θ	Cf_x	R_x	R_θ	H
AL	300	8.46	0.0001559	0.169	0.103	0.00830	74937	465	1.64
OX	600	19.86	0.0001557			0.00670	176019		
	1100	36.46	0.0001587	0.144	0.102	0.00617	317056	1952	1.42
Grade	1400	45.31	0.0001561	0.115	0.075	0.00617	400425	1812	1.54
100	1500	50.68	0.0001626			0.0060	430144		
	1600	52.68	0.0001589	0.121	0.081	0.00594	457380	2237	1.50
Glass	1900	67.26	0.0001571	0.170	0.103	0.00890	590844	3670	1.65
Paper	1450	48.49	0.0001571	0.186	0.116	0.00920	425992	3000	1.60
Grade	1000	33.34	0.0001571	0.216	0.134	0.0102	292905	2373	1.61
36									

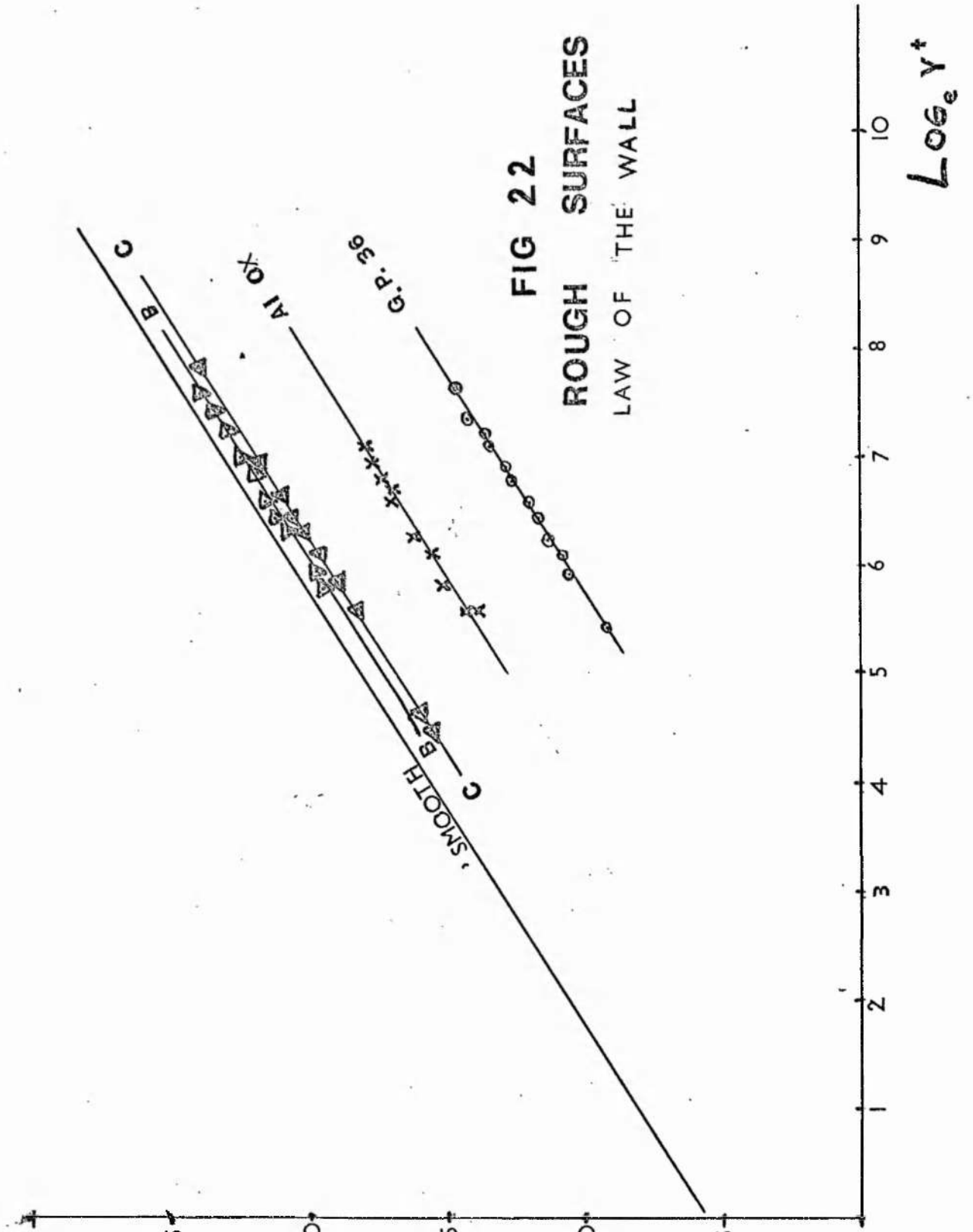

FIG 22

ROUGH SURFACES

LAW OF THE WALL

TABLE 3B

LAW OF THE WALL PLOT see (FIG. 22.)
(Para. 6.02)

Rough Surfaces x = 1.380 ft.

Surface	U/u_τ	U^+	y ins	$\text{Log}_e yU/\nu$	$\text{Log}_e y^+$
Sand Blasted Brass Plate 'B'	24	23.90	1.40	10.75	7.57
	24	23.40	1.20	10.59	7.41
	23	22.70	1.10	10.35	7.22
	23	22.30	0.90	10.15	7.02
	23	21.20	0.50	9.56	6.43
	22½	21.80	0.90	9.95	6.84
	22½	21.50	0.70	9.70	6.59
	22½	20.70	0.60	9.45	6.34
	22	19.75	0.70	9.04	5.95
	22	19.30	0.60	8.89	5.80
Sand Blasted Brass Plate 'C'	18	13.79	0.20	6.60	3.70
	18	16.15	0.50	7.52	4.62
	18	18.25	1.30	8.48	5.58
	21	19.11	0.50	8.68	5.82
	21	19.76	0.80	9.15	6.11
	22	21.90	0.90	9.74	6.64
	22	20.80	0.40	9.50	6.37
	24	15.75	0.06	7.65	4.47
	24	21.90	0.50	9.77	6.92
	24	24.10	0.70	10.10	7.81
Abrasive Paper (Aluminium Oxide) Grade 100	18½	18.10	0.70	10.00	7.08
	18½	17.80	0.60	9.84	6.92
	18½	15.35	0.20	8.75	5.83
	18	17.50	0.60	9.71	6.80
	18	17.13	0.60	9.58	6.69
	18	16.31	0.50	9.16	6.27
	18	15.15	0.30	8.65	5.76
	18	17.50	0.60	9.71	6.80
	17	17.15	1.20	9.45	6.60
	15½	14.40	0.90	8.31	5.57
Abrasive Paper (Glass Paper) Grade 36	14	13.69	1.10	9.87	7.23
	14	12.90	0.80	9.55	6.91
	14	11.76	0.50	9.08	6.44
	14	10.71	0.30	8.57	5.93
	14	14.40	1.30	10.04	7.35
	14	13.51	0.70	9.79	7.10
	14	13.15	0.60	9.64	6.95
	14	12.05	0.40	9.23	6.54
	15	14.71	0.90	10.37	7.66
	15	10.98	0.20	8.87	6.16
	15	9.28	0.10	8.17	5.46

The sand-blasted surfaces fall just outside the hydraulically smooth region and are just in the transition region. The glass paper surface GP 36 falls in the fully rough region where B = -4.23. The limits of B corresponding to the values of R_r quoted above are 5.5 and -2.11.

Nikuradse's roughness function F_r defined in equation (2.03..1) is linked to the intercept B by the following relationship $F_r = 2.5 \text{ Log}_e R_r + B$

...(6.02..1)

This relationship is considered in more detail in para.6.04.

6.03 Stanton-Tube Results

The same technique as described in para. 5.03 for Stanton-tubes on smooth surfaces has been applied to the sand-blasted plates, and the same computer program used. (see flow diagram Fig. 10).

Two values of h were used with the 'C' surface, and only one with the 'B' surface, the two graphs BB and CC can be seen in Fig. 23. The fact that C_{fx} is slightly different is because the surface is rough (see Fig. A3, this no doubt accounts for the slight change in intercept of y^*, due to variation of u_τ, (approximately 5% difference in y^*).

The relationship between x^* and y^* was expressed as a polynomial; the standard Fortran polynomial regression program (POLRG) being used to obtain the necessary regression coefficients, but is not included in this thesis. The range of y^*, and the given polynomial equations can be seen in Appendix 2C, and show that the rough plate calibrations shown in Fig.23 almost coincide with the smooth plate ones.

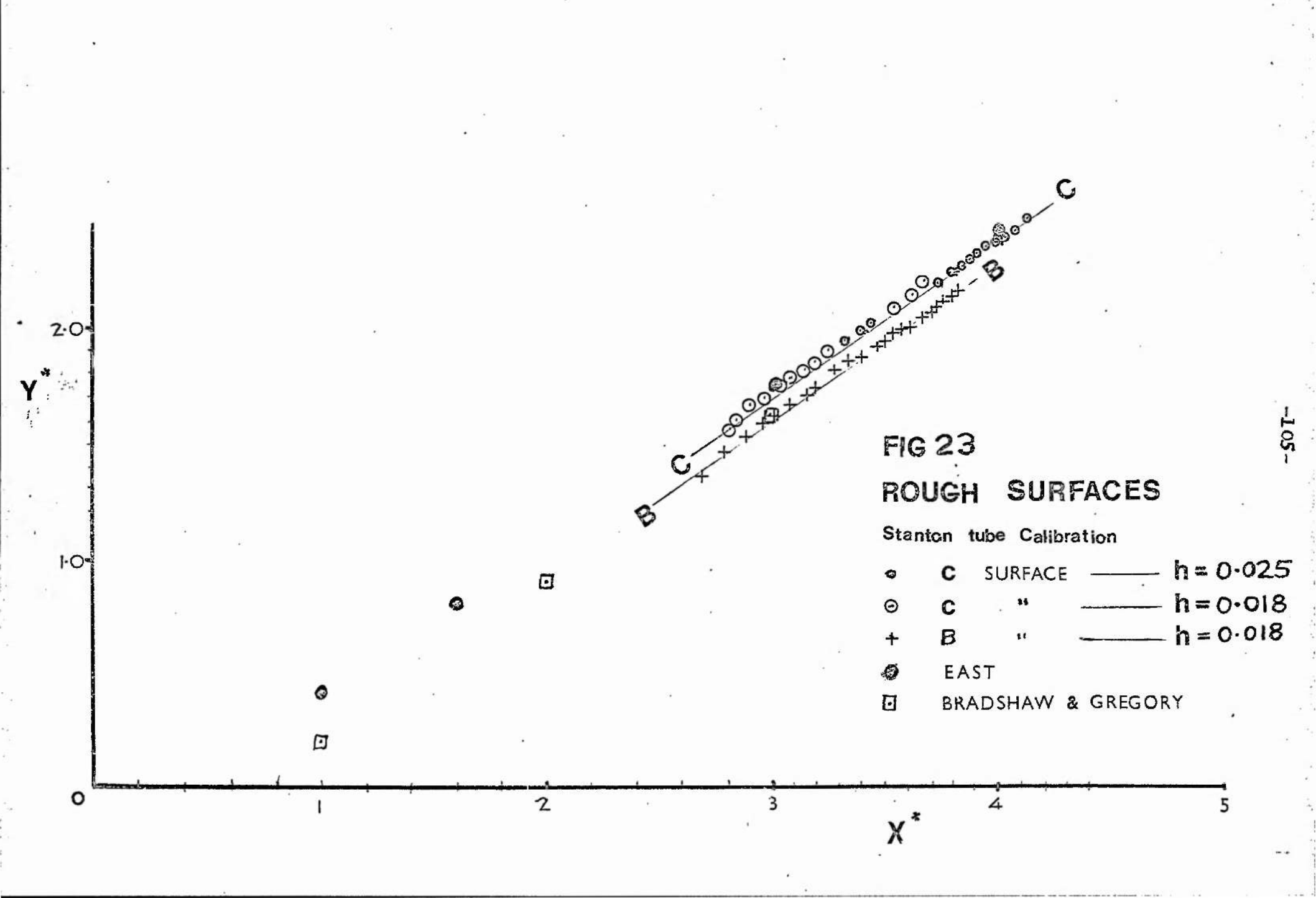
C
B
B
C
2·0
1·0
0
Y*
1
2
3
4
5
X*
FIG 23
ROUGH SURFACES
Stanton tube Calibration
C SURFACE —— h = 0·025
C " —— h = 0·018
B " —— h = 0·018
EAST
BRADSHAW & GREGORY

Due to the difficulty in accurately defining the height h it was not possible to use the Stanton tubes on any rougher surfaces, however these results suggest that the use of such a Stanton tube on rough surfaces similar to the shot-blasted ones used here is quite feasible.

6.04 Assessment of Sand Particle Size

As outlined in para. 4.09, R_r is the primary parameter for all types of roughness. The sand particle size K_s as defined by Nikuradse [40] already referred to in para. 2.03 must therefore be found no matter what type the surface roughness is, if similarity laws are to be followed. Schlichting [46] shows the relationship between various artificial roughness elements, and the sand particle size, however little is known about sand blasted surfaces or abrasive paper surfaces. An arbitrary relationship must therefore be found between the actual roughness height K, and K_s. The centre line average value was used as a roughness value for the brass plates, but for the abrasive paper surfaces manufacturers grit size was chosen as the measure of roughness.

Streeter [47] in his work on rough pipes using internal spirally-cut grooves as the roughness elements refers to values of between 7 and 9 for the ratio of K_s/K; these however appear rather high when compared with Forster's[24] figure of about 1.5 for emery paper fixed to steam turbine blades. It should be pointed out however that Forster was dealing with greater values of Reynolds number based on exit velocity and axial width of blade.

As can be seen in the diagram, a step is formed by the abrasive paper which is stuck on the brass plate. This must result in a step change in surface roughness at the leading edge, which according to Antonia and Luxton [1] could result in greater friction values downstream. Dryden[13] also suggested that an allowance should be made for paper thickness when estimating K_s.

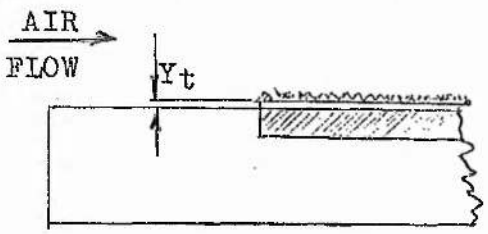

The roughness Reynolds number R_r can only be determined with any degree of confidence when the fully rough condition is satisfied; under these conditions Nikuradse [40] showed that the roughness function F_r (from equation 2.03..1) was equal to 8.5.

Consequently :-

$$U^+ = 2.5\ Log_e(y/K_s) + F_r = 2.5\ Log_e(yu_\tau/\nu) + B$$

$$\therefore \quad F_r = 8.5 = 2.5\ Log_e\ R_r + B$$

$$\therefore \quad 8.5 = 2.5\ Log_e\ R_r + B \qquad \ldots(6.04..1)$$

hence if B is known from the inner law graph i.e. Fig.22, R_r can be obtained as can K_s since $R_r = u_\tau K_s/\nu$.

Considering the above factors, and utilising equation (6.04..1) for the fully rough condition, the following empirical relationship has been obtained between actual grit size K and the Nikuradse sand particle size K_s for use in the intermediate roughness range as defined by $5 < R_r < 70$.

$$K_s = 5.0\ K + y_t \qquad \ldots(6.04..2)$$

where y_t = the abrasive paper thickness.

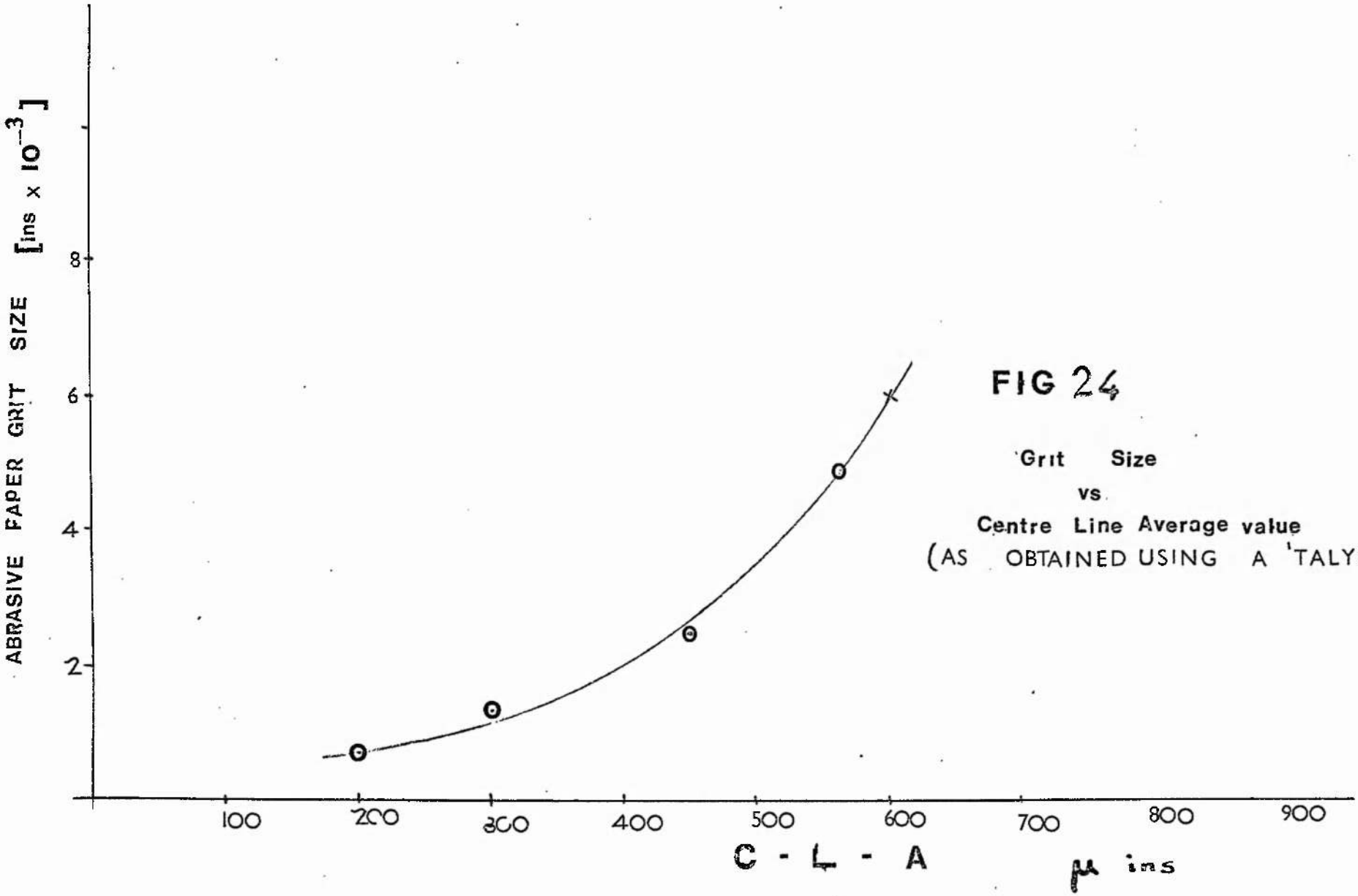

FIG 24

'Grit Size
vs
Centre Line Average value
(AS OBTAINED USING A 'TALYSURF')

The Talysurf readings can naturally only be used on fairly smooth surfaces i.e. less than 600 μ ins. CLA. In Fig. 24 the relationship between actual particle size and CLA values is plotted. This graph has been compiled with the aid of the F.E.P.A. handbook, some results of Forster, and Talysurf measurements and these are shown in Table 4.

The Talysurf is not a means of truly identifying roughness metrology. The geometry and distribution of the asperity heights must be allowed for in any assessment of roughness. A.J.Hunter [34] states that a Talysurf can only be used on isotropic roughness; even so the stylus cannot give a true impression, as it cannot penetrate to the bottom of the valleys. Professor Halling [27] states that it is even quite possible for two surfaces to have the same CLA value but vastly different physical appearances.

The question of roughness texture, and metrology, and the consequent value of K_s will be discussed further in Chapter 8.

6.05 Comparison of Roughness Results

Using the relationship (6.04..2) K_s, and subsequently R_r were obtained for the full range of rough surfaces used; the results can be seen in Table 5.

It has already been shown in para. 4.09 that the intercept B is a function of roughness. From equation 6.04..1 taking $F_r = 8.5$ (Nikuradse [40]) and the lower limit for the fully rough condition as $R_r = 70$ (Schlichting [46] page 557) then $B = -2.11$.

TABLE 4

ABRASIVE PAPER GRADES AND PARTICLE SIZE

Grade	I		II		III	
	µm	thou	µm	thou	µm	thou
36	422	16.6	425		425	16.6
60	251	9.9	250		212	
80		7.0	180	7.1	150	5.9
100	152	6.0	150	5.9	125	4.9
120	124	4.9			106	
220					63	2.5
240	64	2.5			45	1.77
320					29	1.15
400					17	0.67
600					9	0.35

I British Standard 872

II Federation of European Abrasive Manufacturers Handbook.

III F.E.P.A. Graph.

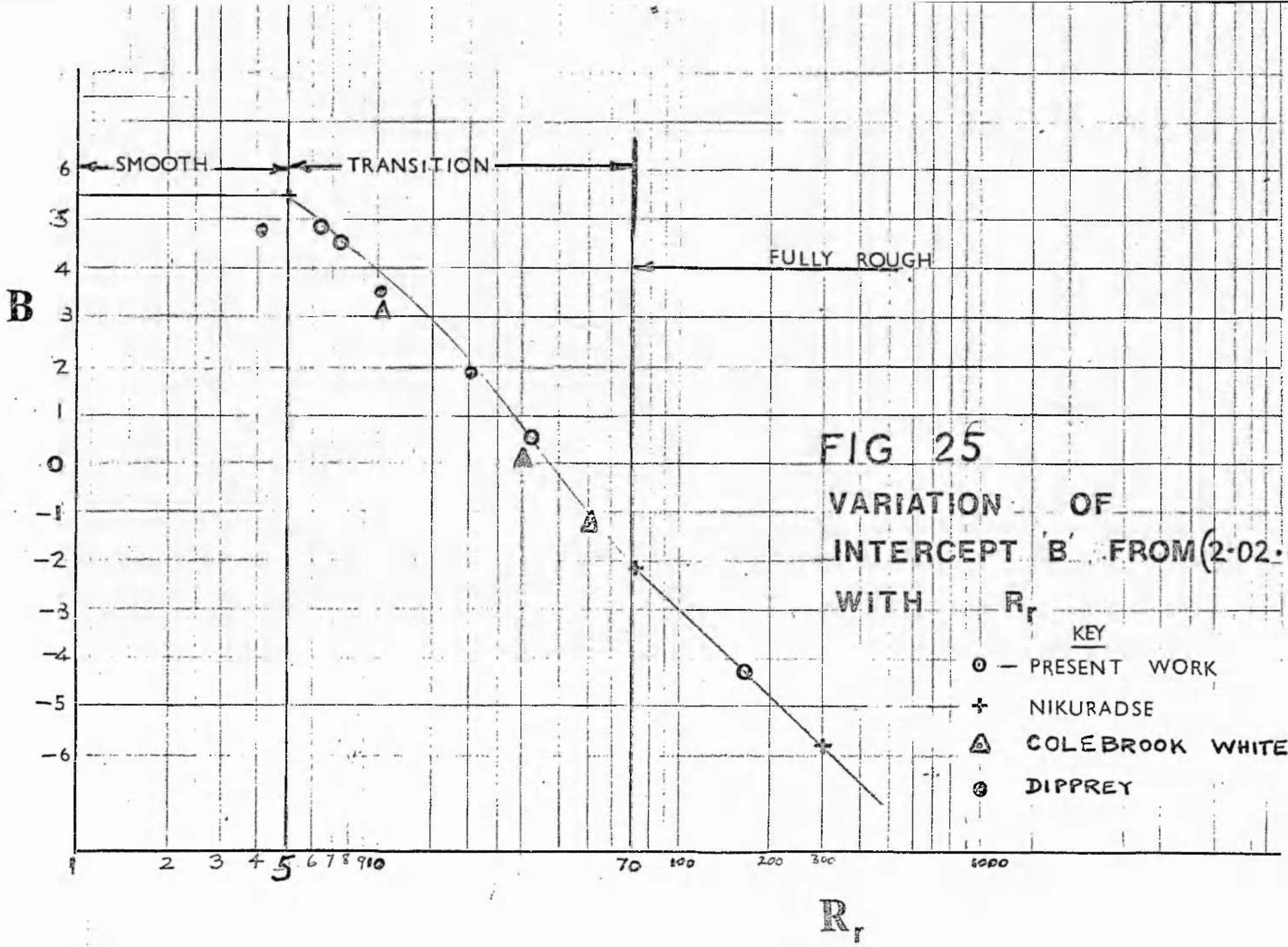
SMOOTH
TRANSITION
FULLY ROUGH
B
6
5
4
3
2
1
0
−1
−2
−3
−4
−5
−6
2
3
4
5
6
7
8
9
10
70
100
200
300
5000
R_r
FIG 25
VARIATION OF INTERCEPT 'B' FROM (2·02·2) WITH R_r
KEY
PRESENT WORK
NIKURADSE
COLEBROOK WHITE
DIPPREY

TABLE 5

LAW OF THE WALL AND ROUGHNESS REYNOLDS NUMBER

$U^+ = 1/k \text{ Log}_e y^+ + B$, or $U^+ = 1/k \text{ Log}_e (y^+, G)$ (see equation 2.03..5)

Surface	Paper yt	CLA† μ in	K in	K_s in	R_r	F_r	B	G
‡Transition Range					5	9.53	5.5	9.05
					70	8.5	-2.11	0.431
Glass Paper 36	0.045	—	0.017	0.1300	165	8.5	-4.23	0.184
Al. Oxide 100	0.021	600	0.006	0.0510	32	9.02	0.52	1.231
'C'	—	250	0.001	0.0050	7.4	9.5	4.5	6.05
'B'	—	210	0.0009	0.0045	6.3	9.35	4.8	6.8

† Obtained by Talysurf.

‡ Nikuradse [40].

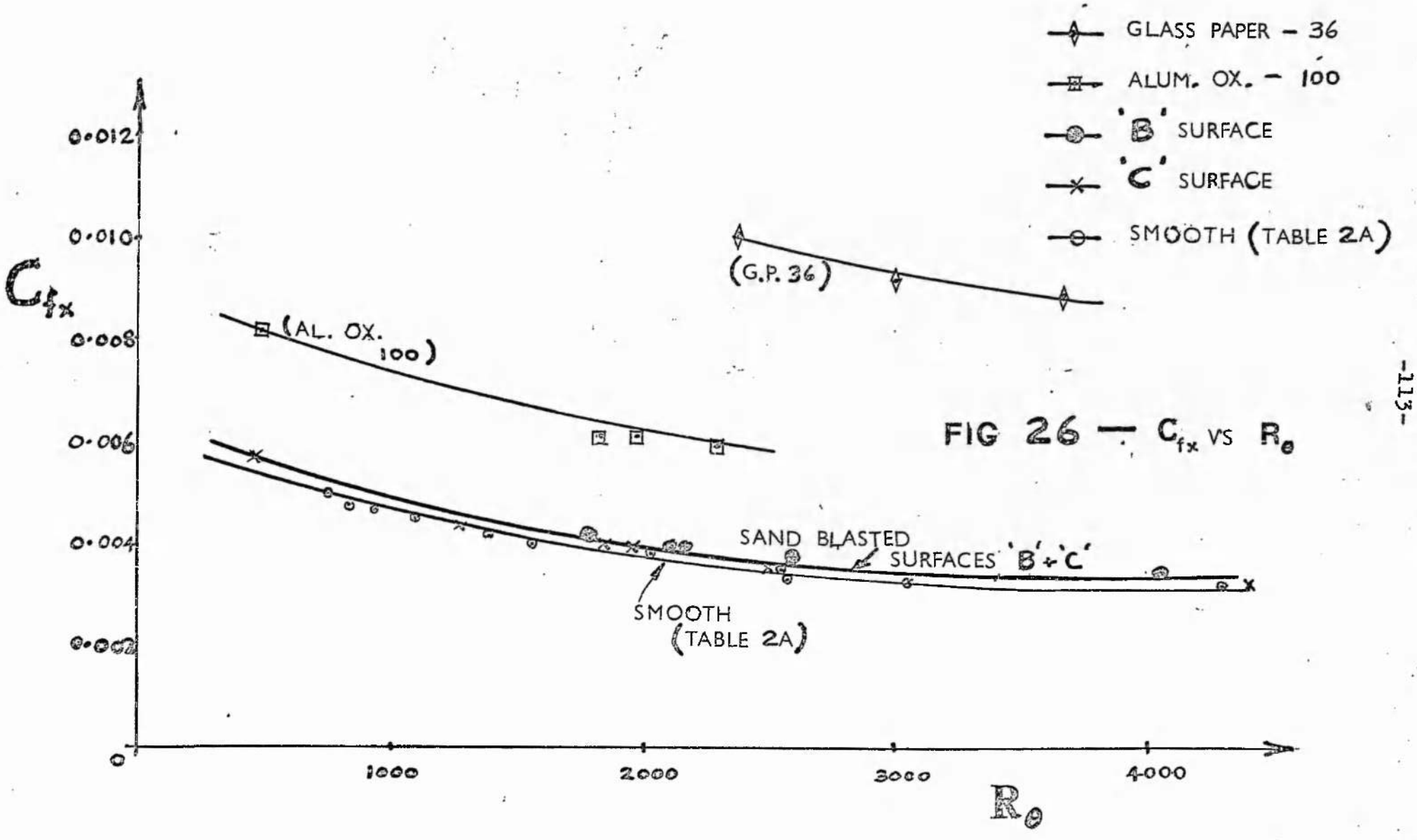

FIG 26 — C_{fx} VS R_θ

Hence when intercept B is less than -2.11 the surface is defined as being fully rough, above this value the roughness is usually taken to be in the transition range. An inspection of Table 5 indicates that most of the rough surfaces fall in this transition range, except for glass paper of Grade 36 which is clearly fully rough.

The graph of intercept B against R_r (Fig. 25) tends to confirm that in the intermediate range ($5 < R_r < 70$) the relationship is non linear whereas in the smooth, and fully rough zones this relationship is linear. This is in good agreement with the findings of Jayatillaka [35], and also Rotta[45] (page 77) etc., some of whose results regarding the linear relationship in the fully rough region are shown in Fig. 25. For the hydraulically-smooth condition, B assumes the generally accepted value of 5.5 until R_r is greater than 5.

Nikuradse's roughness function F_r in equation 2.03..1 is shown plotted against R_r in Fig. 27. Close agreement with Dipprey and Sabersky[12], and also with Nikuradse [40] can be observed. The maximum value of F_r being 9.5 coming slightly after the value $R_r = 8$, and corresponding to the sand-blasted 'C' surface.

The universal velocity distribution plot suggested by Nikuradse for rough surfaces is shown in Figs. 28A and 28B. Fig. 28A shows the abrasive paper results together with the values of F_r obtained from the intercept, and Fig. 28B shows the sand-blasted plate relationships.

A graphical relationship between the universal velocity distribution law of Nikuradse, and the law of the wall equation is shown in Fig. 29 for glass paper Grade 36.

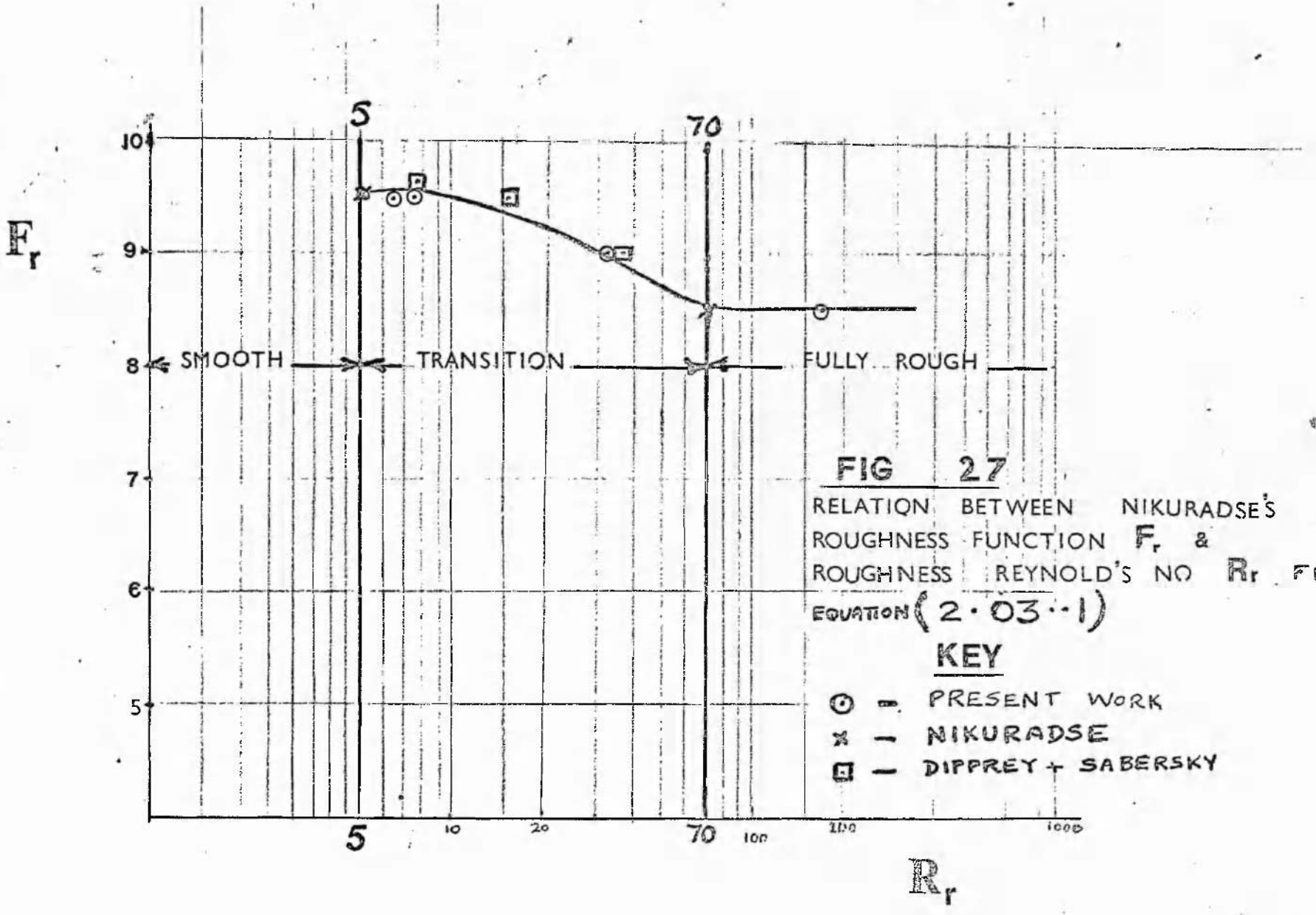

FIG 27

RELATION BETWEEN NIKURADSE'S ROUGHNESS FUNCTION F_r & ROUGHNESS REYNOLD'S NO R_r FROM EQUATION (2·03·1)

KEY

⊙ — PRESENT WORK

× — NIKURADSE

⊡ — DIPPREY + SABERSKY

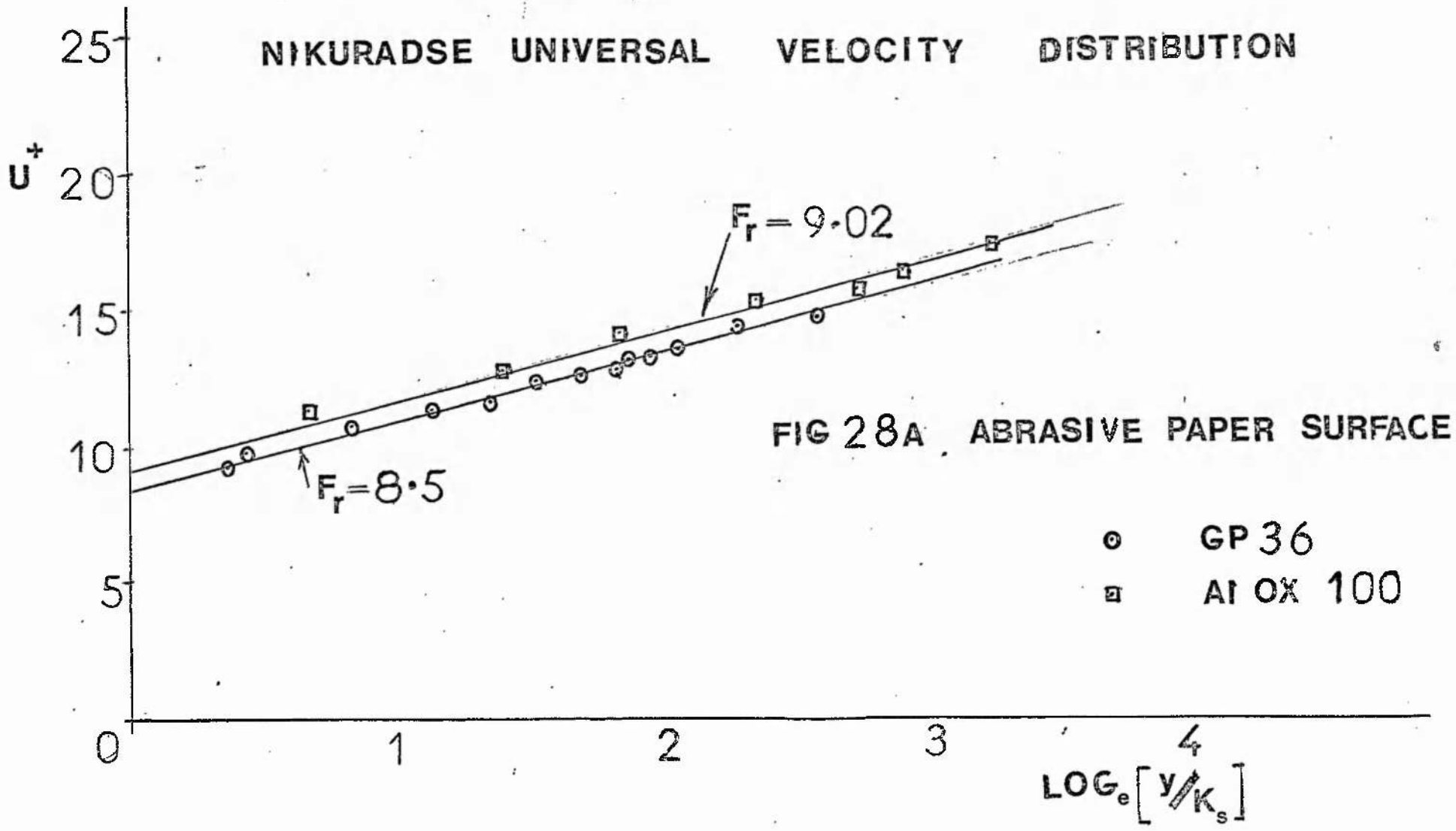

FIG 28A ABRASIVE PAPER SURFACE

For a given value of U^+ it is evident that the horizontal distance between the two lines is a direct measure of $\text{Log}_e R_r$, although this method was not used to obtain the values of R_r in Table 5.

6.06 Shape Factor and Momentum Thickness

The values of momentum thickness θ, and shape factor etc., for the rough surfaces shown in Table 2B have been calculated from the velocity profile using the polynomial regression program, and the momentum thickness program Appendix 5 Program 3, the procedure is shown graphically in the flow diagram Fig. 10.

Friction factor C_{fx} has been plotted against R_θ in Fig. 26, for the reason given in para.5.04 and consists of a family of curves each curve being for a particular roughness. A similar family of curves shown in Fig.30 indicates that in general H increases as R_θ decreases for a particular type of surface. However as roughness increases each curve shifts slightly upwards; this fact is reinforced by the C_{fx} vs R_θ graph (Fig. 26) which also follows a similar pattern.

This could possibly have been predicted from the momentum integral equation (4.02..1). It has been established that the relationship between C_{fx} and R_θ for rough plates takes the form $C_{fx} = \text{const}/R_\theta^{\,n}$, similar to that for a smooth plate in equation (4.07..5) Clauser [9] states that increasing roughness has the effect of making the velocity profile much fuller and consequently increasing θ and H, Dutton[17] has also confirmed this.

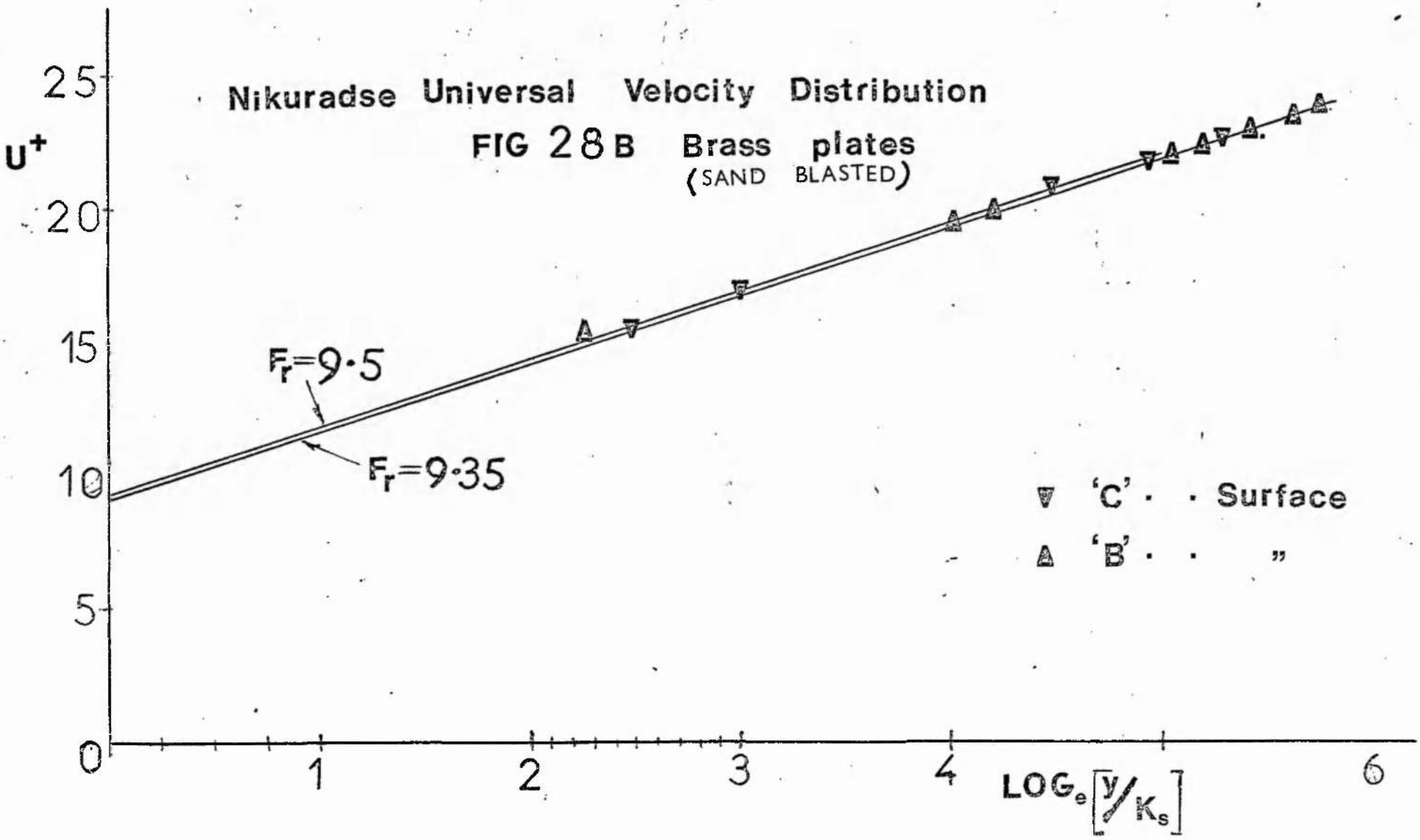
Nikuradse Universal Velocity Distribution
FIG 28 B Brass plates
(SAND BLASTED)
U^+
25
20
15
10
5
0
1
2
3
4
6
$LOG_e\left[\frac{y}{K_s}\right]$
$F_r=9\cdot5$
$F_r=9\cdot35$
'C' · · Surface
'B' · · "

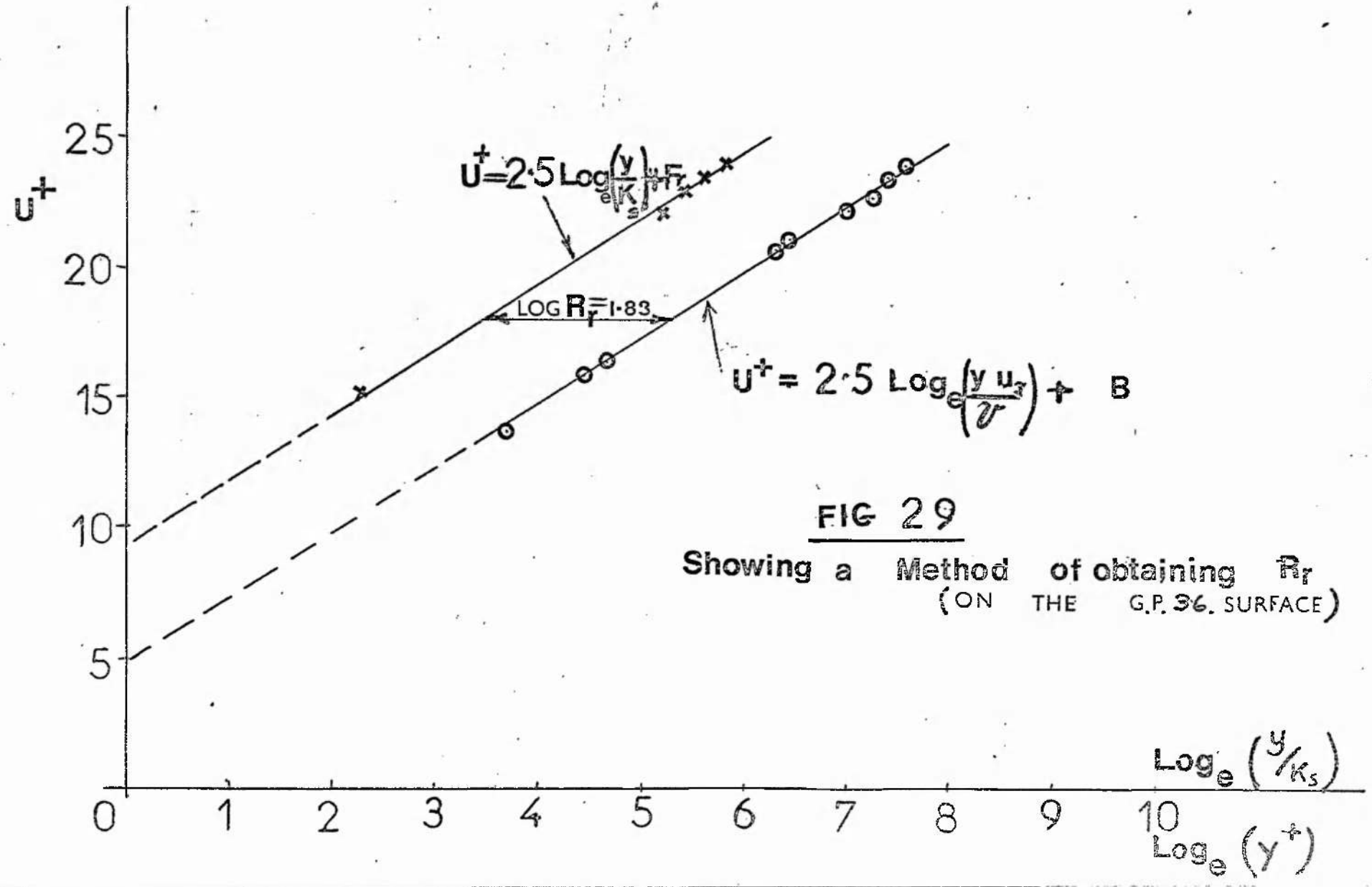

FIG 29

Showing a Method of obtaining R_r (ON THE G.P. 36. SURFACE)

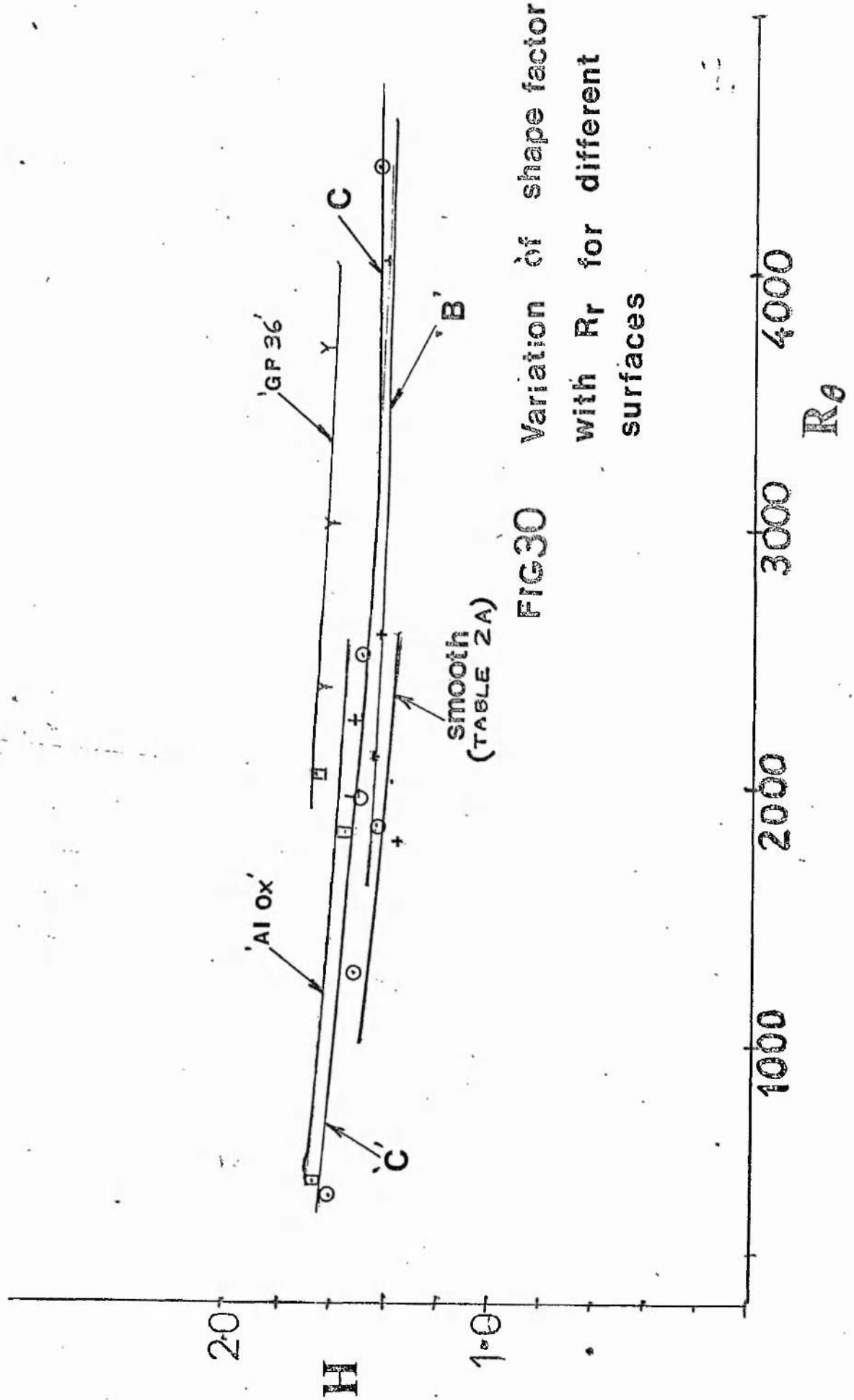

FIG 30 Variation of shape factor with R_r for different surfaces

CHAPTER 7 TURBULENCE EFFECTS

7.01 Turbulence Profile from the Wall

Fig. 12 shows a typical curve showing turbulence intensity variation inwards towards the wall. Substantial work already exists showing this effect notably by such workers as Laufer, Klebanoff and Bradshaw to mention just a few. For this reason little has been done along these lines in this investigation.

7.02 Axial Effect along the Wall at Constant Values of y

Using the sand-blasted surface 'B' and with a constant mainstream velocity of 50 ft/s (15.5 m/s), an axial traverse was carried out for five constant y values. Readings being taken of bridge voltage, and RMS voltage at four measuring stations. The resulting graphs of turbulence intensity against x are shown in Fig. 31.

It is apparent that the blunt edge of the Sindanyo frame has a more pronounced effect on turbulence close to the plate., this is particularly noticeable at the front 3 ins. (76 mm) station. All values of y chosen show that 'I' diminishes as x increases.

Steep rises occur between the 8 and 3 ins. measuring positions, but after 10 ins. very little effect is evident. The large turbulence effect due to the front edge only lasts therefore until about half way along the plate when the calmer, more stable conditions prevail. This effect of the blunt leading edge is discussed further in Chapter 8.

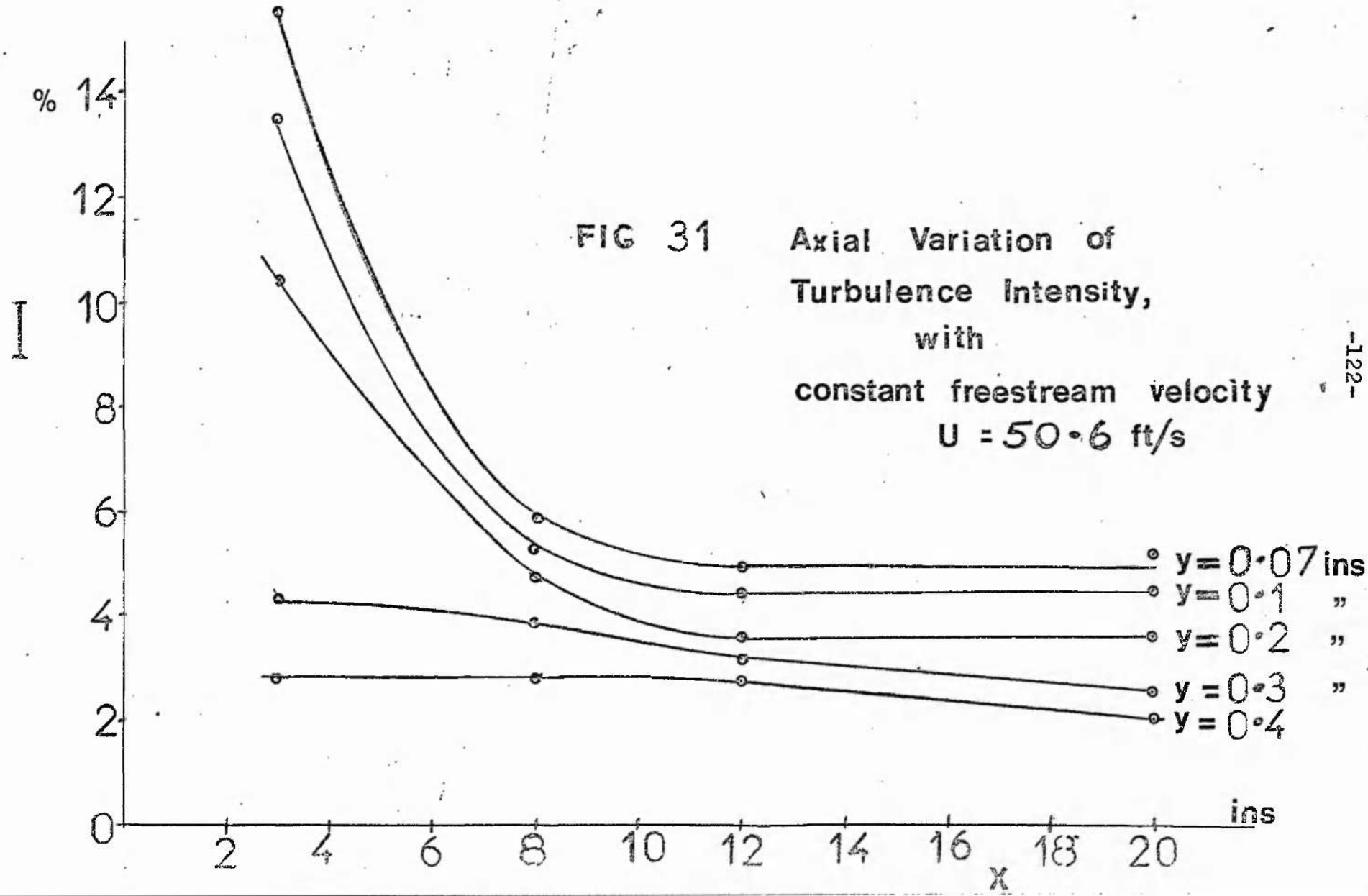

FIG 31 Axial Variation of Turbulence Intensity, with constant freestream velocity U = 50·6 ft/s

It is fortunate that most of the skin friction measurements were taken at stations where x is in excess of 12 ins.

7.03 Effect of Roughness

To ascertain the possible effect that the surface roughness has on turbulence intensity measurements, the following procedure was adopted. The free stream turbulence was measured for four values of flow rate at a position of ½ in. (12.5 mm) in front of the Sindanyo frame.

For the various surfaces considered turbulence intensity 'I' was measured at the trailing edge of each plate and at a height y = 0.2 in. (5.1 mm) from the plate for each value of flow rate shown in Fig.32.

The results for turbulence intensity 'I' and the differing rough surfaces are presented as a series of histograms see Fig. 32. The greater the roughness, the greater turbulence intensity becomes; this is especially apparent at higher velocities. It is hoped eventually and subsequent to the present work to be able to formulate a mathematical model which correlates roughness and turbulence intensity.

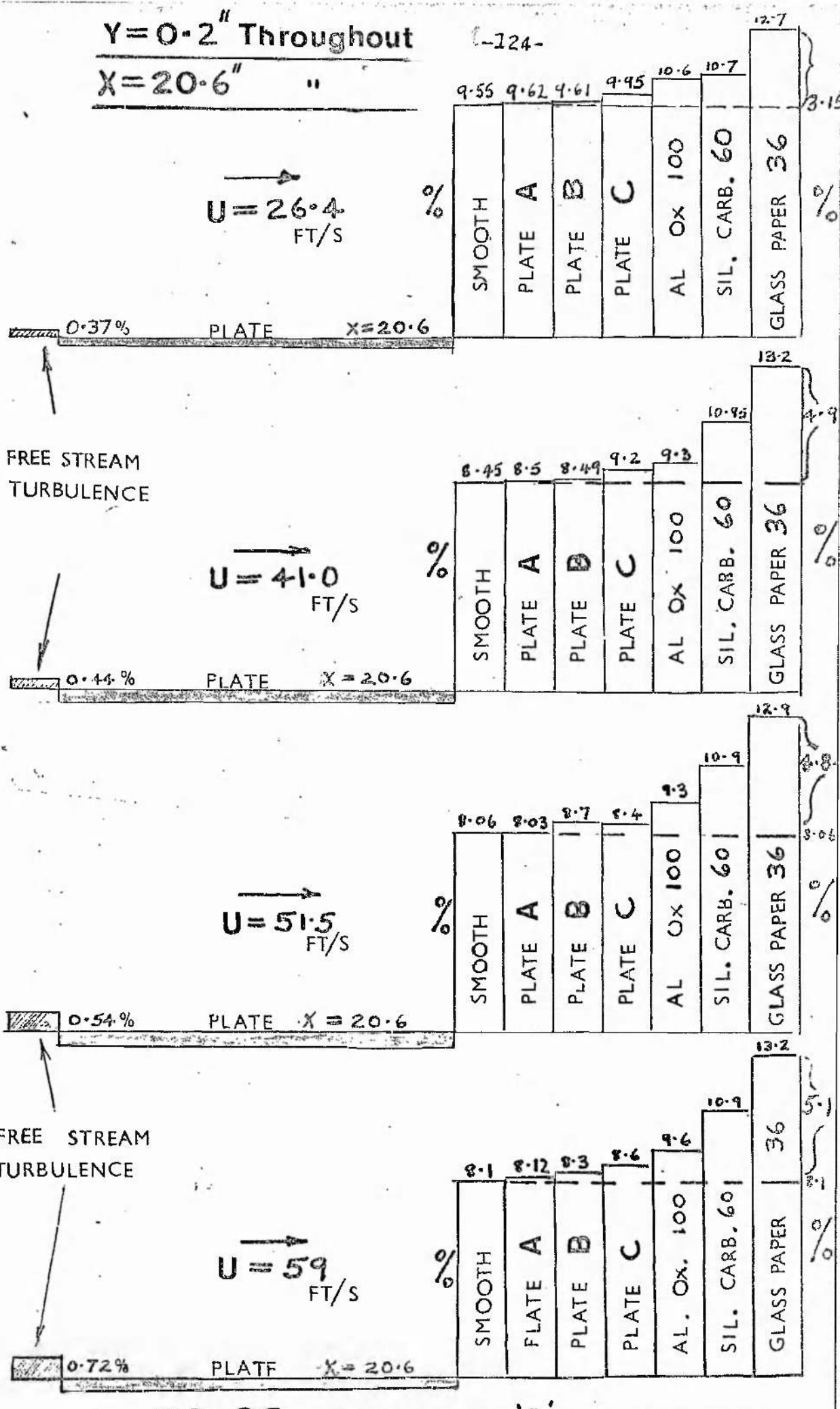

FIG 32. VARIATION OF 'I' WITH ROUGHNESS

CHAPTER 8 DISCUSSION

In this chapter one or two general topics arising from the project, as well as sources of error, and the final conclusions regarding this research are discussed.

8.01 Sources of Error

The errors arising from the project can be classified into two groups; mainly errors in physical measurements, and errors in theoretical computations.

(a) Errors in Physical Measurements

(1) The measurements of pressure difference on the inclined manometer could be liable to some error. MacMillan [39] gives details of techniques used to render liquid manometers more sensitive. As the manometer used for the Stanton tube readings was a commercial one from 'Airflow Developments'; most of these pitfalls had been overcome. It was thought prudent however to allow 7 - 8 minutes to elapse before recording any readings. The tubes between the manometer and the pressure taps on the brass plates were of $\frac{1}{8}$ in. bore except where they passed in the Sindanyo frame when they became approximately 0.125 in. (2 mm) inside diameter. If the maximum error in measuring pressure on the 0 - $\frac{1}{2}$ in. scale was 0.005 in. water, which is half the least count of the scale then the maximum possible error at 0.1 in. water would be of the order $\pm$ 5%.

(2) Defining the distance y measured from the wall could be difficult in some situations, particularly with an abrasive paper surface. The technique of using the dummy probe has already been described, however when this probe gauge rests on the surface and the zero

is obtained it amounts to y being measured from the peaks of the roughness elements. Possibly y should be defined so as to include the paper thickness, and the grit size.

The maximum amount of free movement on the traversing equipment was found to be $\pm$ 0.004 in. (0.1 mm) which at a value of y = 0.1 in. (2.54 mm) would cause an error of 4%.

(3) Errors can arise due to the vibrations of hot wire anemometer filaments. Perry and Morrison [42] refer to errors which can arise either by vibration due to fluctuating aerodynamic loads, or forced vibrations due to vibrations of the wind tunnel. Turbulence readings may be in error by as much as 50% because of filament vibration. As the dangerous region for vibrations referred to by Perry and Morrison (High level - narrow band turbulence) where frequencies are in excess of 4kHz was found to be well outside the range of these tests it was considered that errors due to vibrations would be negligible.

(4) Errors in obtaining kinematic viscosity ν using the Sutherland formula could arise if an error in temperature, or atmospheric pressure arose. Suppose an error of $\pm$ 0.5°C, which represents the maximum conceivable error in reading the thermometer, occurred, this would only cause an error of 0.6% in ν when using the Sutherland formula. Atmospheric pressure measurement using a Fortin's barometer is very reliable and accurate, and can be discounted as a source of error.

(5) Another source of error should not be overlooked, and that is the question of static pressure taps protruding above the surface of the plates.

Zogg and Thoman [50] state that a protruding pressure tap records a lower pressure than the true wall static pressure; in spite of this they obtained close agreement to Preston's calibration for Preston tubes. In the case of the Stanton tubes great care was exercised to maintain a completely flat surface on the brass plate. Hypodermic needle tubing was used for these pressure taps, and a metal plate with a dial gauge ensured that these did not project above the working surface.

(6) The assessment of roughness is open to some sources of error, particularly the use of a roughness meter. Several Talysurf readings had to be taken to obtain a representative value. Readings deviated by as much as 12%.

The grit size as specified by the abrasive paper manufacturers was however more reliable, as strict limits on the mesh sizes are laid down in B.S. 872, and most manufacturers recognise these limits.

(b) Errors in Theoretical Computations

(1) The assumption that the constant K in the law of the wall equation remains constant for varying degrees of roughness has been clearly demonstrated in para. 4.09. This of course is assumed when using the Clauser grid for rough surfaces. Bradshaw and Huffman [33] point out that it may vary by as much as 3% for very low flows. In spite of this, the technique appears to give satisfactory results, and can be used over a wide range of Reynolds number. Possibly the very low flows may be open to error, but for the faster velocities it remains valid.

(2) In using the Bradshaw method which requires the location of intersection of the given velocity profile with the law of the wall equation (refer computer graph Appendix 3 Program 1) a slight error might arise in obtaining the correct value of u/U. Suppose due to uncertainty about the path of the velocity profile through the experimental points an error in u/U of $\pm$ 0.05 occurred. This would represent a substantial error in assessing u/U, normally one would expect greater accuracy; however such an error in u/U would only cause a final error in local friction factor C_{fx} of $\pm$ 1.6%. Since this method relies on an intersection it is more accurate than other methods which require a gradient to be measured.

(3) The Clauser grid procedure is not quite as accurate as the method of Bradshaw. Referring to the grid on Fig. 11 it might be possible to misjudge the gradient of the profile, and obtain an error U/u_τ of $\pm$ 0.5, suppose this occurred at a value of U/u_τ = 20, then the error in the value of friction factor would be $\pm$ 5%. This error would increase, as U/u_τ decreased, however with steeper gradients on the grid the likelihood of making such an error becomes less probable.

8.02 General Comments

(a) Leading Edge

The rapid rise in turbulence intensity close to the blunt leading edge (Fig. 31) may influence local skin friction results to some extent. Dutton [16] states that for normal flow with zero pressure gradient along a flat plate an allowance for turbulence of 2% of $C_{fx}/2$ should be made. With the high figures of 12 - 14% shown in Fig. 31 the values of skin friction close to the leading edge must be somewhat suspect.

Reference was made in para. 5.04 to the family of curves shown in Fig. 16 for each value of x; the explanation given about the uncertainty of the datum for x accounts for much of this, but the question of artificially induced turbulence by the leading edge should also be included.

The effect of a blunt leading edge must frequently occur in practice, and it is for this reason that an average drag law including results that may be useful to designers was developed. For a flat plate at zero incidence the friction factor is usually derived from $C_{fx} = \frac{0.0576}{(R_x)^{1/5}}$, this can be modified to include distance ratio(x/L)such that

$$C_{fx} = f\left[(R_x), \left(\frac{x}{L}\right)^N\right]$$

The value of the index N was obtained by plotting Log C_{fx} versus Log(x/L)using the results given in Table 6 Fig. 33., for a given value of R_x.

As can be seen all curves have the same slope of N = 0.3.

hence local $C_{fx} = \frac{0.0576}{(R_x)^{1/5}} \cdot \left(\frac{x}{L}\right)^{0.3}$ ...(8.02..1)

Considering the plate as a whole

$$\bar{C}_f = \frac{1}{L}\int_0^L C_{fx}\, dx$$

$$= \frac{1}{L}\int_0^L \frac{0.0576}{\left(\frac{x\,U}{\nu}\right)^{1/5}}\left(\frac{x}{L}\right)^{0.3} dx$$

$$= \underline{0.0524 \cdot R_L^{-1/5}} \qquad \ldots(8.02..2)$$

This is an average drag law for a blunt-edged flat smooth plate with free stream turbulence in the range 0.1 to 0.8%.

FIG 33

LOG PLOT C_{f_x} vs (x/L)

FOR VARIOUS R_x

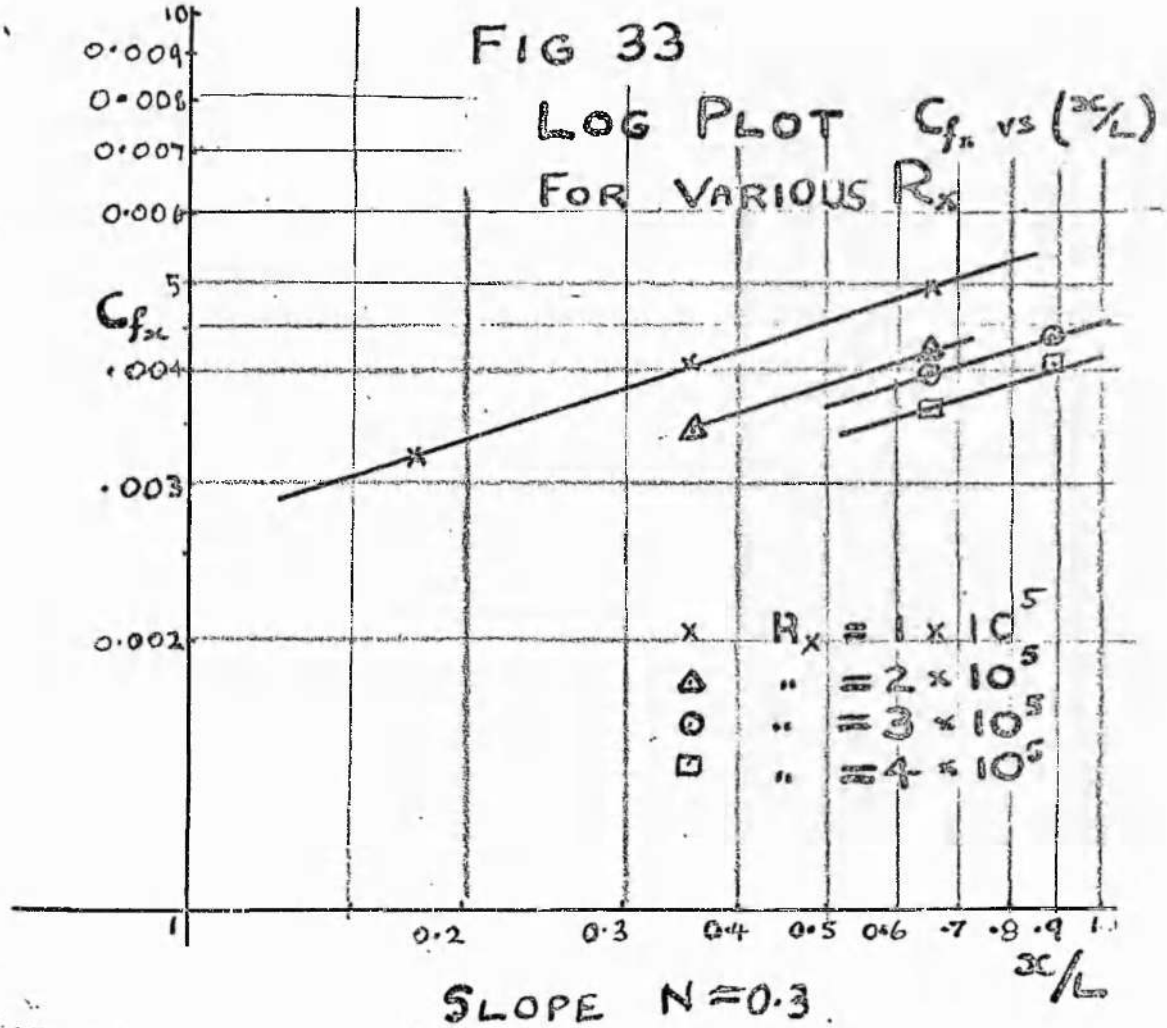

SLOPE $N = 0.3$

TABLE 6.

$\frac{x}{L}$	C_{f_x} for given R_x			
	1×10^5	2×10^5	3×10^5	4×10^5
·178	0·0033			
·356	0·0041	0·0033		
·653	0·0049	0·0042	0·0039	0·0036
			0·0043	0·0041

(b) Velocity Defect Law

The reasons why this method was not generally adopted was discussed in paragraphs 4.07 and 5.02. Such a method could apply to both rough, and smooth surfaces, but in fact the Clauser method appears to be more reliable since it does not require the local boundary layer height δ to be obtained, and relies solely on the law of the wall.

The universal defect-velocity profile as advocated by Clauser does however seem to be a useful means of plotting both smooth, and rough plate results on a single curve; it also has the additional advantage of being applicable in adverse pressure gradients where other methods are not valid.

8.03 Objectives Fulfilled

The aims of the project as listed in para. 1.02 can now be discussed.

(1) The Stanton tubes developed from laminated shim steel appear to give consistent results. Unfortunately it does not appear practical to use them on very rough surfaces, but for measurements on moderately rough surfaces of less than 300 μ inches CLA no difficulty should be experienced.

(2) The results shown in Fig. 25 show how varying R_r affects the intercept B. Further values of intermediate roughness would clarify the position regarding the transition region. The empirical relationship between the actual grit size and the Nikuradse sand particle size K_s appears to agree well with other workers, however further work needs to be done to establish a more formal relationship.

(3) The turbulence intensity 'I' results show positively (a) how turbulence varies along the axis of the plate and (b) how increasing roughness causes increasing values of 'I'. Ultimately perhaps a more mathematical correlation might be arrived at.

(4) Momentum thickness and shape factor results indicate that definite relationships exist between boundary layer and roughness parameters.

The objectives mentioned in para. 1.02 have been fulfilled, but it is obvious that further work of a mathematical nature needs to be carried out at a later date.

8.04 Conclusions

Bradshaw's method for determining friction factor on smooth surfaces appears to be a very reliable and quick method provided that one assumes prior knowledge of the law of the wall, the results agree very well with those derived from momentum thickness.

The Clauser grid technique, using tracing paper provides a quick means of obtaining friction factor on rough surfaces, and is to be advocated.

The only drawback to having a blunt leading edge on the Sindanyo frame is in the precise definition of x, and the high turbulence promoted; however if Reynolds number is based on momentum thickness no trouble should be experienced. Extensive use of computer techniques are essential for obtaining all the required results listed.

CHAPTER 9 FUTURE WORK

9.01 Surface Pitot Tube

The ultimate intention of the author, is to develop a Stanton tube which can be used easily on either rough, or smooth surfaces, requiring only a simple calibration. A format similar to Head and Ram[30] seems to obviate some of the calculations normally encountered. It must be stressed that such a Stanton tube should be constructed so that it complies with the limits $u_\tau h/\nu$ ascribed by Bradshaw and Gregory[6].

It would be a step forward if the pressure tap holes could be dispensed with, and the output could be an electrical signal from a special transducer. This may not however be possible on account of electronic limitations.

9.02 Surface Texture

Further work on roughness geometry, and texture is obviously needed. The shape of grain, and the type of abrasive may affect the value of K_s.

A technique for assessing roughness, other than by a Talysurf is of paramount importance, possibly the light scattering method as discussed by Edwin [20] could be usefully employed.

9.03 Heat Transfer

Reference has already been made to extending this work to include heat transfer. Provision was made for a heating element to be fitted between the brass plates, and no great difficulties can be foreseen.

REFERENCES

1 ANTONIA, R.A. and LUXTON,R.E. 'Response of a Turbulent Boundary Layer to a step change in Surface Roughness'. Pt.2 Rough to Smooth
J. Fluid Mech. 53. Jan 1972 pp 737-757.

2 ARNI,V.R.S. and MYERS,J.E. 'Effects of Internal Roughness on Pressure Drop and Heat Transfer of Integral Finned Tubes'.
Refr. Eng. July 1953 p 757.

3 BRADSHAW,P. 'A Simple Method for Determining Turbulent Skin Friction from Velocity Profiles'.
J. Aero Sc. Vol 26 1959 p 841.

4 BRADSHAW,P. 'The Effect of Wind Tunnel Screens on Nominally Two Dimensional Boundary Layers'.
J. Fluid Mech. Vol 22-24 1965 pp 679-687.

5 BRADSHAW,P. 'The Turbulent Structure of Equilibrium Boundary Layers'.
J. Fluid Mech. Vol 29 1967 p 625.

6 BRADSHAW.P. and GREGORY,N. 'The Determination of Local Turbulent Skin Friction from Observations in the Viscous Sub Layer'.
R&M 3202 March 1959.

7 BRUN,E.A. and PLUM,H. 'Etude Experimentale d'une couche limit le long d'un plaque rugueuse'.
CNRS. No. 53 1960.

8 BRUNELLO,G. 'Contribution A L'etude de la Convection Forcee de la Chaleur sur des Parois Rugueuses'.
Publications Scientifiques et Techniques. No. 332 1957.

9 CLAUSER,F.H. 'Turbulent Boundary Layer in Adverse Pressure Gradient'.
J. Aero Sc Feb 1954 pp 91-108.

10 COLEBROOK,C.F. 'Turbulent Flow in Pipes with particular reference to the Transition Region between Smooth and Rough Pipe laws'.
J. Inst Civ Eng. Paper 5204 1939.

11 COPE.W.F. 'Friction and Heat Transmission Coefficients of Rough Pipes'.
Proc I Mech E. Vol 145 1941 pp 99-105.

12 DIPPREY,D.F. and SABERSKY,R.H. 'Heat and Momentum Transfer in Smooth and Rough Tubes at various Prandtl Numbers'.
Int J. of Heat and Mass Trans. Vol 6 pp 329-353 1963.

13 DRYDEN,H.L. 'Review of Published Data on the Effect of Roughness on Transition from Laminar to Turbulent Flow'.
J. Aero Sc. July 1953 pp 477-482.

14 DUFFY,J. 'Measurement of Turbulent Skin Friction by Pressure Difference Method with special reference to Preston Tube'.
Ph D Thesis Liverpool University 1964.

15 DUFFY,J. and NORBURY,J.F. 'The Measurement of Skin Friction in Pressure Gradients Using a Static Hole Pair'.
Proc I Mech E Thermo Fluid Convention Paper 7
27th - 29th March 1968.

16 DUTTON,R.A. 'The Accuracy of Measurement of Turbulent Skin Friction by means of Surface Pitot Tubes and the Distribution of Skin Friction on a Flat Plate'.
Min Supply Aero Research Council 1957 R & M 3058.

17 DUTTON,R.A. 'The Velocity Distribution in a Turbulent Boundary Layer on a Flat Plate'. Min Supply (A R C Report) C P No. 453 1959.

18 EAST,L.F. 'Measurement of Skin Friction at Low Subsonic Speeds by the Razor Blade Technique'. Min Aviation R A E Report 66277 1966.

19 EAST,L.F. 'Spatial Variations of Boundary Layer in a Large Low Speed Wind Tunnel'. J. Aeronaut. Vol 76 Jan 1972.

20 EDWIN,R.P. 'Light Scattering as a Technique for Measuring the Roughness of Optical Surfaces'. J. Phys E. Sc Inst Jan 1973 Vol 6 pp 55-58.

21 FAGE,A. 'Fluid Motion-Transition from Laminar to Turbulent flow in a Boundary Layer'. Phys Soc. Reports on Progress in Physics. Vol 6 pp 270-279 1939.

22 FAGE,A. and FALKNER,V.M. 'An Experimental Determination of the Intensity of Friction on the Surface of an Aerofoil'. Proc. Roy. Soc. 'A' 1930 Series 'A' Vol 129

23 FAGE,A. and PRESTON,J. 'Experiments on Transition from Laminar to Turbulent Flow in Boundary Layers'. Proc Roy Soc. Series 'A' 1941. Vol 178 p 202.

24 FORSTER,V.T. 'Performance Loss of Modern Steam-Turbine Plant Due to Surface Roughness'. Proc I Mech E. 1966-67 Vol 181 Pt.1

25 GADD,G.E. 'A Note on the Theory of the Stanton Tube'.
A.R.C. Min Aviation R & M 3147 1958.

26 GOLDSTEIN,S. 'A Note on Roughness'.
A.R.C. R & M 1763 1936.

27 HALLING,J. 'Specification of Surface Quality'.
Prod. Eng. (51) May 1972 pp 171-179.

28 HEAD,M.R. 'Entrainment in Turbulent Boundary Layers'.
A.R.C. R & M 3452 1958.

29 HEAD,M.R. and RECHENBERG,I. 'Preston Tube as a means of Measuring Skin Friction'.
J. Fluid Mech. Vol 14 Pl. 1962.

30 HEAD,M.R. and VASANTA RAM,V. 'Simplified Presentation of Preston Tube Calibration'.
Aero Quart. Vol 22-23 pp 295-300 1971.

31 HOLMES,W.E. and LUXTON,R.E. 'Measurement of Turbulent Skin Friction by a Preston Tube in the presence of Heat Transfer'.
J.Mech. Eng. Sc Vol 9 No.3 1967.

32 HOOL,J.N. 'Measurement of Skin Friction Using Surface Tubes'.
Aircraft Eng. 28 p 52 1956.

33 HUFFMAN,G.D. and BRADSHAW,P. 'A Note on von Karman's Constant in Low Reynolds Number Turbulent Flow.
J. Fluid Mech. 53 1 pp45-60 May 1972.

34 HUNTER,A.J. 'On the Distribution of Asperity Heights of Surfaces'.
Journal Phy. D. Vol 5 No.2 pp 319 324 Feb 1972.

35 JAYATILLAKA,C.L.V. 'Influence of Prandtl Number and Surface Roughness on the Resistance of Laminar Sub Layer to Momentum and Heat Transfer'.
Ph. D. Thesis Imperial College 1967.

36 KINNS,R. 'Calibration of Hot Wire Anemometers for Velocity Perturbation Measurement'.
J. Phys E. Vol 6 No. 3 pp 253-256 Mar 1973

37 KLEBANOFF,P.S. 'Characteristics of Turbulence in a Boundary Layer with Zero Pressure Gradient'.
N A C A. 1247 - 1955.

38 LAUFER,J. 'The Structure of Turbulence in Fully Developed Pipe Flow'.
N A C A. Report 1174 - 1954.

39 MAC MILLAN,F.A. 'Liquid Manometers with High Sensitivity and Small Time Lag'.
J. Sc. Ins. Vol 31 pp17-20 1954.

40 NIKURADSE,J. 'Stromungsgesetze in Rauhen Rohren'.
V D I Verlag Aug 1933 Forschungsheft 361.

41 PATEL,V.C. 'Calibration of Preston Tube and the Limitations on its use in Pressure Gradients'.
J. Fluid Mech. Vol 23 - 1 pp 185-208. 1965

42 PERRY,A.E. and MORRISON,G.L. 'Vibration of Hot Wire Anemometer Filaments'.
J. Fluid Mech. Vol 50 Pt 4 Dec 1971.

43 PRESTON,J.H. 'Determination of Turbulent Skin Friction by means of Pitot Tubes'.
J. Roy. Aero. Soc. Vol 58 1954.

44 PRANDTL,L. and SCHLICHTING,H. 'Das Widerstandsgesetz Rauher Platten'.
Werft Reed Hafen 1934 - 1.

45 ROTTA,J.C. 'Turbulent Boundary Layers in Incompressible Flow'.
Progress in Aeronautics Sc. - 2 1962. Pergamon Press.

46 SCHLICHTING,H. 'Boundary Layer Theory'.
6th Edition McGraw Hill.

47 SMITH,K.G. GAUDET,L. and WINTER,K.G. 'Use of Surface-Pitot Tubes as Skin Friction Meters'.
Aero. Res. Coun. Report. R & M 3351 1962.

48 STANTON,T.E. MARSHALL,D. and BRYANT,C.N. 'On the Conditions at the Boundary of a Fluid in Turbulent Motion.
Proc. Roy. Soc.(A) Vol 97 p 413 1920.

49 STREETER.V.F. 'Frictional Resistance in Artificially Roughened Pipes'.
Am Soc. Civ. Eng. pp 163-186 1935.

50 TAYLOR,G.I. 'Measurements with a Half Pitot Tube'.
Proc. Roy. Soc. (A) Vol 166 1938.

51 TEWFIK,O.E. 'Some Effects of Surface Roughness on the Turbulent Boundary Layer'.
A I A A Journal Vol 1 No.9 1963.

52 ZOGG,H. and THOMAN,H. 'Errors in Static Pressure Measurement due to Protruding Pressure Taps'.
J.Fluid Mech. Vol 54 - 3 Aug 1972.

APPENDIX 1

Typical Calibrations

(A) Wind Tunnel Calibration

Heads measured in Inches W.G.		
Fan Speed rev/min	Kinetic Head	Static Head
700	0.124	0.121
900	0.214	0.208
1000	0.264	0.258
1200	0.388	0.380
1400	0.545	0.541
1500	0.626	0.602
1600	0.730	0.718
1700	0.824	0.798
1800	0.930	0.905
1880	1.010	0.980

Date :- 8th November 1972.
Barometric Pressure 770mm Hg.
Temperature 20.5°C.

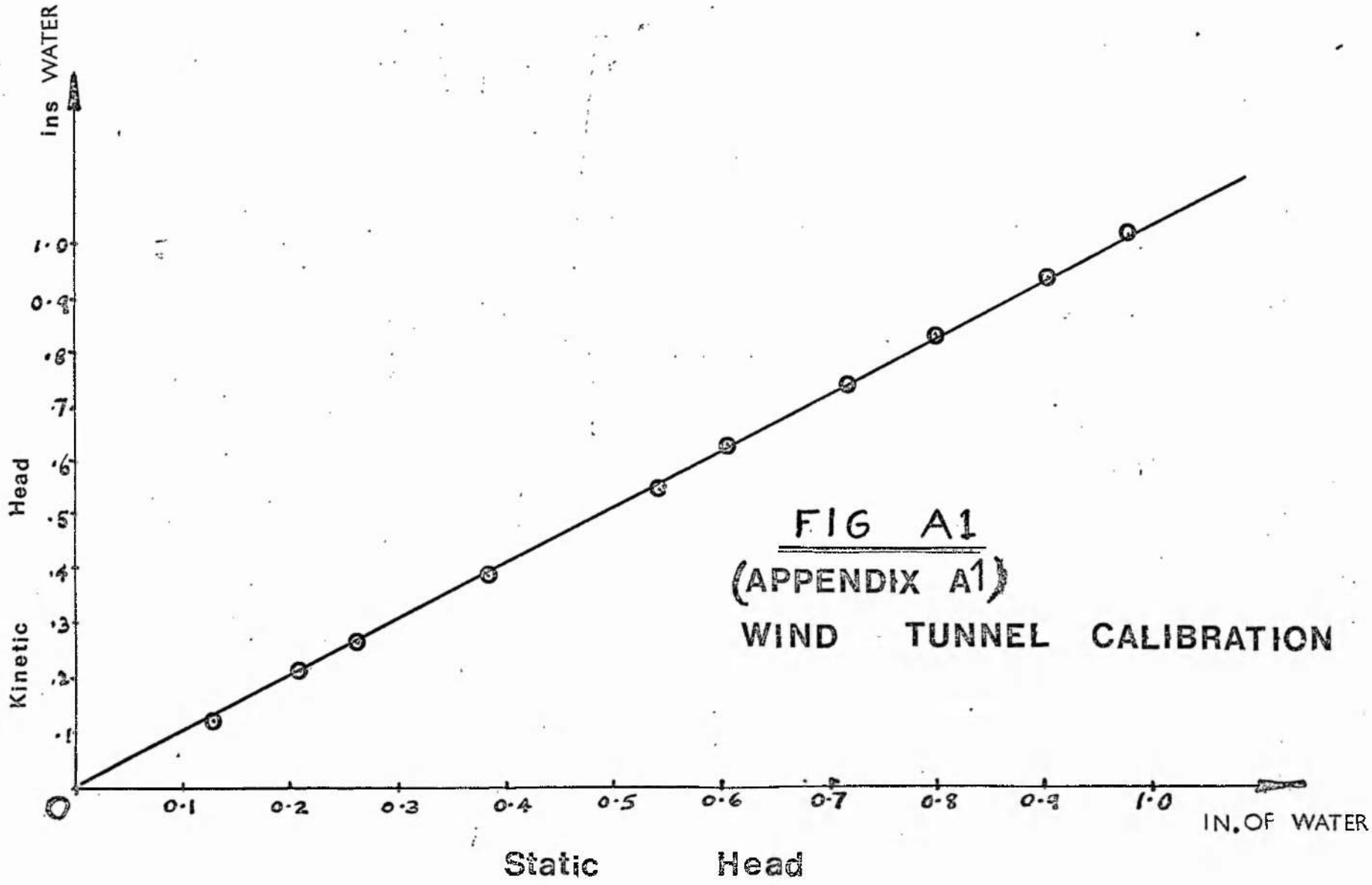

FIG A1
(APPENDIX A1)
WIND TUNNEL CALIBRATION

APPENDIX I

(B) Kinematic Viscosity of Air

Temperature		Density ρ	Viscosity μ	Kinematic Viscosity ν	
$t^{\circ}C$	T K	gm/cc	poise	c/stoke	ft^2/s
14	287	1.230×10^{-3}	1775×10^{-7}	14.42	15.5×10^{-5}
15	288	1.225 "	1780 "	14.51	15.6 "
16	289	1.221 "	1782 "	14.60	15.7 "
17	290	1.215 "	1790 "	14.72	15.8 "
18	291	1.212 "	1795 "	14.80	15.9 "
19	292	1.210 "	1799 "	14.88	16.0 "
20	293	1.205 "	1800 "	14.95	16.1 "
21	294	1.201 "	1810 "	15.07	16.2 "
22	295	1.196 "	1813 "	15.19	16.3 "
23	296	1.192 "	1820 "	15.25	16.4 "
24	297	1.191 "	1822 "	15.30	16.5 "
25	298	1.186 "	1825 "	15.40	16.6 "

Correct for Atmospheric Pressure Multiply by $760/P_a$.

APPENDIX 1

(C) Typical Hot Wire Probe Calibration

Example:- Calibration for Aluminium Oxide Grade 100.

Air Temperature = 19.1°C (292 K) (525.6 R)

Barometric Pressure = 780.4mm (15.1 lbf/in^2)

Kinetic Head measured in ins. Water- P_{ke}

$$u = \sqrt{\frac{2g\ \rho_w\ P_{ke}}{\rho_a}} = M\sqrt{P_{ke}}$$

and $$M = \sqrt{\frac{2 \times 32.2 \times 62.5 \times 53.3\ T}{P_a \times 12 \times 144}} = \text{Manometer Const.}$$

$$= \sqrt{\frac{124T}{P_a}}$$

where T = temperature in °R, and P_a = atmospheric pressure (lbf/in^2)

$$\therefore M = \sqrt{\frac{124 \times 525.6}{15.1}} = 65.7$$

E	P_{ke}	u	$\sqrt{u}$	E^2
1.805	0.526	47.6	6.89	3.26
1.754	0.324	37.4	6.11	3.07
1.824	0.586	49.1	7.01	3.32
1.655	0.154	25.8	5.08	2.74
1.896	0.925	63.2	7.95	3.59
1.700	0.250	32.9	5.73	2.89
1.790	0.515	47.2	6.87	3.20
1.562	0.085	19.1	4.37	2.44

from **FIG. A2.** A = 3.23 C = 1.12, where A and C are probe constants (4.06..1) used in the computer program shown in Appendix 3.

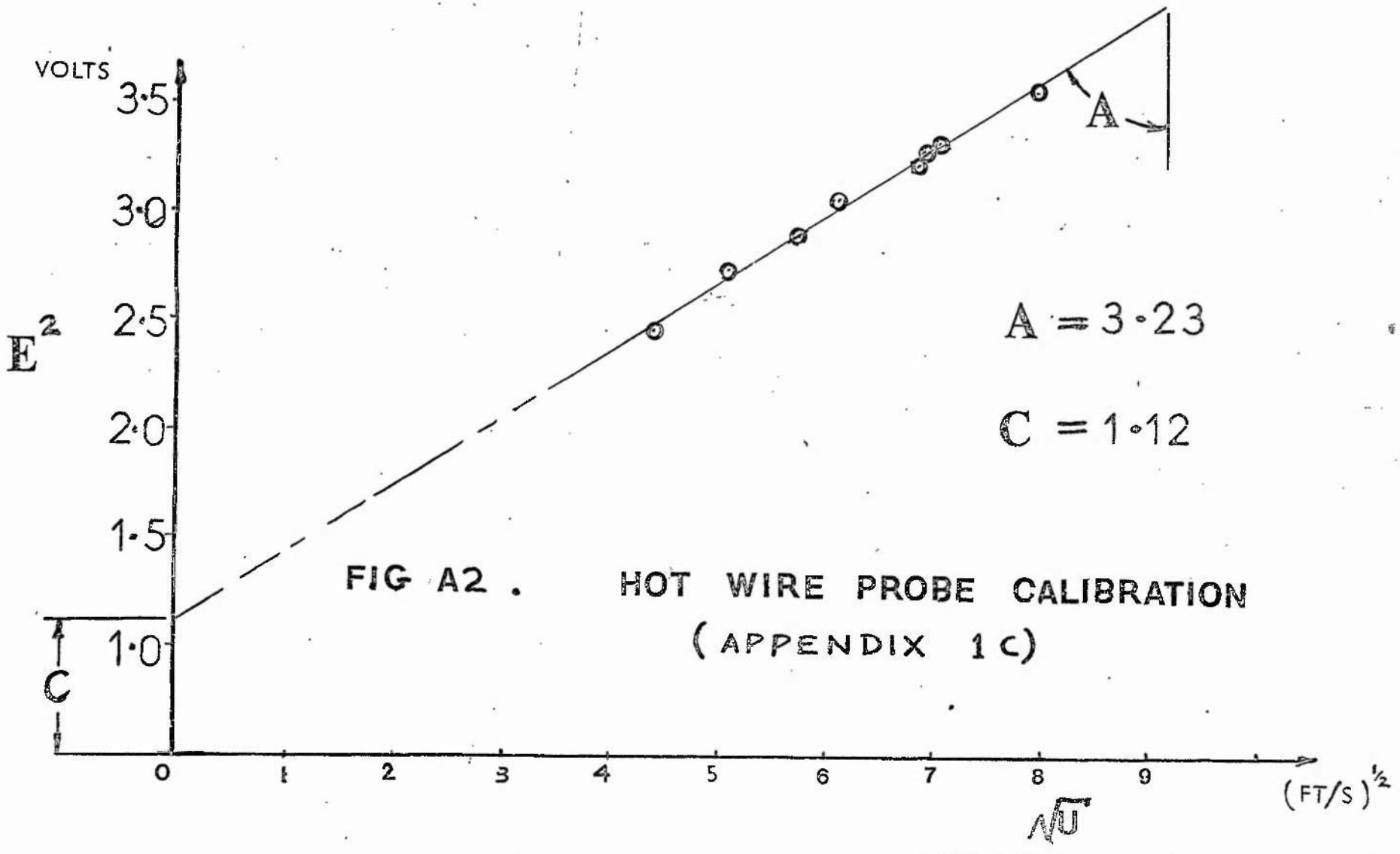

FIG A2 . HOT WIRE PROBE CALIBRATION
(APPENDIX 1C)

APPENDIX 1

(D) Calibration of Plates

The calibration for the various plates is obtained by plotting $\text{Log}_{10} R_x$ against $\text{Log}_{10} C_{fx}$ using the hot wire results for C_{fx} and R_x from Table 1.

The relationship takes the form

$$C_{fx} = \frac{\text{const}}{(R_x)^N}$$

The results shown on the graph in Fig. A3 indicate $N = 0.21$ and the constant varies between 0.055 and 0.060.

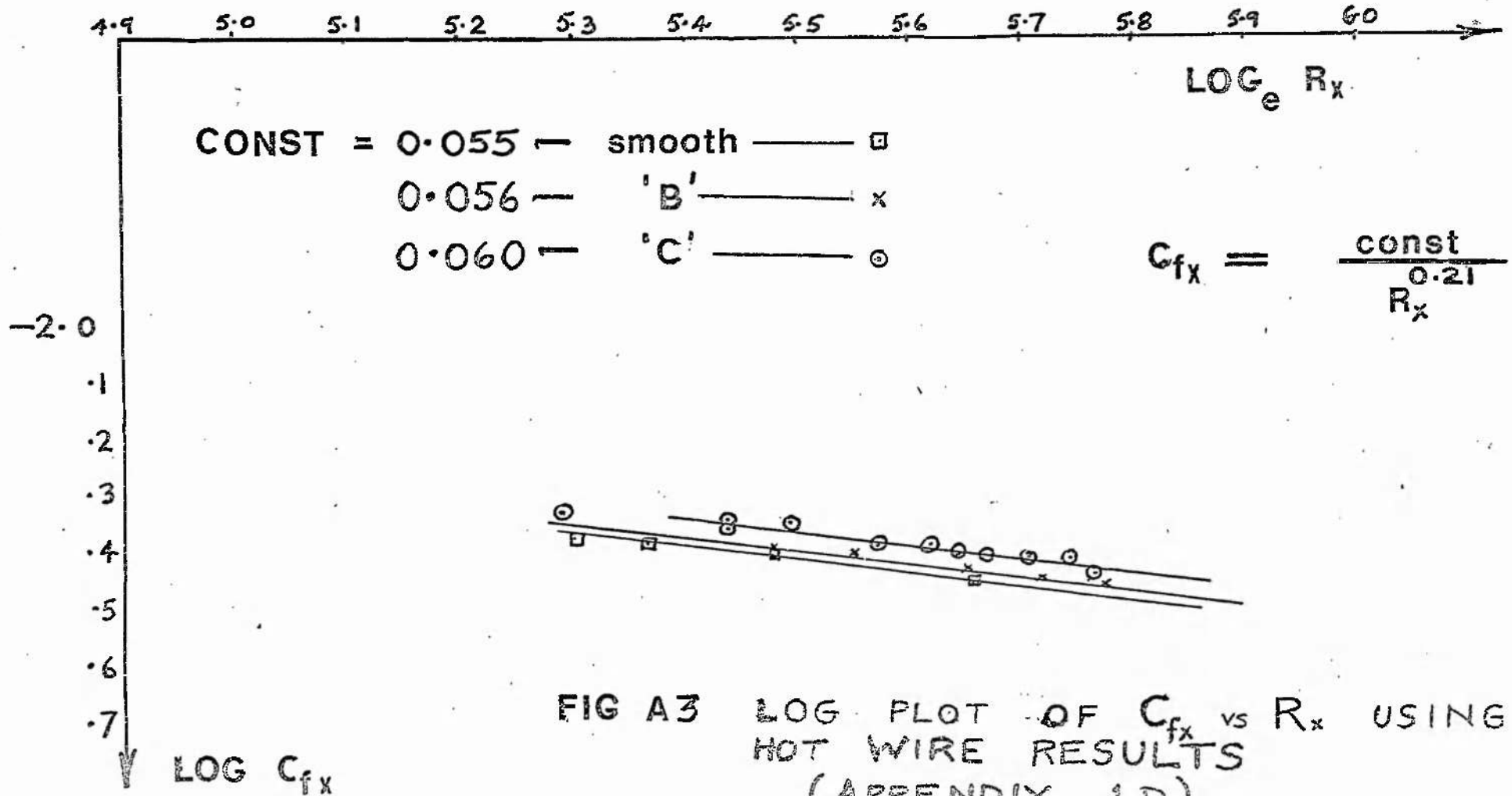

FIG A3 LOG PLOT OF C_{fx} vs R_x USING HOT WIRE RESULTS (APPENDIX 1D)

APPENDIX 2

Specimen Calculations

(checked by slide rule)

(A) Stanton Tube Calculations

Example:- Surface C
Measuring station x = 1.224 ft
h = 0.025 ins.
At 1400 rev/min, P_a = 753.5 mmHg
t^oC = 16.8 (289.8K, 521 R)
Kinetic Head = 0.54 ins Water.
Δp = 0.08 ins. Water.

$\therefore$ Viscosity $\nu = (0.00014205 + 16.8 \times 9.37 \times 10^{-7}) \frac{760}{753.5}$

$= 0.0001591 \text{ ft}^2/\text{s}.$

Manometer const. (m) $= \sqrt{\frac{124\ T}{P_a}}$

$= \sqrt{\frac{124 \times 521}{14.58}}$

$= 66.61$

Mainstream Velocity (U) $= 66.61 \sqrt{0.54}$
$= 49.0$ ft/s

Stanton Tube Velocity (u_p) Equivalent. $= 66.61 \sqrt{0.08}$
$= 18.83$ ft/s

Reynolds Number(R_x) $= \frac{49.0 \times 1.224}{0.0001591}$

$= 376000$

Friction Factor (C_{fx}) (Local) $= \frac{0.0602}{(3.76 \times 10^5)^{0.21}}$ (Obtained from Fig. A3)

$= 0.00405$

$U/u_\tau = 22.21$, $\therefore$ $u_\tau = 2.20$ ft/s

Derived from $u_\tau = U\sqrt{\frac{1}{2}C_{fx}}$

APPENDIX 2 (continued)

(A) Stanton Tube Calculation

$$\frac{1}{8}\left[\frac{u_p\, h}{\nu}\right]^2 = \frac{1}{8}\left[\frac{18.83 \times 0.025}{12 \times 0.000159}\right]^2$$

$$= 7600$$

$$\frac{1}{4}\left[\frac{u_\tau\, h}{\nu}\right]^2 = \frac{1}{4}\left[\frac{2.20 \times 0.025}{12 \times 0.000159}\right]^2$$

$$= 208$$

$$x^* = \text{Log}_{10}\ 7600 = \underline{3.880}$$

$$y^* = \text{Log}_{10}\ 208 = \underline{2.318}$$

These values of x^* and y^* are plotted either on Fig. 14 or Fig. 23, and program POLRG then applied (see Appendix 20.)

(B) Surface Tube - Bradshaw Limits - Using Method of Bradshaw and Gregory [6]

‡ Upper Limit:- $u_\tau h/\nu = 30$; Say maximum U = 68 ft/s, and minimum $C_{fx} = 0.0037$ then $u_\tau = 2.93$ ft/s and $\nu = 16 \times 10^{-5}$ ft^2/s

hence $\left(\frac{u_\tau h}{\nu}\right) = \frac{2.93 \times h \times 10^5}{16 \quad 12} = 30$

∴ the maximum height (h) should not exceed 0.020 in.

‡ Lower Limit:- $u_\tau h/\nu = 2$

hence $\frac{1.21 \times h \times 10^5}{12 \quad 16} = 2$

∴ the minimum height (h) should be greater than 0.003 in.

Note:- at 740 rev/min $C_{fx} = 0.0043$ and $u_\tau = 1.21$ ft/s

‡ The maximum and minimum values of u_τ have been taken from Table 1 to achieve these limits.

APPENDIX 2

(C) Polynomial Regression - Stanton Tube Results

(i) Smooth Surface

h	Y^{*} range	hu_γ/ν range	Equation
0.023	2.435,1.481	33 , 11.1	$Y = -0.045X^2 + 1.00X - 0.974$
0.018	2.214,1.226	25.6,8.21	$Y = 0 + 0.6978X - 0.483$
0.014	1.984,1.102	19.7,7.10	$Y = -0.101X^2 + 1.34X - 1.5$
0.011	1.827,1.202	16.4,7.98	$Y = -0.107X^2 + 1.28X - 1.22$
0.008	1.523,0.716	11.6,4.55	$Y = -0.52\ X^2 + 3.05X - 3.04$
0.004	0.796,0.156	5, 2.29	$Y = -0.082X^2 + 0.95X - 0.733$

Polynomial Regression for the complete range (61 readings)

$Y = -0.01266X^2 + 0.7985X - 0.6758$

East $Y = 0.0165X^2 + 0.637X - 0.455$

‡ Note :- the * in x^* and y^* are omitted for clarity in these equations.

(ii) Rough Surfaces

	h	Y^{*} range	hu_γ/ν range	Equation
C	0.025	2.489,1.826	35,16.35	$Y = -2.036X^2 + 15.351X - 26.558$
C	0.018	2.204,1.570	25.3,12.2	$Y = -0.101X^2 + 1.367X - 1.462$
B	0.018	2.172,1.353	24.4, 9.5	$Y = -0.067X^2 + 1.127X - 1.16$

APPENDIX 2

(D) Clauser Method Calculations

Example:- Smooth surface N = 1000 rev/min; x = 1.225 ft.
ν = 0.0001585 ft^2/s. R_x = 298780. U = 38.66 ft/s.

y ins	u ft/s	u/U	yU/ν	Log_eyU/ν
1.2	38.66	1.000	24400	10.10
1.1	38.24	0.989	22400	10.10
0.9	36.72	0.949	18300	9.81
0.7	35.91	0.928	14220	9.56
0.5	34.58	0.984	10150	9.22
0.4	33.28	0.860	8120	9.00

Clauser grid line coincides with U/u_τ = 23
hence u_τ = 1.67 ft/s.

(E) Clauser Defect Velocity Profile - Fig. 21

Example:- Abrasive Paper Surface :- Aluminium Oxide Grade 100.
N = 1600 rev/min; x = 16.55 in.
from computer output δ^* = 0.1211 in.
U = 52.68 ft/s; y = 0.6 in.
u_τ = 2.87 ft/s, u = 50.19 ft/s; U/u_τ = 18.375.

hence $\frac{y}{\delta^*} \frac{u_\tau}{U} = \frac{0.6}{0.1211 \cdot 18.375}$

$= 0.269$

$\frac{u-U}{u_\tau} = \frac{50.19 - 52.68}{2.87}$

$= -0.875$

These quantities are plotted on the defect velocity profile curve see Fig. 21.

Appendix 3

Program 1

```
// JOB
// FOR
*IOCS(1132PRINTER,TYPEWRITER,PLOTTER,CARD)                    ①
*LIST SOURCE PROGRAM
**  J.A.HARRISON  MECH ENG DEPT.
C      VELOCITY PROFILE  FLAT PLATE   330RPM
       DIMENSION Y(20), E(20),U(20)
C  INSTRUCT OPERATOR TO SET PLOTTER AT CENTRE
         WRITE(1,99)
         PAUSE  3
   99 FORMAT(1H,'PLEASE LOCATE PLOTTER IN CENTRAL POSITION')
C       TO FIX SCALES AND ORIGIN
       CALL SCALF (5.0, 5.0,-0.2,0.6)
C         DRAW GRID
C      PLOT+X AXIS
        CALL FGRID(0,0.0,0.0,0.2,7)
C    PLOT +Y AXIS
        CALL FGRID(1,0.0,0.0,0.2,5)
C         TITLE
        CALL FCHAR(0.3,1.2,0.2,0.2,0.0)
        WRITE (7,200)
  200    FORMAT(35HVELOCITY PROFILE, FLAT SMOOTH PLATE)
C  TO TABULATE X SCALE
        XN =-0.03
       RX=0.001
       DO 20J=1,7
        CALL FCHAR (XN,-.05,0.1,0.1, 0.0)
        WRITE(7,202) RX
  202  FORMAT (F3.1)
       XN=XN+0.2
       RX=RX+0.2
    20 CONTINUE
       CALL FCHAR(1.45,-.05,0.1,0.1,0.0)
       WRITE(7,203)
   203 FORMAT(6 HINCHES)
       CALL FCHAR(0.9,-.1,0.2,0.2,0.0)
       WRITE(7,204)
   204 FORMAT(1HY)
C      TO TABULATE Y SCALE
       YN=0.0
       YA=0.0
       YAU=0.0
       DO 21 J=1,6
       CALL FCHAR(-0.08,YN,0.1,0.1,0.0)
       WRITE(7,205)YAU
   205 FORMAT (F3.1)
       YN=YN+0.2
       YA=YA+0.2
       YAU=YA+0.01
    21  CONTINUE
       CALL FCHAR(-0.3,0.70,0.2,0.2,0.0)
        WRITE (7,206)
   206 FORMAT(3HU/U)
       CALL FCHAR(-0.18,0.68,0.1,0.1,0.0)
       WRITE(7,207)
   207 FORMAT (1HO)
       KOUNT=19
       READ(2,10)(Y(I),E(I), I=1,KOUNT)
    10 FORMAT(5(F5.3,1X,F5.3,3X))
       WRITE(3,16)(Y(I),E(I),I=1,KOUNT)
    16 FORMAT(5(2X,F5.3,1X,F5.3,3X))
```

```
      J.A.HARRISON  MECH ENG DEPT.
   16 FORMAT(5(2X,F5.3,1X,F5.3,3X))
      A=2.88                                                    (2)
      C=1.70
C     RATU= U/UO
      U(KOUNT)=((E(KOUNT)**2-C)*A)**2
      WRITE (3,12)
      DO 100 I=1,KOUNT
 1000 FORMAT (100X,F5.3)
      WRITE(3,1000)  Y(I)
      B=(E(I)**2-C)*A
      RATU=(B**2)/U(KOUNT)
      CALL FPLOT(-2,Y(I),RATU)
      CALL POINT(1)
      CALL FPLOT (-1,Y(I), RATU)
   12 FORMAT  (1H,10X,'Y',12X,'U/UO',12X,'E')
      WRITE(3,11) Y(I),RATU,E(I)
   11  FORMAT (3(10X,F5.3))
  100 CONTINUE
      CALL EXIT
      END

FEATURES SUPPORTED
 IOCS

CORE REQUIREMENTS FOR
 COMMON       0  VARIABLES     150  PROGRAM     562

END OF COMPILATION
```

VELOCITY PROFILE, FLAT SMOOTH PLATE

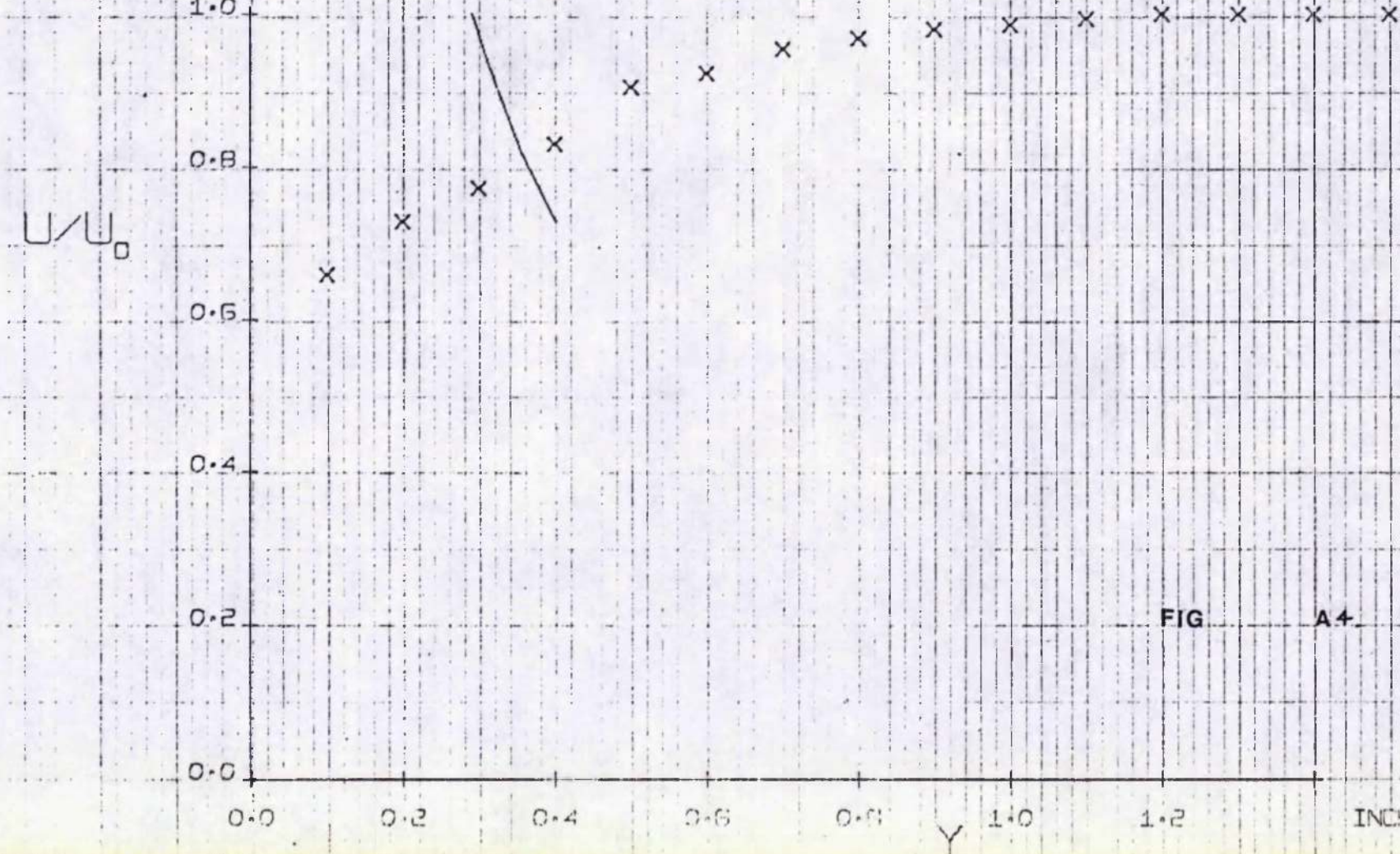

FIG A4

PAGE 2 16/3/73 J.A. HARRISON MECH ENG. DEPT. ①

```
      DIMENSION Y(100),E(100),L(100)
      PAUSE 6666
         WRITE (7,300)
  300  FORMAT ('33JAN')
      CALL SCALF(2.0,10.0,4.0,0.8)
      CALL FGRID(0,5.0,0.5,1.0,5)
      CALL FGRID(1,5.0,0.5,0.1,5)
      CALL FCHAR(5.1,1.1,0.2,0.2,0.0)
      WRITE (7,200)
  200 FORMAT (59HCLAUSER METHOD FOR TURBULENT FLOW PAST RELGH PLANE SURF
     1ACES)
      XN= 4.925
      RX=5.001
      DO 20 J=1,6
      CALL FCHAR(XN,0.485,0.1,0.1,0.0)
      WRITE (7,202) RX
  202 FORMAT (F4.1)
      XN=XN+1.0
      RX=RX+1.0
   20 CONTINUE
      CALL FCHAR(8.1,0.42,0.2,0.2,0.0)
      WRITE(7,205)
  205 FORMAT(3HL (YU /Y))
      CALL F CHAR(3.2,0.41,0.1,0.1,0.0)
      WRITE (7,209)
  209 FORMAT(9HA        0)
      YY=0.5
      RY=0.501
      DO 21 J=1,6
      CALL FCHAR(4.8,YY,0.1,0.1,0.0)
      WRITE(7,215)RY
  215 FORMAT(F4.1)
      YY=Y +0.1
      RY=RY+0.1
   21 CONTINUE
      CALL F CHAR(4.5,0.87,0.2,0.2,1.571)
      WRITE(7,222)
  222 FORMAT(3HU/U )
      CALL FCHAR(4.6,0.94,0.1,0.1,1.571)
      WRITE(7,228)
  228 FORMAT(1H0)
      DO 90 I=1,6
      K = I-1
      READ(2,12) N,TC,A,C,BARP,X
   12 FORMAT (2X,I2,1X,F5.2,1X,F4.2,1X,F4.2,1X,F5.1,1X,F5.3)
      IF(N) 108,108,128
  128  CONTINUE
      WRITE(5,16)I
   16 FORMAT(//5X,3HI =I2,/)
      WRITE(5,18)N
   18 FORMAT(5X,3HN =I2,/)
      WRITE(5,24) A,C
   24 FORMAT(5X,3H A =F4.2,10X,3HC =F4.2,//)
      WRITE(5,25) TC, BARP
   25 FORMAT(5X,3HTC=F5.2,10X,7HBAR.PR=F5.1,//)
      VISC=((1.420E-4)+(TC*3.37E-7))*760.0/BARP
      WRITE(5,26)VISC
   26 FORMAT(5X,11HVISCOSITY =F9.7,//)
      WRITE(5,22)Y
```

CLAUSER METHOD FOR TURBULENT FLOW

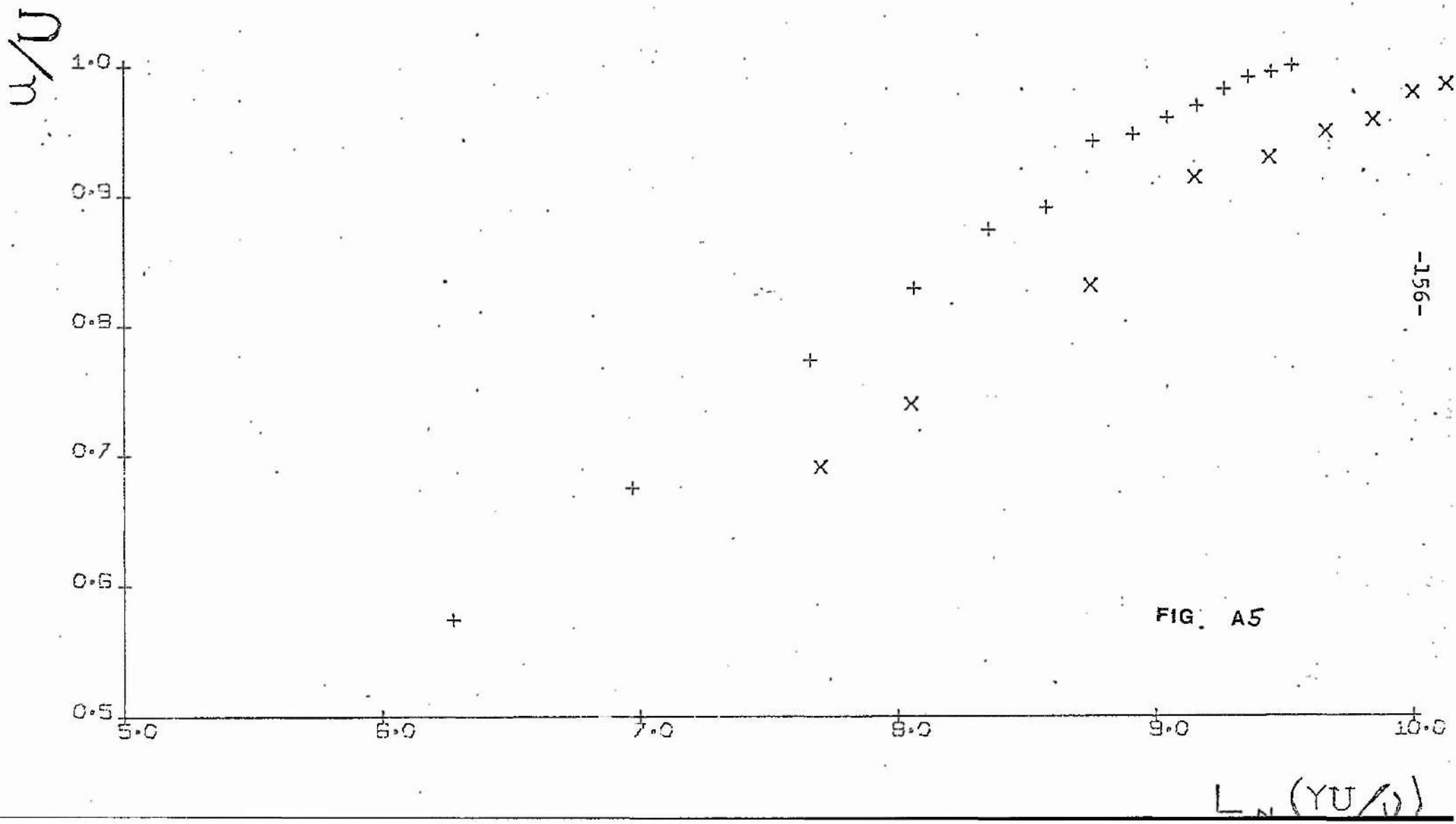

FIG. A5

```
PAGE   3    16/3/73    J.A. HARRISON  MECH ENG. DEPT.                    ②
     22 FORMAT(5X,3HX =F5.3,//)
        READ(2,10)(Y(L),E(L),L=1,N)
     10 FORMAT (5(F5.3,1X,F5.3,3X))
        WRITE(5,14)
     14 FORMAT(1H ,5X,'Y',6X,'E',6X,'U',5X,'U/UO',3X,'REY',4X,'LOG(REY)')
        DO 100 L=1,N
        U(N)=((E(N)**2-C)*A)**2
        B=(E(L)**2-C)*A
        RATU = (B**2)/U(N)
        U(L)= RATU*U(N)
        REY=(Y(L)*U(N))/(12*VISC)
        H=ALOG(REY)
        WRITE (5,28) Y(L),E(L),U(L),RATU,REY,H
     28 FORMAT(3X,F5.3,2X,F5.3,2X,F5.2,2X,F5.3,2X,F7.1,2X,F5.2)
        CALL FPLOT (-2,H,RATU)
        CALL POINT (7)
        CALL FPLOT (-1,H,RATU)
    100 CONTINUE
        REX = U(N)*A/VISC
        WRITE(5,30) REX
     30 FORMAT(//5X,5HREX =F8.1,/////)
     90 CONTINUE
    108 CALL EXIT
        END

FEATURES SUPPLIED
 ICCS

CORE REQUIREMENTS FOR
 COMMON      0  VARIABLES     644  PROGRAM     740
```

TYPICAL "PRINT OUT"

I = 2

N =13

A =2.90 C =1.22

TC=20.00 BAR.PR=777.8

VISCOSITY =0.0001571

X =1.380

Y	E	U	U/UO	REY	LOG(REY)
0.100	1.766	30.32	0.625	2572.4	7.85
0.200	1.815	36.18	0.746	5144.8	8.54
0.300	1.835	38.77	0.799	7717.2	8.95
0.400	1.842	39.71	0.818	10289.6	9.23
0.500	1.856	41.62	0.858	12862.1	9.46
0.600	1.868	43.31	0.893	15434.5	9.64
0.700	1.877	44.61	0.919	18006.9	9.79
0.800	1.884	45.63	0.940	20579.3	9.93
0.900	1.896	47.43	0.977	23151.7	10.04
1.000	1.902	48.34	0.996	25724.2	10.15
1.100	1.903	48.49	1.000	28296.6	10.25
1.200	1.903	48.49	1.000	30869.0	10.33
1.300	1.903	48.49	1.000	33441.4	10.41

Prog. 3

```
C     BOUNDARY LAYER
      DIMENSION A(6)
      DO  90   K=1,6
      READ(2,16)UG,VISC, D, X1,X2
   16 FORMAT (2X,F5.2,2X,F9.7,2X,F5.3,2X,F6.3,1X,F6.3)
      WRITE(5,18) K ,UG
   18 FORMAT (//2X,3HK =I2,6X,10HVELOCITY = F5.2,//)
      WRITE(5,14) VISC  , D
   14 FORMAT(10X,6HVISC = F9.7,5X,9HDISTANCE=F5.3,//)
      READ (2,99) (A(I),I=1,6)
   99 FORMAT(6 F11.7)
C     THE COEFFICIENTS ARE RENUMBERED, A0 BECOMES A(1) ETC
      X=X1
      DX=(X2-X1)/100
C       X1 AND X2 STRADDLE X=.99 (CORRECTED VALUES)
      DO 20 J=1,100
      Y=A(1)+X*(A(2)+X*(A(3)+X*(A(4)+X*(A(5)+(A(6)*X)))))
C        N=5 HAS BEEN TAKEN AS HIGHEST LIKELY ORDER OF POLYNOMIAL
      X=X+DX
      IF(0.0001-ABS(Y-0.99))20,25,25
   20 CONTINUE
   25 Z=X* (A(1)+X*(A(2)/2+X*(A(3)/3+X*(A(4)/4+X*(A(5)/5+A(6)*X/6)))))
C       Z IS THE INTEGRAL OF Y DX AND X=D
      C=X-Z
C       C IS THE DISPLACEMENT THICKNESS
      B=X*((A(1)*A(1))+X*((A(1)*A(2))+X*((2*A(1)*A(3)+A(2)*A(2))/3+X*
     1((2*A(1)*A(4)+2*A(3)*A(2))/4+X*((A(3)*A(3)+2*A(1)*A(5)+2*A(2)*A(4)
     2)/5+X*((A(1)*A(6)+A(2)*A(5)+A(3)*A(4))/3+X*((A(2)*A(6)*2+A(5)*A(3)
     3*2+A(4)*A(4))/7+X*((A(3)*A(6)+A(4)*A(5))/4+X*((A(4)*A(6)*2+A(5)*
     4A(5))/9+X*((A(5)*A(6))/5+X*(A(6)*A(6))/11)))))))))))
C       B IS THE INTEGRAL OF Y SQUARED DX
      E=Z-B
C         E IS THE MOMENTUM THICKNESS
      WRITE(5,100)C,E
  100 FORMAT(10X,10HDISP. TH =F10.8,3X,11HMOMENT TH = F10.8,//)
      REX = UG*D/VISC
      REE =E *UG/(12*VISC)
      CF =  0.0256 /(REE **0.25)
      WRITE(5,106)  REX , REE
  106 FORMAT (5X,5HREX =F8.1,5X, 6HRTHETA = F6.1,///)
      WRITE (5,98) CF
   98 FORMAT(10X, 4HCF = F9.7,//////)
   90 CONTINUE
      CALL  EXIT
      END
```

```
FEATURES SUPPORTED
 IOCS

CORE REQUIREMENTS FOR
 COMMON       0  VARIABLES     96  PROGRAM     794
```

TYPICAL "PRINT OUT"

```
K = 2       VELOCITY =62.38

            VISC =0.0001631      DISTANCE=1.380

            DISP. TH =0.07820107    MOMENT TH =0.04844690

      REX =527801.3      RTHETA =1544.1
```

Appendix 6 Program, 4.

```
PAGE    2     14/5/73    J.A.HARRISON  MECH ENG.

C       STANTON  TUBE  CALIBRATION
        DIMENSION BARP(30),TC(30),REV(30),HKIN(30),DP(30),REX(30),B(30)
        DIMENSION C(30),A(30),VISC(30)
         X=1.224
           GAP=0.022
         KOUNT= 8
        D=GAP/12.
        READ(2,10)(REV(I),BARP(I),TC(I),HKIN(I),DP(I), I=1,KOUNT)
   10 FORMAT(2X,F6.1,2X,F5.1,2X,F5.2,2X,F5.3,2X,F5.3)
         WRITE  (5,6)  X
    6 FORMAT ( 10X, 5H'X' =F5.3)
         WRITE  (5,8)  GAP
    8 FORMAT (10X,5HGAP =F6.4)
        WRITE(5,12)
   12 FORMAT(1H ,3X,'REVS',4X,'VISC',7X,'A',6X,'UG',5X,'UP',6X,'REX',7X,
     1'CF',7X,'B',9X,'C',5X,'XSTAR',2X,'YSTAR')
        DO 100 I=1,KOUNT
        VISC(I)=((1.4205E-4)+(TC(I)*9.37E-7))*760.0/BARP(I)
        TAB =1.8*(273+TC(I))
        A(I)= SQRT(6410.*TAB/BARP(I))
        UG =A(I)*SQRT(HKIN(I))
        UP =A(I)*SQRT(DP(I))
        REX(I)=X*UG/VISC(I)
        CF=0.055/REX(I)**0.21
        UTOR = UG *SQRT(CF/2)
        B(I)=0.125*(UP*D/VISC(I))**2
        C(I)=0.250*(UTOR*D/VISC(I))**2
        XSTAR= ALOG(B(I))/2.3026
        YSTAR= ALOG(C(I))/2.3026
        WRITE(5,11)  REV(I),VISC(I),A(I),UG,UP,REX(I),CF,B(I),C(I),XSTAR,Y
     1STAR
   11 FORMAT(2X,F6.1,2X,F9.7,2X,F5.2,2X,F5.2,2X,F5.2,2X,F8.1,2X,F7.5,2X,
     1F8.2,2X,F6.2,2X,F5.3,2X,F5.3)
  100 CONTINUE
        CALL EXIT
        END

FEATURES SUPPORTED
 IOCS

CORE REQUIREMENTS FOR
 COMMON       0  VARIABLES     632  PROGRAM     440

END OF COMPILATION

// XEQ
```

```
// FOR
*IOCS(1403 PRINTER,CARD)
**J.A.HARRISON  MECH ENG.

FEATURES SUPPORTED
 IOCS

CORE REQUIREMENTS FOR
 COMMON       0  VARIABLES    632  PROGRAM    440

END OF COMPILATION

// XEQ

          'X' =1.224
          CAP =0.0250
   REVS      VISC          A      UG      UP        REX          CF          B          C      XSTAR   YSTAR
 1725.0  0.0001580    66.47   60.63   24.96   469684.7   0.00386   13538.58   308.70   4.131   2.489
 1650.0  0.0001583    66.52   57.68   23.33   445776.1   0.00390   11770.24   281.14   4.070   2.446
 1600.0  0.0001591    66.61   56.09   22.68   431383.1   0.00393   11025.60   265.10   4.042   2.423
 1550.0  0.0001589    66.59   54.09   21.47   416560.5   0.00396    9901.70   249.02   3.995   2.396
 1500.0  0.0001591    66.61   52.62   20.42   404699.2   0.00398    8934.54   236.47   3.951   2.373
 1450.0  0.0001579    66.46   50.00   19.37   387558.8   0.00402    8168.49   218.84   3.912   2.340
*1400.0  0.0001591    66.61   48.95   18.84   376475.6   0.00404    7603.87   207.77   3.881   2.317 *
 1350.0  0.0001592    66.62   47.34   18.12   363917.3   0.00407    7027.65   195.52   3.846   2.291
 1300.0  0.0001588    66.58   45.40   16.71   349706.9   0.00411    6003.21   182.15   3.778   2.260
 1250.0  0.0001591    66.61   43.37   15.90   333597.6   0.00415    5417.75   167.33   3.733   2.223
 1200.0  0.0001585    66.54   41.61   15.02   321165.1   0.00418    4872.08   156.33   3.667   2.194
 1100.0  0.0001583    66.52   37.92   12.79   293055.2   0.00426    3540.64   132.69   3.549   2.122
 1000.0  0.0001591    66.61   34.16   11.34   262735.0   0.00436    2756.40   109.13   3.440   2.037
  950.0  0.0001578    66.45   32.21   10.50   249832.0   0.00441    2404.54    99.72   3.381   1.998
  900.0  0.0001589    66.59   30.80    9.67   237199.1   0.00446    2094.59    90.88   3.321   1.958
  850.0  0.0001589    66.59   28.71    8.93   221137.6   0.00452    1713.75    80.16   3.233   1.903
  800.0  0.0001578    66.45   25.82    8.13   200263.8   0.00462    1442.72    67.12   3.159   1.826
// * END OF DECK

// PAUSE
```

* See specimen calculations